College of Engineering, Design and Physical Sciences

Department of Mechanical, Aerospace and Civil Engineering

A thesis submitted for

the degree of

Master of Philosophy

Nonlinear behaviour of Offshore Flexible Risers

Supervisors:

Professor Hamid Bahai

Dr. Giulio Alfano

By:

Shayan Norouzi

Dedicated to

My parents, my sibling, and Sara

Abstract

As the search for exploration of oil and gas moves to deeper waters, flexible unbounded risers have become the main means of extracting hydro carbonates from deep waters. In this context, structural integrity of flexible risers has become a crucial issue for the offshore industry.

In this study, experimental tests and detailed finite element analyses were carried out on a scaled down model of a flexible riser pipe. The model used consists of four layers which include two cylindrical polycarbonate tubes and two steel helical layers. One helical layer represents the carcass layer in an actual flexible riser whilst the other represents the riser tendon armour layers, wounded around the pipe assembly.

The model was first subjected to a three point bending load in order to study its bending-curvature behaviour experimentally. Then, the specimen was tested under compressive load with different pressure values to investigate the effect of pressure on the pipe deformation. Additionally, the effects of pure axial load and pure pressure with no load on the model were examined. The effects of static load on the deformation of a single helical tendon layer and creep behaviour (Shetty, 2013) of the layer were also studied.

The investigation of a single tendon under axial load using finite element based software shows residual strains results are in good agreement with the experiments. The numerical model also shows a non-linear behaviour in bending-moment curvature for flexible pipe which is in a good agreement with the experimental data.

Declaration

This thesis is written based on the research carried out in Brunel University London in United Kingdom. No part of it has been submitted elsewhere for any other qualification or degree. It is all my own research except some sections which the works of others were used and the related authors' names are mentioned in references.

Acknowledgements

The author tends to thank his supervisors, Professor Hamid Bahai and Dr. Giulio Alfano for their helpful recommendations and guidance during the research process.

Also thanks to Mr. Keith Withers, whose guidance and ideas helped a lot to improve the experiments, the previous researchers of offshore engineering, the staff of mechanical engineering workshop, and the other related staff of Brunel University.

Contents

List of Figures

Chapter 1

Chapter 3

Chapter 4

List of Tables

List of Symbols

d_o	outer diameter
d_i	inner diameter
E	module of elasticity
GF	gauge factor
I	area moment inertia
L	length of beam
M	bending moment
M_a	bending moment at point A
M_y	yield moment
P	bending load
R_a	reaction force at point A
R_i	inner radius
R_G	initial resistance of gauge
R_m	mean radius
R_o	outer radius
Rev	Number of revolutions (pitches)
t	thickness
x	horizontal direction at bending
X	bending curvature
y	vertical direction at bending
y	maximum bending radius
ΔR	strain made resistance
ϵ	strain
π	Pi number
σ	stress
σ_y	yield stress

Chapter 1:

Introduction

1.1 Overview

In recent decades, as global oil demand has been rising, oil exploration and production has been progressing into deeper water. As a result, industrial competition for designing efficient and reliable facilities to reach the hydro-carbonates in ultra-deep waters in areas such as Gulf of Mexico, southern shores of Caspian Sea, Norwegian Sea and Greenland waters has become inevitable. This has led to the rapid development of the flexible risers capable of functioning in a harsh environment in deeper waters often exceeding 3km below sea level.

One key development has been the unbounded flexible risers used to transport oil and gas at high internal and external pressure between the seabed and surface in deep waters. Flexible risers consist of several polymer and steel layers that are, to a certain extent, free to move internally relative to each other. This gives low bending stiffness and makes them highly valuable tools for subsea oil and gas companies. Their ability of withstanding against both horizontal and vertical displacements made them ideal for floating platforms.

Due to the complex geometry of flexible risers, the conventional stress prediction and fatigue analysis tools based on analytical formulations and linear methods are not adequate. Instead, detailed non-linear finite element methods or experimental methods are required to take into account the contact and friction between the layers, radial contraction and delamination. In this thesis both detailed finite element methods and experimental techniques are used to analyse the complex structural behavior of flexible risers.

In this chapter, first the main configurations for flexible risers are briefly explained. Then, the components of a typical flexible riser are described. Finally, the objective, scope of the research, and outline of the thesis are presented.

1.2 Subsea Risers Configurations

As shown in figure 1.1, flexible risers can have the following configurations:

- Steep wave,
- Lazy wave,
- Steep S,
- Lazy S.

The first two configurations perform through incorporate buoyancy modules (Tong and Tang, 1997); in these configurations, synthetic foam used to make buoyancy elements which are connected to the longer length of the pipe; hence, negative weight results to wave shape, which separates the movements of risers of Touch down point (TDP) from vessel motion. The steep wave requires a base and a bend stiffener at sea floor and therefore the lazy wave is more desired; in some projects where internal fluid density changes with life of the riser, steep wave configurations is a good solution. Buoyancy elements would lose volume if the pressure is high and submerged weight would increase (Løseth, 2011).

The next two configurations are known as S-configurations in which anchored buoyancy modulus is used; the buoy component is attached to the pipe and creates an S-shape; it might either be fixed or floated. Tension variation is absorbed by buoy and minimized at TDP. S-configurations are expensive because of the infrastructure requirements (Løseth, 2011).

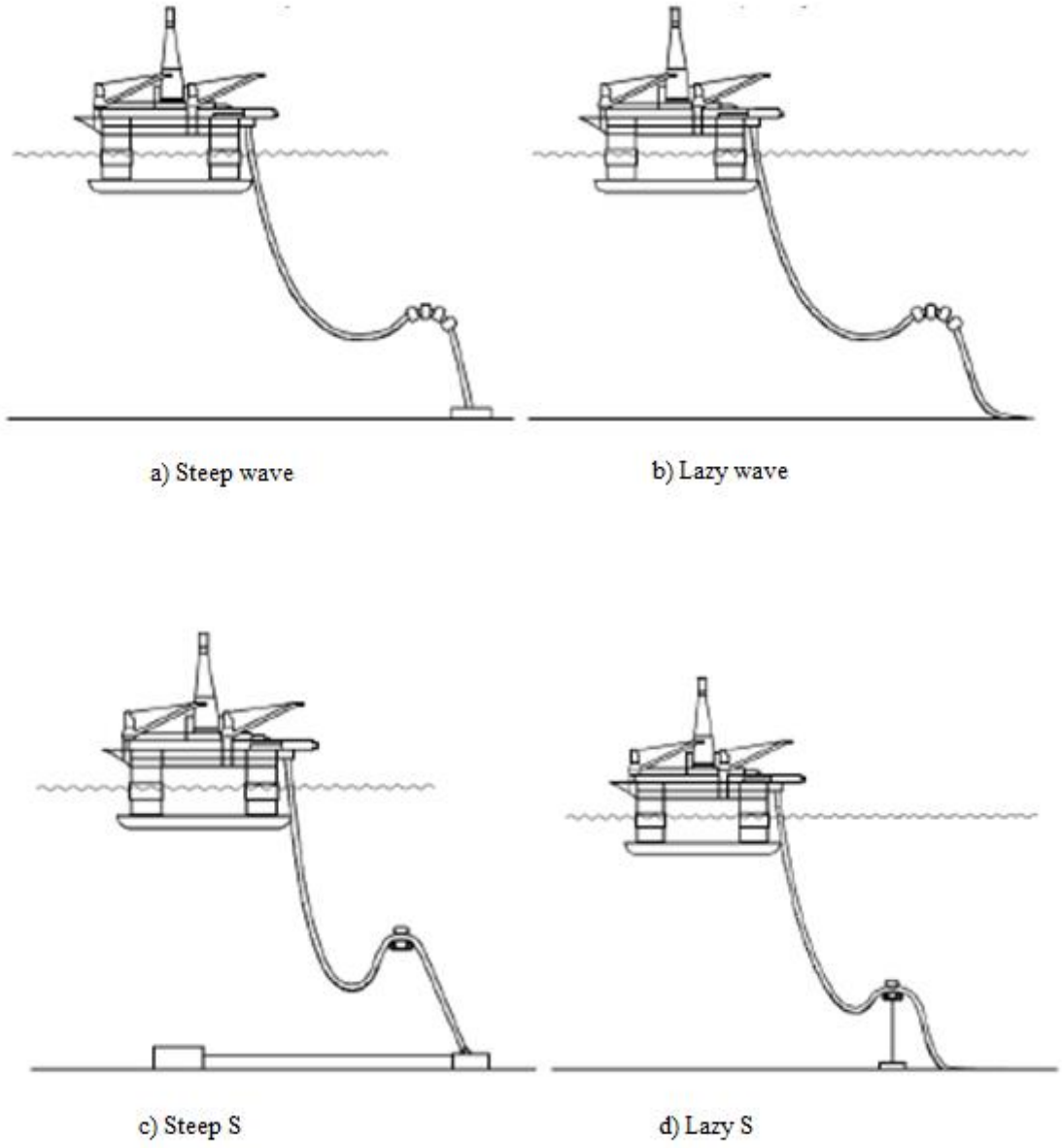

Figure 1.1 Flexible Riser Configurations (Løseth, 2011)

1.3 Flexible Risers Layer[1]

A typical unbounded flexible riser consists of six to twenty layers with different materials and cross-sections (Løseth, 2011). The layers of a typical flexible riser are shown in figures 1.2 and 1.3.

(1) A detailed discussion upon layers is presented in Bai and Bai (2010).

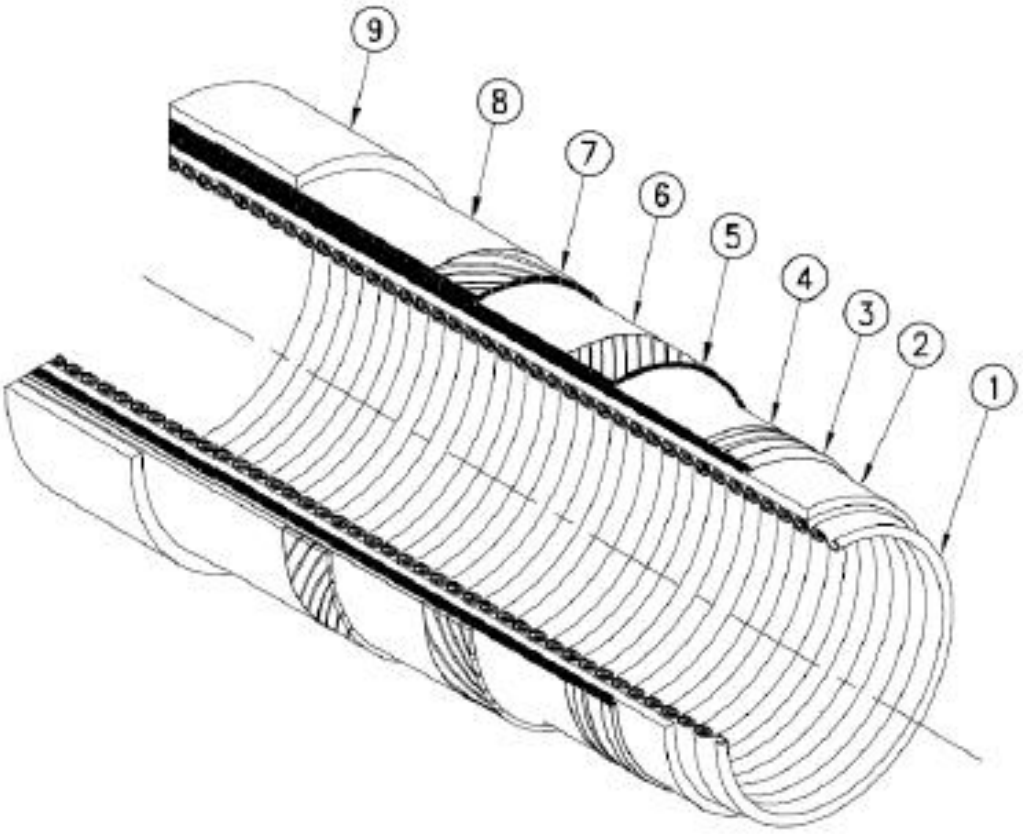

Figure 1.2 Flexible Riser and its layers 3D view (Løseth, 2011)

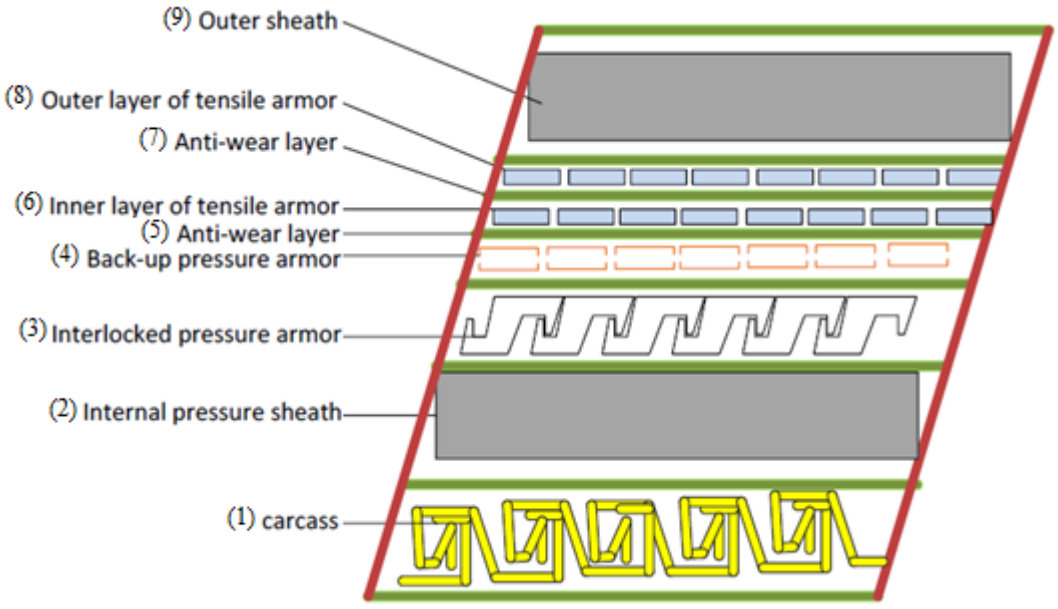

Figure 1.3 Flexible Riser and its layers Cross-Section (Zhao, 2013)

1.3.1 Carcass

An interlocked carcass is the innermost part of the pipe structure; it has an interlocking cross section with a high lay angle with respect to the pipe longitudinal direction. The profile of carcass is demonstrated in figure 1.4. Carcass is commonly made from steel AISI 304, steel AISI 316, or Duplex steel (Løseth, 2011). Its function is to contact with internal fluid directly in the bore and make resistance against the external pressure. The fluid freely flows through the carcass in the bore.

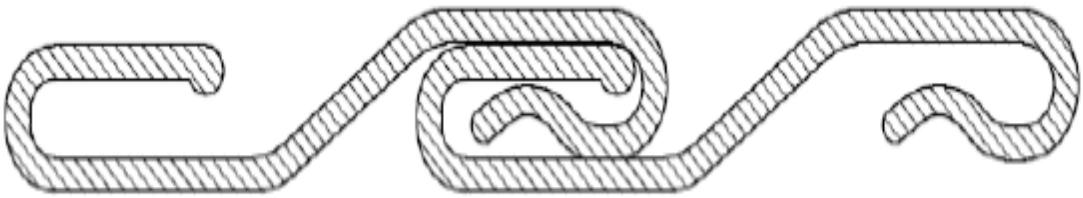

Figure 1.4 Carcass Profile (Løseth, 2011)

1.3.2 Internal Pressure Sheath

This layer ensures internal fluid integrity and is used as sealing component; is made from thermoplastic polymer, either extruded over the carcass or tape wrapped. This layer guarantees the fluid temperature (Bai and Bai, 2010). The possible material options of internal pressure sheath have listed below (Zhao, 2013):

- Polyamide (nylon), PA11 or PA22
- Poly vinylidene fluoride (PVDF)
- High density polyethylene (HDPE) and cross-linked polyethylene (XLPE)

1.3.3 Inner and Outer Liner

These layers are made from polyethylene (e.g. HDPE, XLPE), or polyamide (e.g. PA11) and polyvinylidene fluoride (e.g. PVDF). They have the ability to withstand high mechanical and thermal strains which makes them crucial; the thermal properties of these layers mostly are defined as design limits (Løseth, 2011).

1.3.4 Anti-wear Layer

The aim of considering this layer in flexible risers is separating metallic armour layers and therefore reducing the friction. Typically, they are made from polyethylene, polyamide, or polyvinylidene fluoride (Løseth, 2011).

1.3.5 Pressure Armour

Also called Zeta pressure spiral or flat spiral, this layer has zeta shaped cross-section and similar to carcass, its lay angle with respect to the pipe longitudinal direction is high (about 89 degree). A typical pressure armour profile is shown in figure 1.5. The zeta shaped profiles let the layer to bend easily and the gap between armour wires would be controlled; hence, internal sheath through this layer would not be extruded. This layer is mainly designed for the applied hoop stresses made from internal pressure; in addition, it can resist against external pressure, accidental loads, and crushing effects from the tensile armour layer. The material used for this layer is mainly low carbon steel alloys, which have bigger yielding strength around 700 to 1000 MPa. Profiles used for pressure armours designs are: Theta shaped, C-Clip, X-LINKT, and K-LINKT. As a reinforcement, zeta profile might be assembled by a flatted steel helix (Løseth, 2011 and Zhao, 2013).

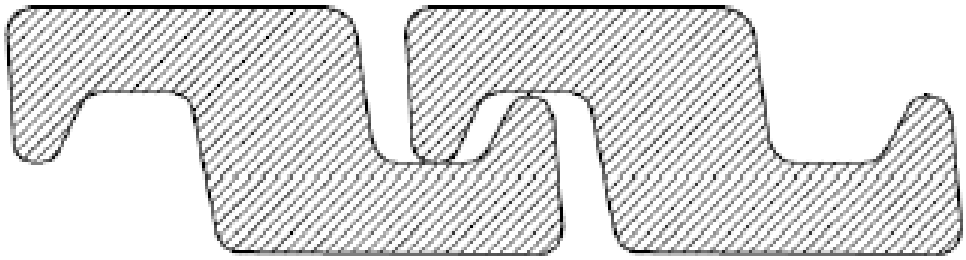

Figure 1.5 Pressure Armour Profile (Løseth, 2011)

1.3.6 Tensile Armour

Also known as axial armour or helical tendon, this layer consists of two or four cross wounded layers (pairs), which are made from flat rectangular wires with low lay angle with respect to the pipe longitudinal direction (30 to 55 degree). This layer provides longitudinal strength (axial loads) and supports the structure weight by transferring it to the termination point atop. When axial load is applied, the induced torsion on helical cross wounded layer can be balanced by using another layer with different angular assembly; hence, the number of cross wounded in the structure is always even. It also transfers some longitudinal loads to radial direction similar to the direction of the external pressure. They are made from low alloy steels with yield points of 700 to 1500 MPa (Løseth, 2011, Zhao, 2013 and Norouzi, 2012).

1.3.7 Outer Sheath

Also known as external thermal plastic layer, this layer is the only visible layer of the flexible pipe from outside. It has designed for protecting the structure from sea-water intrusion, corrosion, abrasion, damages during the handling, and binding the armour layers (Zhao, 2013 and Norouzi, 2012).

1.4 Failure Causes

According to Zhao (2013) the main causes of fatigue failure of flexible risers are as follows:

- "*First order wave loading (wave frequency)*
- *Second order floater motion due to wind, wave and current*
- *Vortex induced vibration (VIV)*
- *Floater vortex induced motion (VIM)*
- *Floater vertical heave induced vibration (HVIV)*
- *Installation fatigue damage*
- *Slugging loads*
- *Transportation*
- *Start up and shut down*"

First order wave loading has a very significant effect on the reduction of flexible riser fatigue life. The transportation and installation loads should be carefully examined after construction. The failure tree of flexible pipe is demonstrated in figure 1.6. It is important to study the fatigue failure and the causes of the failures in order to prevent some of the defects shown in this figure.

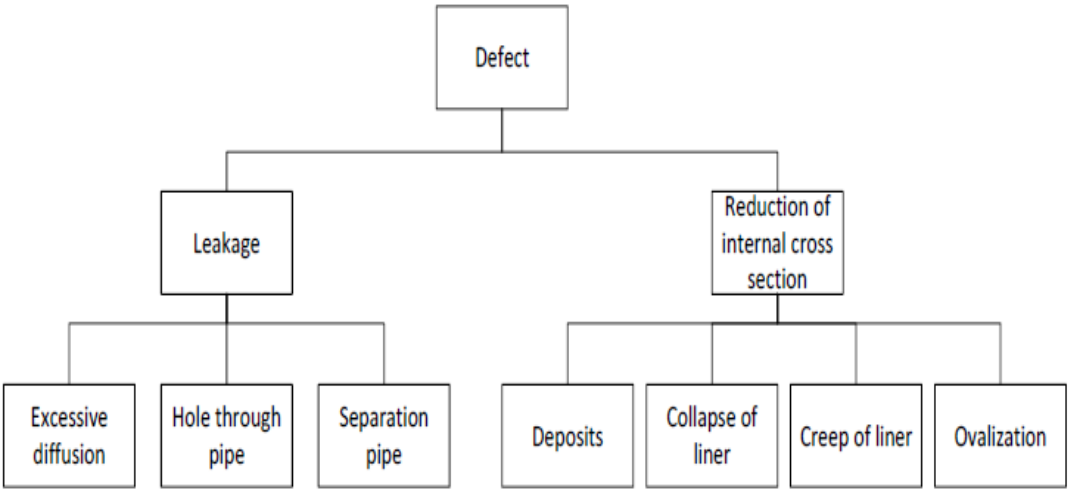

Figure 1.6 Failure tree of flexible pipe (Zhao, 2013)

1.5 Problem Statement

Even though the importance of using flexible risers for subsea technology in offshore oil and gas production is well known, the complex structural behaviour of flexible risers is not sufficiently understood for many design and development purposes. On the one hand flexible risers must be reliable enough to safeguard the environment. On the other hand, they must make the exploitation of the subsea hydrocarbons economically feasible. It is clear that due to ultra-deep water usage, the processes of repairing the risers are very expensive. The major incidents rate per riser operational year is shown in figure 1.7. The solid line shows the incident rate reported to Petroleum Safety Authority (PSA) Norway while the dotted curve shows the estimated total number of riser incidents, including unreported major issues. Despite the fact that many attempts have been made to develop highly reliable flexible risers, they are not meeting their recommended service life. This is because the basic technology is relatively new (compared to steel pipes), and has to be evolved to support more challenging application for deeper waters and harsher environment. The major reported failure in most of flexible risers is usually fatigue-failure in helical metal armoured layers, also called tendon, which is considered by the oil industry as a very significant problem.

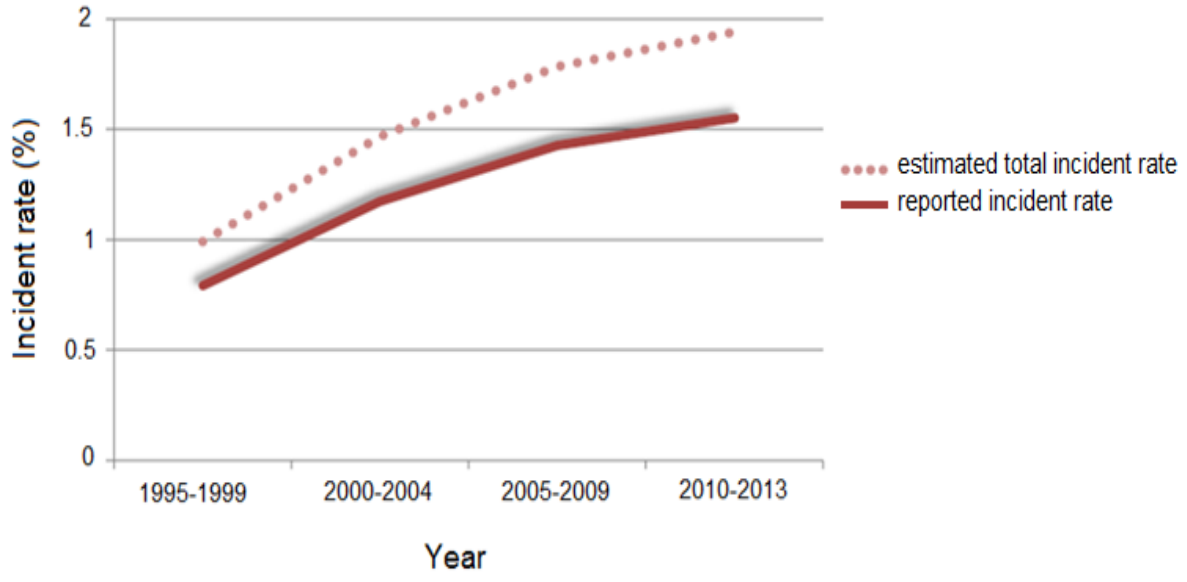

Figure 1.7 Major Incident rate per riser operational year reported to PSA, Norway (PSA, 2013)

Experimental tests on the tendon layers and flexible risers and detailed numerical methods are essential to understand the structural behaviour and failure mechanism of flexible risers.

1.6 Research Objectives

The objective of this study is the development of experimental and numerical models to analyse the structure of flexible risers. This will help us to understand the failure mechanism of flexible risers. In particular, the intention of this thesis is to use accurate numerical and experimental modelling to investigate the followings:

- Stress and strain analysis and creep behaviour of a single helical armour wire of tendon layer under various loads.
- The structural behaviour of a simplified prototype of a flexible pipe with four layers under bending moment and axial load.
- Capability of finite element methods for prediction of the structural behaviour of flexible risers.

1.7 Thesis Outline

The thesis is organized in five chapters to report the work carried out to achieve these objectives. A review of literature in the field of flexible risers is presented in **Chapter 2**. The major existing methods for analysing flexible risers are outlined in this chapter. The methods are also classified according to their accuracies. **Chapter 3** deals with the experiments on a model of flexible riser. The tensile testing on the helical tendon under various axial loads is described. Also the bending moment, axial extension and compression tests on the model are explained and the results are discussed. **Chapter 4** contains the finite elements methods for numerical modelling of a flexible riser. The geometry of the model, mesh generation, contacts modelling and solution methods are explained in this chapter. Also the numerical results are compared with the experimental data. **Chapter 5** draws conclusions about the work presented with a summary and suggestion for future work.

Chapter 2:

Literature Review

2.1 Overview

This chapter is concerned with literature relevant to the present research. The aim is to obtain an understanding of a variety of methods which have been used for analysing offshore flexible pipes with their assumptions, level of complexity and capabilities. For the objectives of this thesis it is convenient to classify them into three broad categories; analytical, computational, and experimental methods. In analytical methods, simple formulations developed for linear elastic models e.g. methods based on Euler-Bernoulli beam theory (Bauchau and Craig, 2009) are used for analysing flexible risers. In computational methods, flexible risers are analysed by a model-based simulation through numerical methods implemented on digital computers. Experimental methods subject a small scale of the riser to the ultimate test of observation under various loads and displacements.

2.2 Analytical Methods

A common approach in analysing flexible pipes is to assume them as composites or cross-sectional models. In this simple and straightforward approach, it is assumed that a pipe composed of many independent parts and response of a pipe can be predicted by summing the characteristic responses of the components. Indeed, in this method the global load-displacement relation is calculated from summarizing of individual layer roles; hence, interlaminar effects are neglected. Multi-layer method analyses each layer individually and considers their degree of freedoms separately. In some models a combination of FE and analytical methods are used. Some analytical studies have been compared by numerical models or experiments which will be demonstrated in this section.

Custódio and Vaz (2002) introduced an analytical model to load unbonded flexible pipes and umbilicals axi-symmetrically; the nonlinear behaviour which calculate the related interlaminar gaps and contact between wires is defined by this model. In order to model the equilibrium of

wires, Clebsch-Kirchhoff equations (Love, 1927) were used instead of Love's equations (Love, 1927); hence, the wires were assumed as bar and not beams.

In the work presented by Féret and Bournazel (1987), a multi-layer model was developed to predict response of bending and axis-symmetrical loading; the model consisted of variables for radial and thickness changes with respect to individual layers and used wire bar assumption. A finite element programme called EFLEX was used, assuming layers are always in contact. Several equations were presented for wire stress, contact pressure, radial changes and the length of pipe. Bending moment-curvature relationship was defined for three distinct regions:

- *Initial stiff section*, there is no significant bending as there is a frictional moment. The frictional moment magnitude has a linear relationship with the internal pressure.
- *Elastic section*, plastic sheaths stiffness is largely responsible for calculating the pipe bending stiffness. It is assumed that the bending stiffness is weakly dependent on the pressure.
- *High stiff section*, which is limited by contact radius on the lower curvature side.

In this final section, when helical wires contact each other, their lay angles have to be changed for further deformations. So, a blocking radius appears on the high curvature side and bending stiffness in this side is highly increased. This is because pressure armour layer covered a single self-interlocking wire, yet still adjacent hoops can move. At high curvature of the pipe, adjacent hoops will contact each other, which prevents further bending. Authors compared their work with results of a bending test, showing a similar pattern in bending behaviour.

Harte and McNamara (1993) proposed a method based on the changes of stiffness matrices for layers with deformation. They assumed helical armour as wire bar and global stiffness

matrix was made from assembly of individual layer stiffness matrices. As the global contact pressures were unknown, radial constrains which keep the layers in contact were assumed. The authors compared their study with results of a finite element model, modelled the structure as axi-symmetric and bonded. The verification of analytical method was introduced by the numerical results; for large deformation the prediction using the analytical method is not satisfactory as the nonlinear deformations are not taken into account.

Huang (1978) conducted research on an elastic strand finite deformation with a core surrounded by helical armours loaded by axial forces and torsional moments. The core was regarded as straight circular rod while tendons were considered as thin curved rods; both have circular cross-sections. The theory of the research was based on curved and slender rods. Nonlinear behaviour of changes in geometry caused by reduction in helical angle and cross section between core and wires were added to the analysis. Extension of the core, causes the helical wires to separate from each other, especially if the material of the core and surrounding armours are the same. For each helical angle caused by various axial forces, stress of core and armours and contact forces between them were analysed. Examples of finite extension of strands with both free ends and fixed ends were demonstrated. The examples had a central core with six helical armour wires. The strand could be either fixed or free end to twist. In latter strand, extension was coupled by untwist. As the wire extensional rigidity reduced by untwist, the total extensional rigidity of structure decreased and stress in core was increased. At rotation-free end analysis, untwist causes a considerable reduction of tensile strength.

Knapp (1979) derived a stiffness matrix for helical armoured wires under tensile and torsion. Strain expressions were developed for the wires under axial loading, twisting and bending, and radial contraction of the layers. The expression of wire strain under bending are obtained using equations of Love (1927) without derivation to explain bended wire response. Radial contraction was given form an analytical method which considered underlying layer

as a thick tube with elastic material; hence, the interlayer contact is not directly considered. Because of the geometrical restrictions of the method, the expressions are only valid for initially straight wire sections.

In the study presented by Kraincanic and Kebadze (2001), a model developed to predict wire slippage during bending. In this model, a gradual and non-linear transition area between small curvatures with high stiffness and large curvatures with low stiffness for moment-curvature relationship was predicted. This is because the helical wires start to slip at various points. Interlayer nonlinear behaviour between individual armours of tendon layer was studied; bending stiffness was defined as a function of "*bending curvature, coefficients of interlayer friction, and interlayer contact pressure*". By increasing the curvature of the pipe, wires slip at neutral axis. The curvature expressions which were defined as cause of slip in an individual wire was developed and assembly of the forces, caused the slip in individual wires, can predict the moment-curvature relationship at bending for flexible pipes. They hypothesized Coulomb friction model as their theoretical base and compared their nonlinear formulations of helical layers on unbonded flexible riser with experiments. The force at neutral axis of cross section was at its maximum value; hence, at neutral axis inter-layer slip started. As a proof practical observations reported the initial failure was near neutral axis. All in all, the results of this study were very similar to the experimental data.

Lanteigne (1985) worked on treatment of helically armoured cables, analysed Aluminium Conductor Steel Reinforced (ACSR) material by assuming the central core as rigid. For modelling components, wire bar assumption has used and linear expressions for wire strains at axial, twist, and bending have been developed. For bending analysis it was assumed that plane sections remain the same during the bending, then global stiffness matrix was calculated. The cables were considered as assembly of helical wound wires (multi-layers). For wire deformation, bent helix assumption was considered because of the higher fill-factor and high values of frictional forces which prevented wires to respond naturally (geodesic).

The author mentions that increasing or decreasing the axial force of structure would cause interlayer slip and proposed an expression for slip based on the radial load and a coefficient of friction. Lanteigne (1985) assumed that in a cable including multiple layers of wounded wires, when conductor is bent, the axial force carried out by outer layer is greater than the one carried out by other layers. If the slip occurs, the outer layer axial force would decrease to the value of first neighbourhood inner layer. Thus, he developed the expressions of radial force for each layer. The lay angle[1] changes of wires caused by deformation were neglected and it was assumed they have no effect on torsion. In this research, the influences of radial stress and tension of cable on frictional forces were studied and some prediction methods in terms of resisting against slip were obtained through considering axial forces of each layer individually.

Leroy et al. (2010) compared three models to predict stress of flexible pipe layers:

- *A developed single wire analytical model*, which was a development of previous research of Leroy and Estrier (2001); it was focusing on lateral contact between armour layers and their neighbourhood layers. Contact was defined via penalty method, wire frictions were neglected. Wire transverse curvature was affected by inter-wire contact.
- *The periodic FE model*, used to model a helical single layer and other layers around it were assumed to be rigid. The value of pitch divided by the numbers of wires was used as model length; boundary conditions at the end were modelled as periodic values.
- *The explicit FE model,* represented as a full pitch model in which all layers were considered. In this model, kinematic coupling method of one reference point to the nodes of end surface (constraint) was used.

Cross-validation between the models showed good agreement in axial stress in armour layer. In terms of outer layer, the predicted stresses using the explicit model were greater than the other two models. This was because the constraints of the explicit model do not

(1) Please refer to Edmans (2012).

have effects on helical wires as it was stabilized by higher frictional loads. A comparison of transverse curvature showed close agreement between the models. The comparisons of the 3D explicit model with experimental results showed good agreement in terms of stress.

McIver (1995) proposed a method for modelling the detailed component and overall structural behaviour of flexible pipe sections. In this method, the helical armour wires are assumed as beams with consideration of torsional stiffness, interlaminar friction, and separation. Love's equations were used for equilibrium and the kinematic analysis of the armour wires defines the accuracy of the model. Serret-Frenet equations taken from derivation of Serret-Frenet vectors were used to introduce a pair of axes for simple directions of wire section. Using tangent vector of the wire, undeformed axes were defined. The Serret-Frenet related curvature is calculated via two factors in the axes; hence, a set of equations was made for defining local basis vectors based on curve of undeformed configuration of helix. Then, variables of the displacement and rotation related to the deformation were defined through local basis vectors. Basis vector at this step was defined by initial vectors using a rotation matrix. Local curvature, local torsion, and axial strain expressions were calculated through the displacement vector of wire, vector of initial tangent, vector of current basis and their derivations due to parameter of the wire and were expanded by comparing to the vector of initial basis. Expressions for the curvature, torsion, and axial strain were written using the local displacement. The varied coefficients of friction were depended on the degree of wear related to the polymer layers.

In the work of Out and von Morgen (1997), armour wire deformation expressions demonstrated by considering geodesic theory (Edmans, 2012). Indeed, through comparison of bent helix and geodesic solutions, normal and bi-normal curvatures were determined. This study was focusing on slip and curvature of the helical wires as they are crucial in fatigue failure studies.

Tan et al. (2005) investigated the effects of geometry on tendons deflection when riser is bended uniformly faraway from any end fittings effects and there is no subsequent bending stress. It was possible to assume either geodesic or bent helix as deflected configuration for simplification. The bending stresses were estimated by measuring geometrical difference of deflected and original helical shape. The effects of cross section of armour, e.g. width and thickness ratio, were neglected. The authors presented a strain energy analytical model to obtain the effect of width-thickness ratio on final deflection. Higher order influences were considered to determine the deflection via exact mathematics, wire deformations, and stress analyses. In addition, combined deformations of pipe in axial-bending directions were discussed. The analysis were compared and validated by finite elements model in terms of deflection and normal, bi-normal, and total bending stresses.

Velinsky et al. (1984) improved a theory for predicting armours with complex cross-section in terms of static responds. Equilibrium nonlinear solutions were linearized; results were used on a 6x19 scale rope which had independent core (wire rope). At rotation-prevented case, the maximum value of tensile stress occurred in the core. The actual stress depended on both axial load and the axial-twisting moment in crude sense. In theory, the effective modulus of structure decreased by adding strands. A Seale rope in terms of load-deformation curve tested and compared with theory. If there was no rotation, tensile stress of Seale rope would be at its maximum value. At bending over a sheave, this value was depended on curvature of the sheave; possibly shifted to the centre wire in one of the outer strands because of the bigger diameter of the outer strand centre wire. Effective modulus was lower in practice because contact deformation was neglected. In addition, the theoretical assumption that "*plane sections in a rope remain plane*" was neglected when the rope ends were held in zinc sockets; they decrease while the rope length increased. In practice, when there is no rotation, the maximum tensile stress will be at centre wire of IWRC (Independent wire rope core); if this value exceeded the material elastic limit, and if there was nearly no external load, the centre wire stresses would be compressive.

Witz and Tan (1992) studied bending behaviours of flexible pipe based on the beam model for wires. Parameters such as axial strain, curvature local changes, and torsion, were defined through analytical assumption of pipe deformation as a whole. Stress/strain changes at wire cross section neglected. The Love's equations were simplified for the study of helical elements by assuming external forces (or moments) were acting on the wires and their resultants along the tape were constant. The distributed force was towards the axis of the pipe. The geometric properties of the wire were constants because of the constitutive relation of curvature and stress resultants. Wire local bending and torsion might be limited via the friction of surrounding parts. The mechanism and the start of axial/twisting slip of the wires inside the pipes were explained.

Witz and Tan (1995) extended the method for predicting stress/strain for the helical tendon wire under bended condition. The analytical model used in this study, used bent helix assumption for the wires configurations and deformed configuration calculated via a linear expression. They showed that when the ends of the flexible pipe were constrained, slip was mostly in the lateral direction and axial strain of slipped wires is non-zero.

2.3 Numerical Models

Major established industries in the field of flexible risers, rely on computational mechanic software to analyse and design flexible pipes. The software can be classified based on the discretization methods used to discretize the continuum mathematical model in the space. Few software use Finite Difference Method (FDM), Finite Volume Method (FVM) or Boundary Element Method (BEM) to discretize the model in the space. The Finite Element Method (FEM), however, is the dominate method and the most powerful numerical method ever devised for the analysis of engineering problems. It is capable of handling geometrically complicated domains, a variety of boundary conditions, nonlinearities, and coupled phenomena that are common in flexible risers. Several FE methods used for analysing flexible pipes are presented in this section.

Bahtui et al. (2009) proposed "*a new constitutive model for flexible risers*" using multi-scale approach. This method which is one of the earliest multi-scale approach used for flexible risers is based on the elasto-plastic constitute model. The model is based on analogy friction slip of riser layers with micro planes of a continuum medium in non-associative elasto-plasticity. In the model an initial linear elastic relation for the initial response is considered followed by non-associative rule with linear kinematic hardening for full slip phase. By modelling the small scale using a non-linear Finite Element (FE) programme, ABAQUS, the behaviour of full scale pipe was estimated.

Felippa and Chung (1981) presented formulations for non-linear beam model geometry. Element displacements and strains were defined as coordinate systems which were convected and changes with their related elements. For formulation of axial strain in bending a component was extensionally considered. Simple expressions presented for loading, external pressure, and fluid flow inside the pipe. The software package used for dynamic analysis is called "Orcaflex".

Larsen (1992) obtained results of mechanical loading on offshore flexible risers done by an in-house FE software. The aim of his research was to:

- Measure numerical modelling error of the FE software for flexible risers,
- Define a benchmark for developers and users of numerical software.

Major results of Larson's paper were:

- The numerical modelling of static analysis was relatively accurate compare with the experimental data.
- Compare to static tensile analysis, the dynamic analysis however show a bigger difference (10 to 15 per cent). The uncertainty observed mostly at hydrodynamic loading and structural damping.

- The work was able to be develop a “benchmark” for verifying other methodologies

Le Corre and Probyn (2009) used ABAQUS to model a single core umbilical with three concentric cylindrical sheaths, assumed to be shells. Between sheaths, helical wounded tubes, cables and fillers were assumed, which were modelled as circular beams. Explicit solver used for the simulation via general contact algorithm taken from tests data. In the general contact algorithm an effective cylindrical surface for the contact in beams axis are assumed. The beam cross section was assumed circular to compute the contact interactions.

Rial et al. (2013) worked on the fatigue analysis of some hydro-formed metal tubes with constant amplitude load as well as a constant internal pressure, causes three dimensional stress-strain relations. They showed that the life cycle decreases when there was lateral distance between axes; in other word, in straight tubes the life cycle is maximum. In addition, practically cracks were started at welding line. The structure life number of cycles at the crack initiation for variable loads extracted. Then, a FE model was made to calculate residual stresses of hydro-forming process. The results of the numerical simulation in the following several approaches were compared with experiments:

- A stress-strain life method (widely used),
- A critical plane method,
- An energy method,
- A continuum damage based method.

It was shown by the FE model that residual stresses of forming process had crucial influence on the mechanical behaviour of risers. Finally, it was demonstrated that the critical plane and continuum damage based are much easier to predict, in terms of fatigue life, when residual stresses were included.

Risa (2011) worked on the FE analysis of an umbilical using ABAQUS software. Two helical conductors with circular cross-sections were assumed to be wrapped around a cylinder. General contact algorithm was considered for contact, explicit dynamic were used for the analysis. Kinematic constrains were helpful to model boundary conditions at the end sections. Repeated hot points were observed by contact along the length of conductor, even though both geometry and loads were uniform in that direction.

Sævik (1993) developed a curved beam with eight degrees of freedom (DOF) to analyse stress and slip in armouring wires of flexible pipe. Tendon layer was slipped between its surrounding layers and thus structure degree of freedom was minimized. In order to explain each armour reference system and loading, differential geometry was used and large transformations were prevented. Numerical models were compared with a test specimen and the results were verified. The analysis was done base on the Lagrange method (ANSYS Inc., 2012) of large displacements and rotations. Hence, a large group of transformations was neglected and instead, pipe/armour layer was solved via an assembly of hyperelastic and elastoplastic springs at nodes. Then, the Newton-Raphson method with load increments solved the equations.

Sævik (2010) compared stresses of bending FE models with related experiments for flexible pipe. He used two different models:

- *First model*, a cross section stress resultant method was used; the model was moment based. Three possible areas of slip were considered for individual tensile armour, relying on local frication positions for various components. Delimiting conditions were formulated based on the local curvature and resulted to a constant value of the critical curvature which was defined as a function of number, material properties, coefficient of friction, and cross-section of the wires. The moment of each layer was then defined; as the geometry and material varies, frictional moment was calculated from summing its individual values at the layers. Then constitutive relation of moment resultants and slip of the wire were

calculated in layers. Plasticity was developed through applying two moments to demonstrated stresses, and frictional moment to show slip-yield surface, and the slip curvatures as made strains.

- *Second model*, was a sandwich beam formulation. It used multi-layer modelling and all components were modelled independently; in terms of constant valued contact, structure was modelled as a composite beam. Bent helix assumption was used in this model. Each helical armour potential energy was assumed to be summed from the strain and the purely elastic slip energies along the helix path. The stick-slip response of the wire was possible through a spring with weak penalty and constant stiffness.

Good agreement between the FE models and experiment in terms of the curvatures were obtained.

Sævik (2011) presented a finite element model to predict axisymmetric effected stresses as well as two equations to predict bending stresses in tendon layers in non-bonded flexible risers. Then the experiments were carried out via fibre-optic Braggs to compare with the equations of bending stresses and fatigue. By applying differential geometry the local bending in wounded armour layers were formulated while shear analysis of frictional interlayer behaviour were calculated in two ways:

a) Considering the cross section output of frictional moment (MM),
b) Applying a similar beam formulation for each tendon (SBM).

The Same axisymmetric model was used to analyse the boundary conditions with regards to initial contact pressure in both formulations. In terms of computational efficiency, the first method was ten times faster because more computational effort required for building stiffness matrix in the second method.

Tan et al. (2007) used FE models for studying the bending hysteresis time-dependent in flexible risers. Two models were analysed, the software of both were developed as subroutines for Orcaflex:

- *First model*, the software extension used in this section was introduced by the manufacturer of Orcaflex; three dimensional increments for bending moment of the springs were available for curvature increments (which were given). Hence, the researchers were able to work on the moment-curvature of single-plane bending as it was common because of much higher cost of combined bending analysis. Using the single-plane bending moment-curvature relationship as input data, the model introduced acceptable scalar stiffnesses, which were multiplied to 3D increments of curvature for the related pipe and bending moment increments were obtained. Curvature and bending then were calculated through sum of curvature increments, introducing smaller increase for moment. In this model, hysteresis behaviour was able to be simulated as the process of increasing and decreasing curvature was similar.
- *Second model*, in this model the extent of the slip region in a pipe element using the current curvature data and internal history variables recording the element's previous curvature and slip states were calculated. Using these results, the section moments was calculated and returned to the main model. Finally, stresses in tendon wires are calculated in a subsequent formulation.

Vaz and Rizzo (2011) calculated the displacement inside metallic/polymer layers of flexible pipes which had a high axial stiffness at tension and low axial stiffness at compression. Typically, under condition of installing or production processes in deep waters, flexible risers can be compressed or bended; if the design is not reliable enough, the possibility of failure of structure is high. A non-linear FE model was developed in terms of instability of unbonded flexible pipe tendon layers under axial compression load and modes of failure. The model was an axisymmetric using assembly of beam and spring components. For each helical armour layer one wire were required to be modelled to optimise computational cost. A typical

flexible riser with variable armours' coefficient of friction and variable external pressure was studied. It was shown that the most critical situation was when annular was flooded because of reduction of COF and lack of support of hydrostatic pressure on helical wires. There were four instability modes; two were in lateral direction and other two in radial directions. It was shown that:

- At bird-caging condition, the inner layers[1] are neutral. The failure is mostly inelastic with dry annular condition; when wetted, the instability might be elastic.
- The anti-bird caging tape was not harmed in lateral modes, armour wires might stabilize independently for low friction force and vice versa for high values.
- The radial modes might depend on the failure of anti-bird caging tape and elastic buckling of foundation.
- In both conditions couple lateral displacement observed in wires.

Østergaard et al. (2012a) studied lateral wire buckling of helical tendons inside flexible pipes. The armour layers defined as two layers of helically steel wires with opposite directions. In ultra-deep conditions, flexible pipe is bended repeatedly and compressed longitudinally; if the compression load exceeds the armour layers load carrying ability, the structure may fail. A helical armour was modelled as a long and thin curved beam surrounded by a frictionless cylinder sheath. Both small geometrical beams and perfect beams were studied. The equations were based on curved beam equilibrium and therefore large deflections were possible. The equilibrium of a single helical wire inside the flexible riser was determined based on the model. The tests with same conditions were examined. Nonlinear Softening (Prasad, 2009) was obtained in the calculated force-displacement diagrams. The most crucial parameter of solution was the pitch of helical armour. It was shown that when the pitch is increased, softening happens at much lower load value.

(1) interlocked carcass, pressure amour and plastic sheath

Østergaard et al. (2012b) introduced a model for analysing lateral buckling failure inside helical tendon layers. Flexible pipes normally buckle laterally under repeating of bending loads or longitudinal compression, mainly when pipe is left in deep waters. The mechanical behaviour of both armour layers was determined using the multiple single-wire analyses. Since failure in one armour layer induces torsion to the structure of pipe, lateral buckling is mostly observed with twisted riser. Two models of buckling, with and without twisting, were modelled. The limit compressive load can be obtained with deformation modes, with the assumption of flooding the interior of riser, and compared with experiments. The observation verified sensitivity of armours to initial defects, caused the inner layer gaps of helical wires to deform at lateral buckling. The maximum value of compressive load can be estimated from the discussed method for both twisting and not twisting conditions.

2.4 Experiments

Very few reported experimental studies regarding flexible risers are available. In this section, some test data from previous studies are described.

Beden et al. (2009) worked on the fatigue life modes and the prediction of the fatigue life modes with constant and variable load amplitude. Different models confirmed the fact that there was no standard methodology for crack propagation. They concluded that:

- From constant amplitude crack growth data and methods of estimating load interaction influences, a logical prediction of specimens failure for random loads can be achieved,
- An optimization between computation cost and accuracy of prediction was essential in model selection,
- Accurate prediction was relied on low value of crack growth rate data.

Clarke et al. (2011) argued that although flexible risers are recently desirable to be used instead of rigid types in offshore oil-exploration industry, they are not easily inspected

through Non Destructive Testing (NDT). Finding a single technique to detect armour failure reliably was desired, however, the recent researchers verified that to take advantage from a combination of different instruments is safer. They worked on a full-scale dynamic loading on a 6 metres long specimen with end fittings equipped with some sensors. Torsional angle, axial displacement, and Acoustic emission were compared. A detection pattern was resulted when there was rupture of outer tendon layer. Although acoustic emission is a desired NDT method because of its non-instructiveness, due to sensitivity to noise, it has some errors; hence, its in-field responds were omitted. To increase the accuracy, the combination of the method with other methods was recommended. The position of sensors has a vital role in accuracy of this method.

MacFarlane (1989) highlighted an experimented viewpoint about problems associated with the behaviour of flexible pipes with solutions. The main problem of the research was pipe terminations of performances, materials and assembly of layers. By explaining safety, testing, and inspection processes, major unknowns were defined as material performance under service conditions, compression and finally, erosion/corrosion in long period. He showed that:

- The connection of the pipes to platforms or sea floors was the most important problem for the designers; the unknowns were defined as the "*the performance of the polymer materials*" under servicing circumstances, corrosion/erosion effects, and performance of risers at compression.
- Safety in design was crucial when termination failure occurs,
- Flexible risers were classified through umbilicals and tethers,

Numerical modelling for analysing mechanical, thermal, electrical, and chemical properties of flexible risers were recommended.

2.5 Conclusion

There are three broad methods for analysing flexible risers; analytical, computational and experimental methods. The analytical method is the simplest and most straightforward method. However, the mathematical model, in most practical cases, does not admit analytical solution due to the geometric complexity and nonlinearities arise from changing geometry, contacts between layers, or material behaviour. In most cases, in particular for small scale modelling of flexible risers, it is necessary to use non-linear finite element methods to compute an approximate solution to the mathematical model. However, it is essential to determine the degree to which the finite element represents the physical reality of the riser model by conducting an experiment. Although validating numerical results using experimental data is a must, very few experimental data regarding structural analysis of flexible risers are available. In the next chapter an experimental study is described.

Chapter 3:

Experiments

3.1 Introduction

In this study, three experiments on a scaled down model of a flexible pipe were conducted. First and foremost, a single helical armour wire of tendon layer was tested under variable axial loads. In addition, the behaviour of this layer in creep circumstances for three various loads has been reported. Second, a prototype of flexible pipe was tested by applying variable bending loads to check the nonlinear behaviour of the specimen in the bending moment-curvature relationship. The prototype consists of two helical armour layers as carcass and helical tendon layers, and two tubes as outer sheath and anti-wear layers. Finally, the behaviour of the prototype under axial load was studied. Also, the effect of internal pressure, when no external load was applied, has been tested. Moreover, the effects of internal pressure on the response of the specimen to the external load have been studied. The methods of experiments and results are described in this chapter.

3.2 Prototype Components[1]

Obviously, because of the size, it is not practical to conduct experiments on a large scale flexible riser in regular labs. So, a small scaled prototype ($\frac{1}{10}$) with only four layers was developed to conduct the experiments. The following four layers were used:

(1) Outer Tube: designed similar to outer sheath layer in real flexible risers, covered all other layers of the prototype (see figure 3.1).

(2) Single Helical Armour (or Tendon): was covered by outer sheath and surrounded the inner cylinder (red helix in figures 3.1 to 3.4).

(1) For more information about size, shapes, and blueprints of each component please refer to appendix B.

(3) Inner Tube: it was designed more accurately in order to seal the pressurized oil inside it; this layer was placed inside tendon and covered carcass (figure 3.1).

(4) Helical Carcass: had more pitches comparing to the tendon layer and it was placed inside the inner tube (yellow helix in figures 3.1 to 3.3).

A schematic view of total assembly of these layers is demonstrated in figure 3.1; for further details of prototype dimensions and materials please see tables 3.1 and 3.2.

Table 3.1 Prototype Dimensions

Layer No.	Layer Name	R_i (mm)	R_o (mm)	R_m (mm)	t (mm)	Rev.	Length (mm)
1	Carcass	44	47	45.5	3	15	651
2	Inner Tube	47	50	49.5	3	-	667.8
3	Tendon	50	55	52.5	5	6	651
4	Outer Tube	55	60	57.5	5	-	681

R_i: inner radius, R_o: outer radius, R_m: mean radius,

t: thickness, Rev.: No. of Revolutions (pitches)

Table 3.2 Material data for each layer

Layer No.	Layer Name	Material Name	E (N/mm^2)	ν	σ_y (N/mm^2)	ρ (kg/m^3)
1	Carcass	Steel AISI1018	2E+5	0.3	740	7860
2	Inner Tube	Polycarbonate	2E+3	0.37	65	1500
3	Tendon	Steel AISI1018	2E+5	0.3	740	7860
4	Outer Tube	Polycarbonate	2E+3	0.37	65	1500

Several more components have been designed in order to keep the layers in right place, to seal the prototype when necessary, or to apply the external load; these additional components have listed below:

(5) End-Caps: were designed to keep the layers of test specimen in desired position, to help other components seal the fluid inside inner-tube, and to help applying load; they were installed at each end of the specimen. The left end-cap for bending test in figure 3.2 was removed to show inside the prototype.

(6) Threaded Rod: was designed to help the end-caps keep the test layers in place. It was adjusted by two nuts at its both ends which are sealed by washers and grease (light blue rod in figure 3.2).

(7) Load Part: was designed to apply the external load. It was installed at the middle of outer sheath for the bending experiment (shown in figure 3.2). It was also installed at the top of the specimen for axial loading tests (see figure 3.3).

(8) Bending bed: was designed and made for the bending test; both bending end-caps were installed on the bed which was installed on loading machine at bottom (magenta in figure 3.2).

(9) Additional Cylinders: these extra components were made for tests on tendon layer (see figure 3.4).

Both end-caps in axial and bending loading test contain notches to add pressured oil or let the air exit. At each end-cap two (totally four) O-rings were placed to seal pressure oil, one pair between end-caps and inner tube and the other between end-caps and the threaded rod. Hence, the size of inner tube was reduced for housing the O-rings.

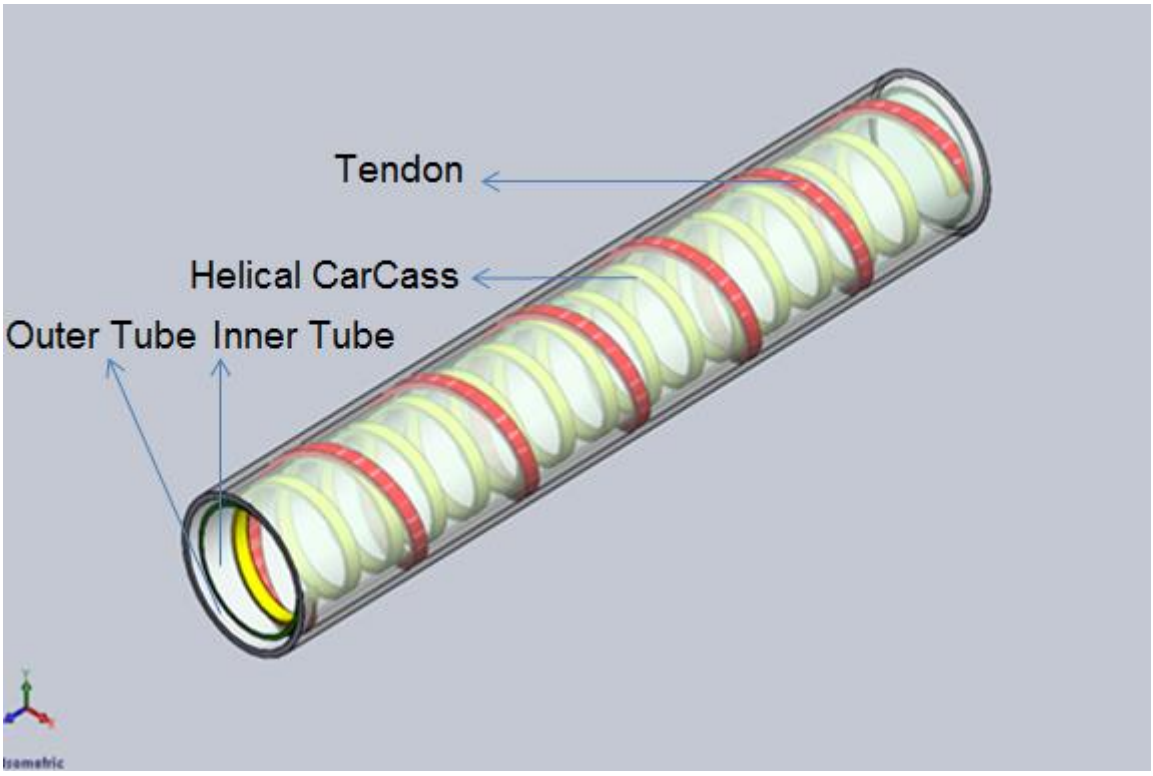

Figure 3.1 Schematic assembly of prototype layers 3D view

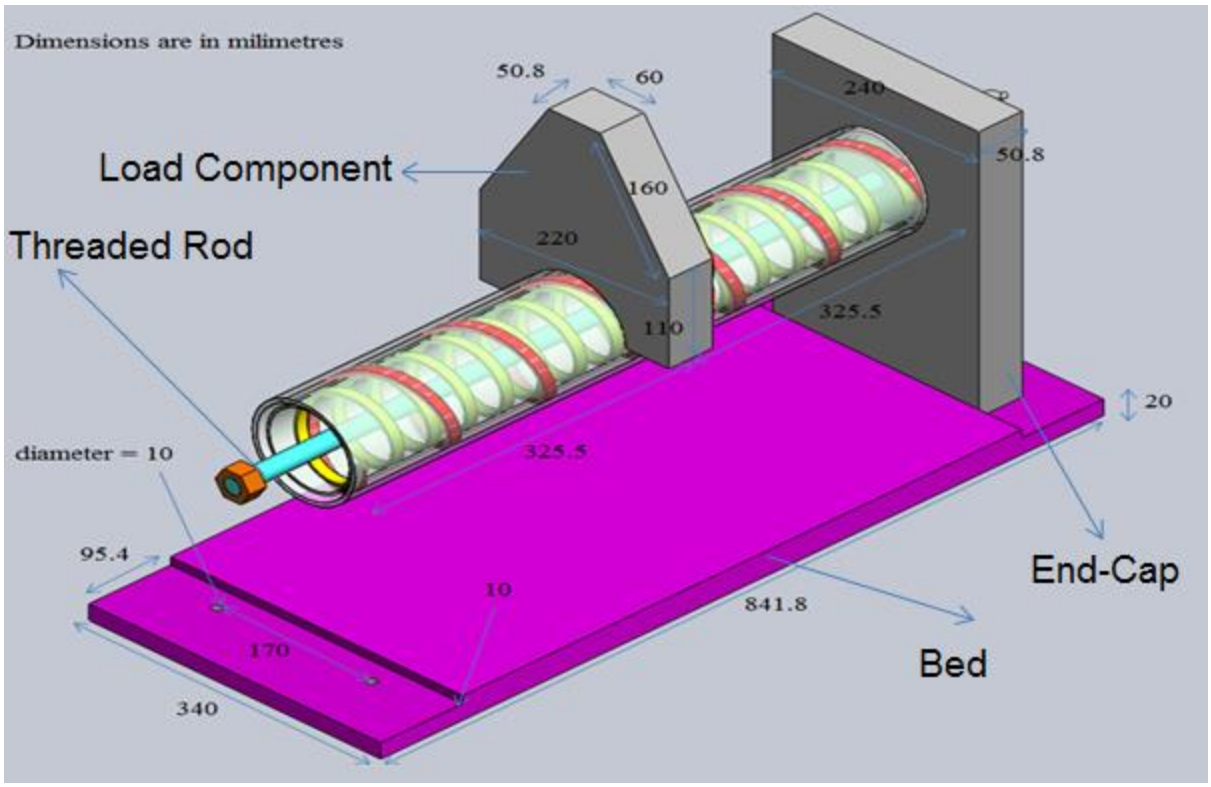

Figure 3.2 Schematic assembly of bending test 3D view

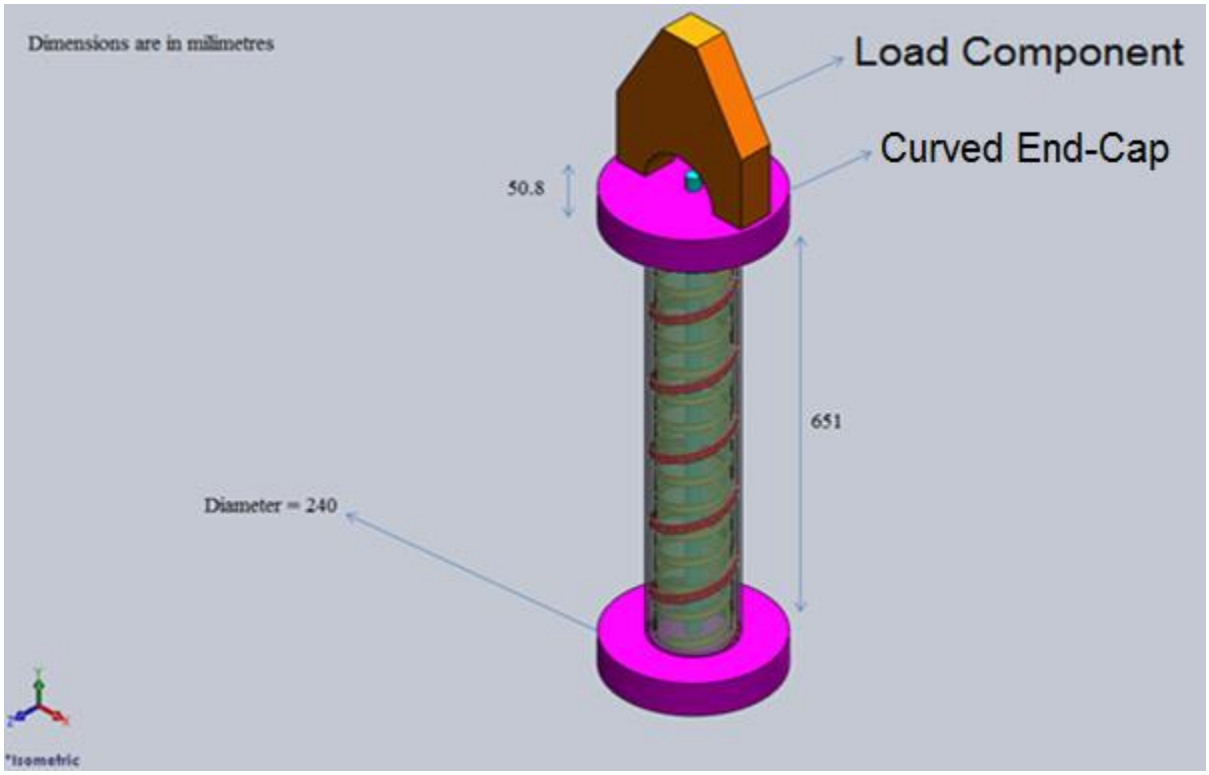

Figure 3.3 Schematic assembly of axial test 3D view

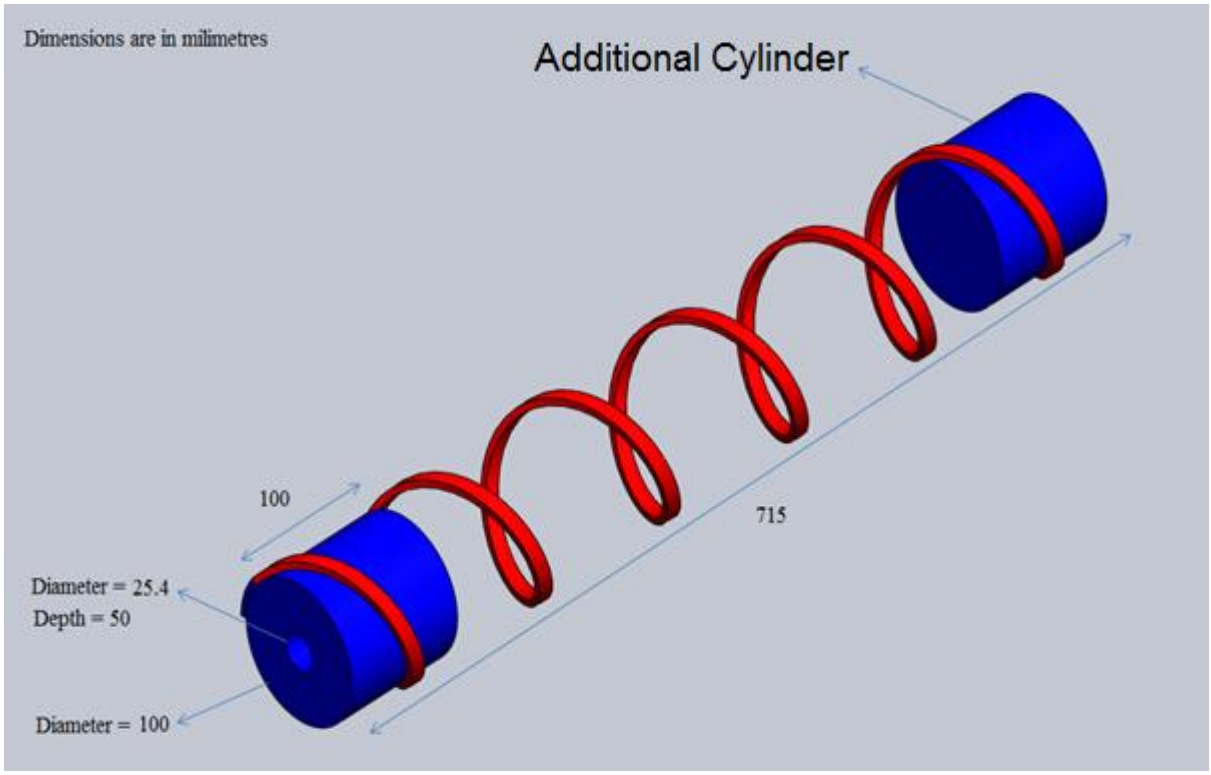

Figure 3.4 Single Tendon assembly for dead loading test 3D view

3.3 Strain gauges

A device for measuring strain on various materials is called *strain gauge*, introduced first time by Edward E. Simmons and Arthur C. Ruge in 1938. The simplest and common design includes an insulating backing which is flexible and supports a main part: metallic foil platform.

Strain gauges must attach to desired objects by any suitable cohesive material, thus changing in object size under tensile, or compressive, loads will change the size of foil and the electrical resistance will change. There are many ways to measure this resistance, usually using *Wheatstone bridge* via a value called *gauge factor*; in all tests in this chapter *Quarter Bridge* was used.

Gauge Factor, also called GF, can be calculated from:

$$GF = \frac{\frac{\Delta R}{R_G}}{\epsilon} \tag{3.1}$$

In which ΔR is strain made resistance changes, which is made by length changes of strain gauge after loaded or unloaded, R_G is the initial resistance of gauge, and ϵ is strain. For most of metallic foils, the GF is between 2.05 to 2.2; for all strain gauges used in this thesis, gauge factor considered as 2.12, which was previously measured.

In bending tests five strain gauges used with approximately the same position. For axial loading this number increased to seven: four on one side of the specimen and three on other side. The same number of gauges used with different arrangement for the dead-loading (figure 3.5). All of the strain gauges were calibrated before each test.

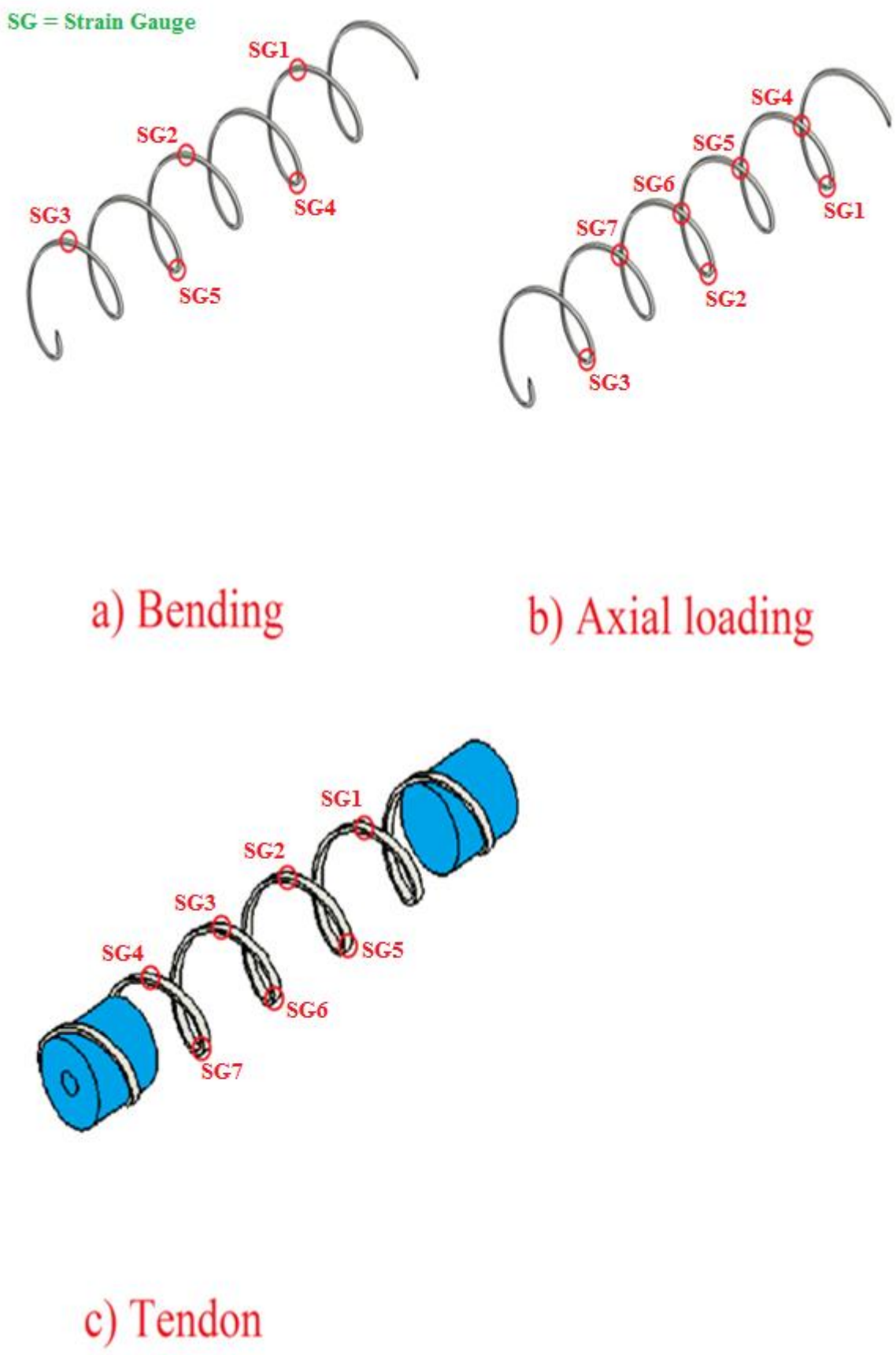

Figure 3.5 Schematic views of Strain gauges positions

3.4 Scorpio

Scorpio is a computer program that reads and plots the information of strain gauges. The Scorpio software includes five applications shown in figure 3.6. They are:

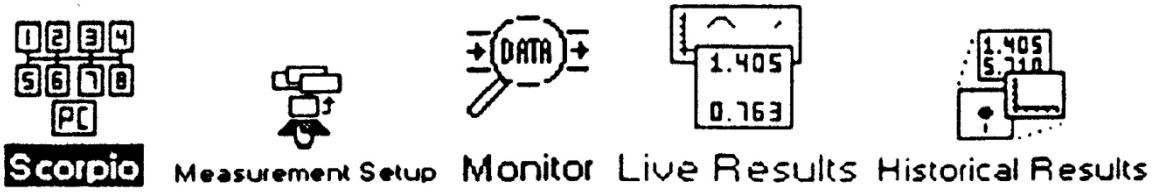

Figure 3.6 Scorpio applications and their icons (Solartron Instruments Ltd., 1993)

a) **Scorpio System Configuration:** It was shown by the first icon on the left in figure 3.6. The main application that prepares the PC system for starting the other four applications.

b) **Measurement Setup:** Using three methods, this application is responsible for preparing the data logger for measuring data; the methods are:
   - *File*: the logger commands are sent through a disk-based file; this file can be prepared via either Learn feature or editing text feature.
   - *Interactive*: in the data logger a command line is saved for further control or plotting.
   - *Panel*: data logger front panel is simulated.

c) **Monitor:** This application for displaying raw data from connected logger(s). The data is divided to three types:
   - *Channels*: They are separated measurements of the tasks.
   - *Task*: A single test results taken from the data logger are assembled in the task.
   - *Headers*: Are the “Task-headers” gathered from all tasks of the data logger and plotted on the screen.

   Measurement setup application controls the Monitor results through its local on/off options.

d) Live Results: It is used to show, plot, save and export the live results data when it was necessary; the data might be demonstrated as:

- *Text*, for the task.
- *Trend graphs*, for the channels.

Transient data through two options might be saved:

- *Interactive*: The data is plotted in a chart and components can be saved in the disk.
- *Standalone*: The data is taken continuously and saved directly to the disk but no plot is provided.

e) Historical Results: The already saved-to-disk data can be record and playback with this application through either the PC or the data logger. From this application data can be transferred to Microsoft Excel, which is more reliable.

3.5 INSTRON 8801 Loading Machine

INSTRON 8801 is a loading machine designed for fatigue testing systems. The maximum load capacity of the machine is 100kN, which is bigger than the maximum loads required for the experiments. It is possible to apply any static or dynamic tests via this instrument including high/low cyclic loading, thermal fatigue experiments and mechanics of fracture. A picture of this instrument is shown in figure 3.7 (Illinois Tool Works Inc., 2012).

The machine has an operator panel facility which proves users immediate feedback on setting of any test (figure 3.8). So, it is possible to instantly check the operating modes; position, real time load, number of cycles, strain status, wearing, errors. No PC is required when panel is available. (Illinois Tool Works Inc., 2008).

Figure 3.7 INSTRON 8801 (Illinois Tool Works Inc., 2012)

Figure 3.8 Series 8800 Operating Panel (Illinois Tool Works Inc., 2008)

3.6 Tests on Helical Tendon

3.6.1 Tensile Dead Loading

One of the major concerns in flexible risers is fatigue failures observed in helical wires. The aim of this test is to measure the effects of static loads on the deformation and strain changes of single helical tendon layer before the reliability of tendon reached the creep-curved conditions.

In figure 3.9, a single tendon specimen with two metallic cylinders at both ends is shown. The process of loading is called *dead loading*, in which the specimen is tested under static tensile loads; using a hanger, various weights are added to apply a specific value of load on the specimen. A hanger with the mass of 1.75 kg was used. The initial length of the specimen without hangers was 630mm; the length with the hanger was 715mm, which was assumed as initial length in the analysis. The maximum possible value for loading was 2kg.

It is shown in figures 3.10 and 3.11 how the test components assembled, placed and tested. The results of dead loading experiments were used to validate the accuracy of the numerical models in the next chapter. Here, only two samples (one for displacement and one for strain changes) of these results have shown in figures 3.12 and 3.13.

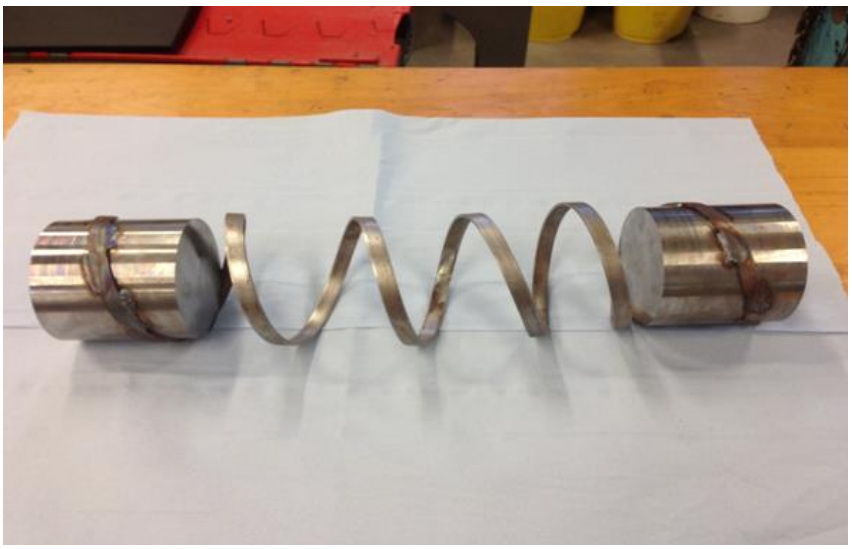

Figure 3.9 Tendon with two cylinders

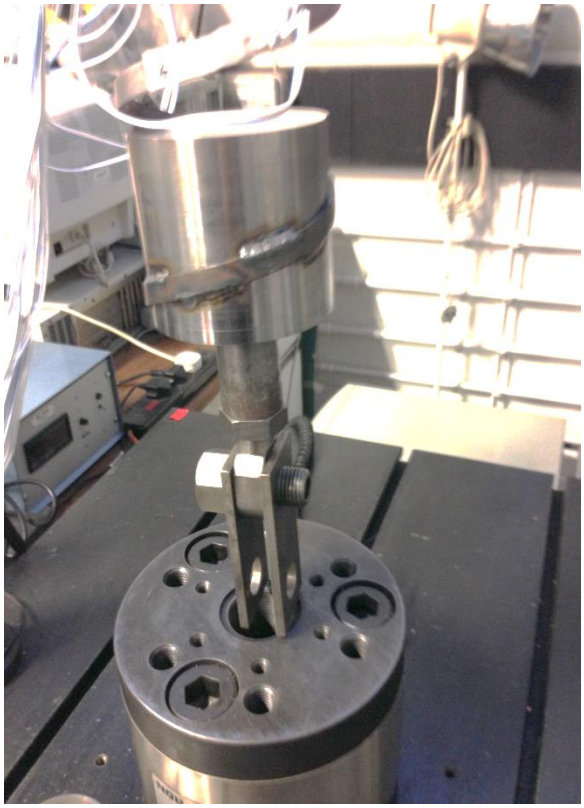

Figure 3.10 Hanger components

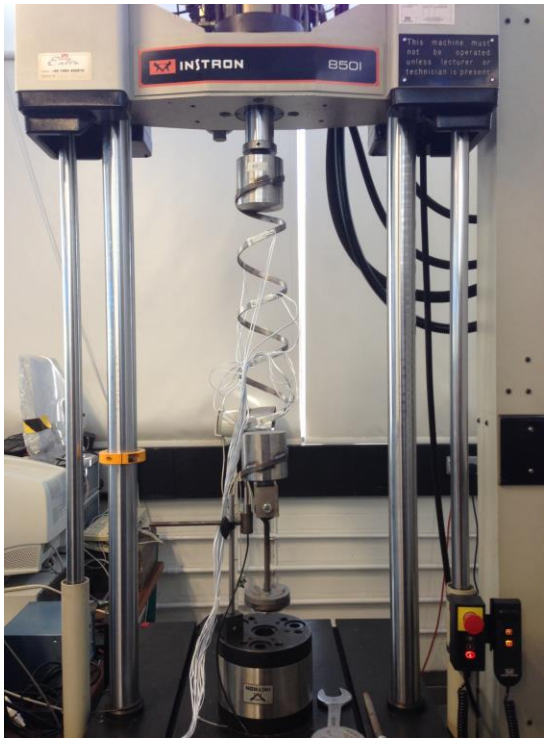

Figure 3.11 Tendon - Testing

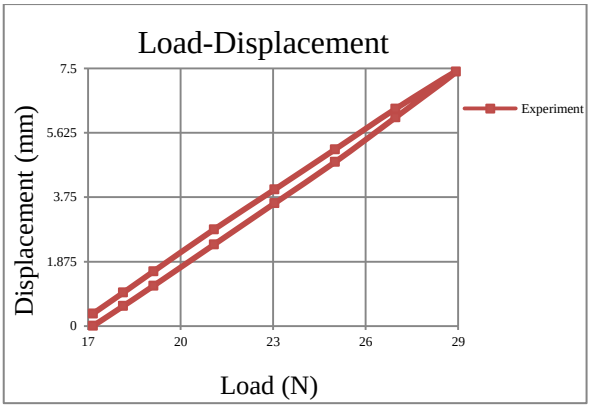

Figure 3.12 Displacement-Load curves

[Single Tendon-Static dead loading]

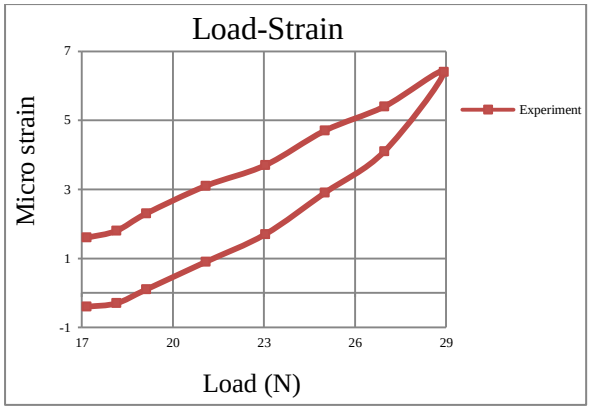

Figure 3.13 Tensile Strain-Load curves at SG1[1]

[Single Tendon-Static dead loading]

3.6.2 Creep Circumstances

During the experiments it was observed that for loads equal or higher than 1.4 kg creep-circumstances appears; in this value, it took a longer time for spring to be balanced and results were reliable to read (twenty minutes for 1.4 kg). The results of this section have split to three groups of figures depend on the weight (load) values:

- **1.4kg**, its displacement-time relationship is shown in figure 3.14 and its strain-time results are plotted in figures 3.15 to 3.21,
- **1.6kg**, its displacement-time relationship is shown in figure 3.22 and its strain-time results are plotted in figures 3.23 to 3.29,
- **1.8kg**, its displacement-time relationship is shown in figure 3.30 and its strain-time results are plotted in figures 3.31 to 3.37.

In order to do some fatigue tests on flexible risers and knowing that the possibility of fatigue failure in the helical wires are much more, cyclic loading on helical layer was desired. The loading machines have the ability to apply loads or displacements for cyclic loading. The results of the tests show that by *adding weight (applying load)*, the reliable time is increased. For the load of 1.4kg the reliable time is just 20 minutes whereas for the load of 1.6kg, it was 45 minutes, and for the load of 1.8kg, it was increased to 80 minutes.

(1) In all sections of this thesis SG means strain gauge

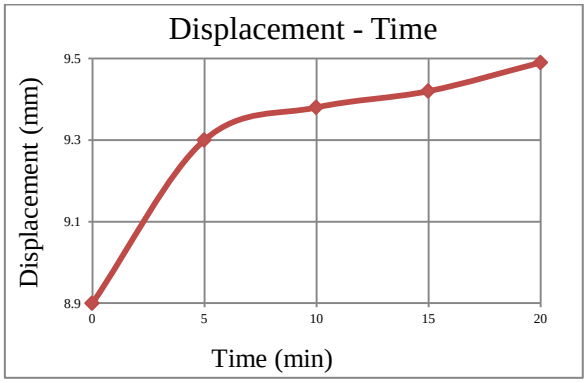

Figure 3.14 Displacement-Time curve

[Single Tendon-Creep Curve-1.4 kg]

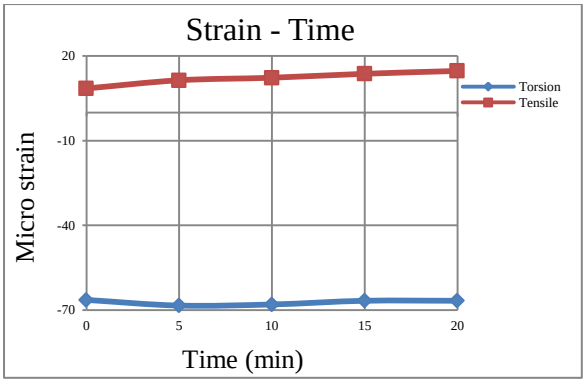

Figure 3.15 Strain-Time curve at SG 1

[Single Tendon-Creep Curve-1.4 kg]

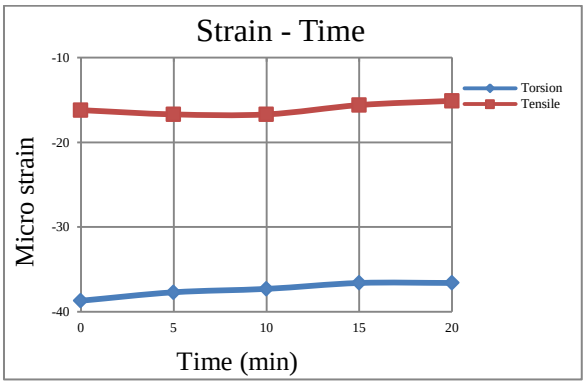

Figure 3.16 Strain-Time curve at SG 2

[Single Tendon-Creep Curve-1.4 kg]

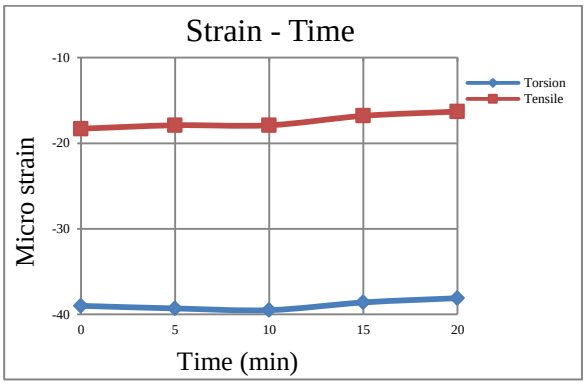

Figure 3.17 Strain-Time curve at SG 3

[Single Tendon-Creep Curve-1.4 kg]

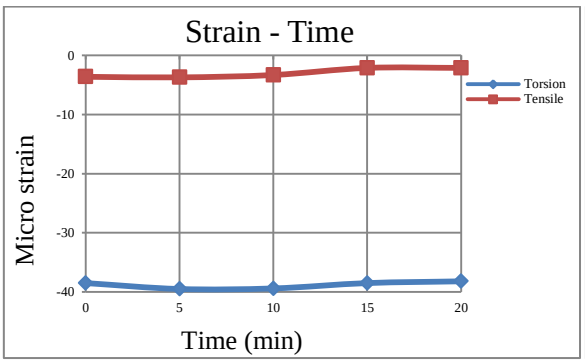

Figure 3.18 Strain-Time curve at SG 4

[Single Tendon-Creep Curve-1.4 kg]

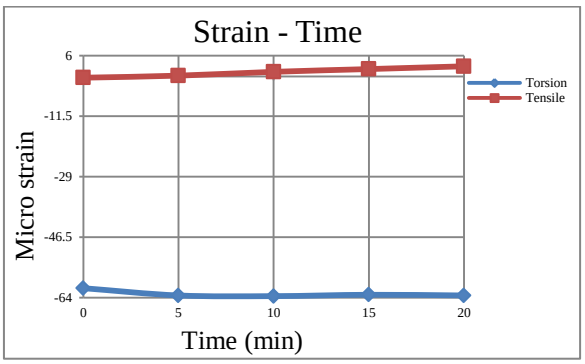

Figure 3.19 Strain-Time curve at SG 5

[Single Tendon-Creep Curve-1.4 kg]

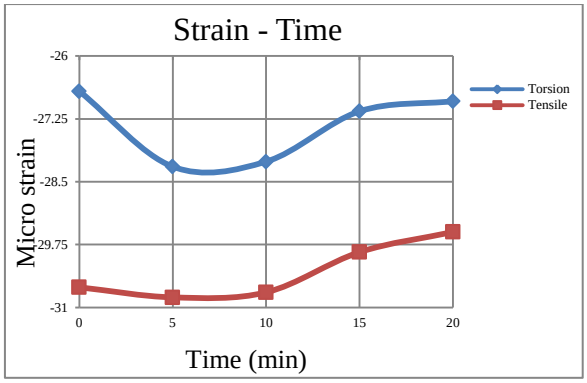

Figure 3.20 Strain-Time curve at SG 6

[Single Tendon-Creep Curve-1.4 kg]

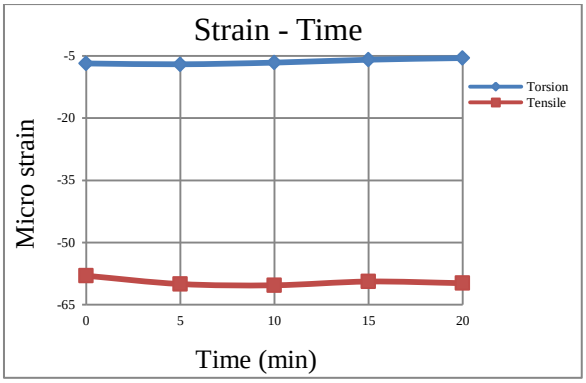

Figure 3.21 Strain-Time curve at SG 7

[Single Tendon-Creep Curve-1.4 kg]

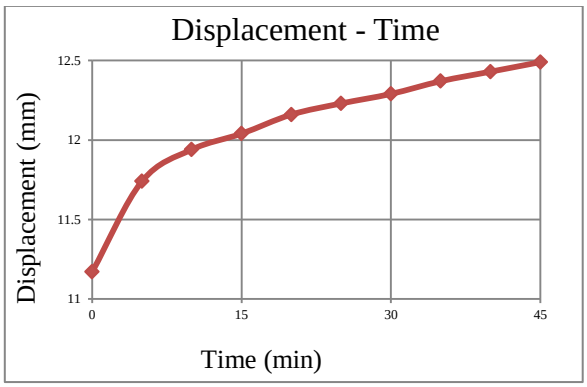

Figure 3.22 Displacement-Time curve

[Single Tendon-Creep Curve-1.6 kg]

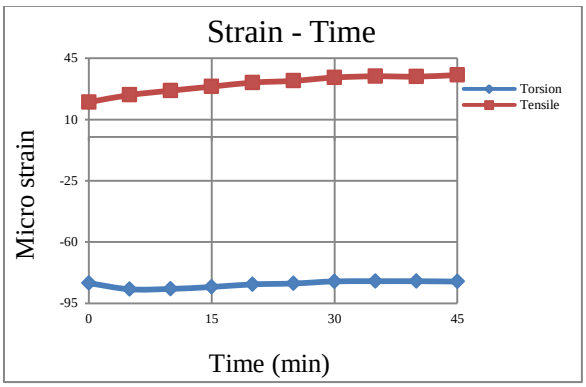

Figure 3.23 Strain-Time curve at SG 1

[Single Tendon-Creep Curve-1.6 kg]

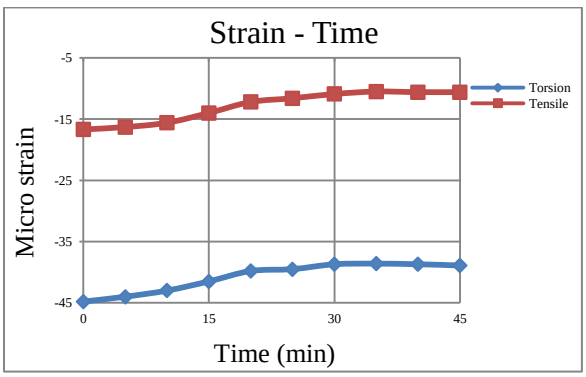

Figure 3.24 Strain-Time curve at SG 2

[Single Tendon-Creep Curve-1.6 kg]

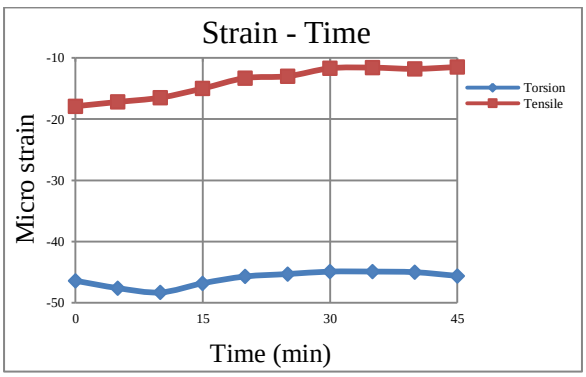

Figure 3.25 Strain-Time curve at SG 3

[Single Tendon-Creep Curve-1.6 kg]

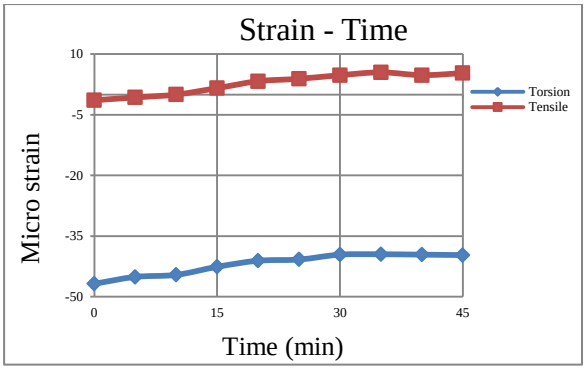

Figure 3.26 Strain-Time curve at SG 4

[Single Tendon-Creep Curve-1.6 kg]

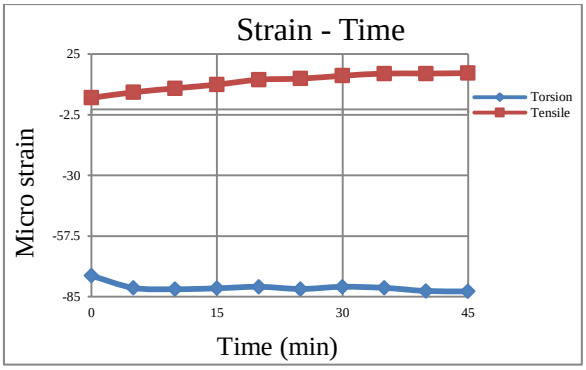

Figure 3.27 Strain-Time curve at SG 5

[Single Tendon-Creep Curve-1.6 kg]

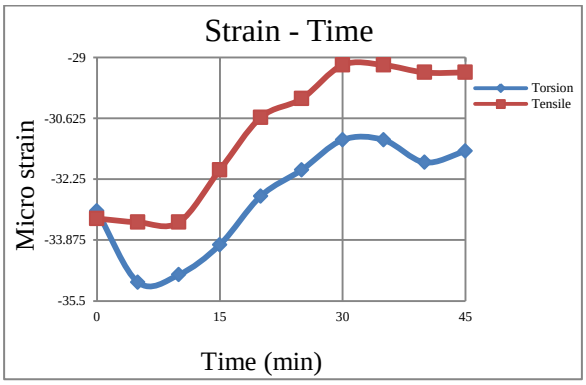

Figure 3.28 Strain-Time curve at SG 6

[Single Tendon-Creep Curve-1.6 kg]

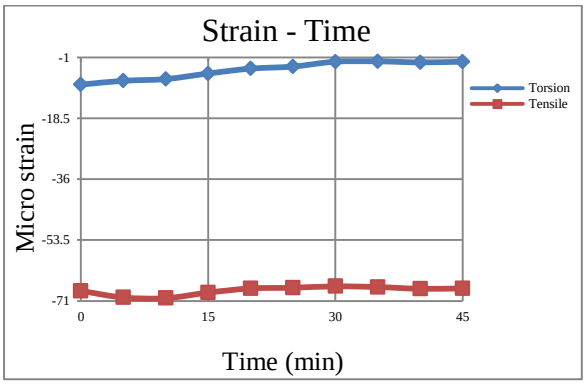

Figure 3.29 Strain-Time curve at SG 7

[Single Tendon-Creep Curve-1.6 kg]

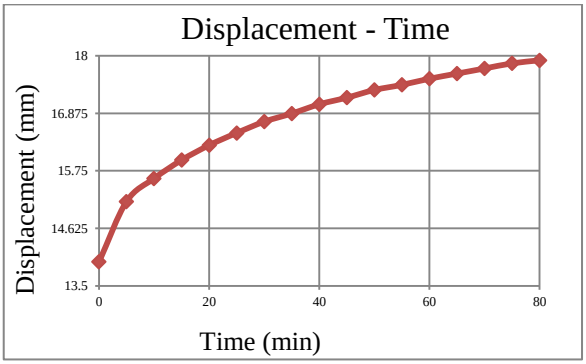

Figure 3.30 Displacement-Time curve

[Single Tendon-Creep Curve-1.8 kg]

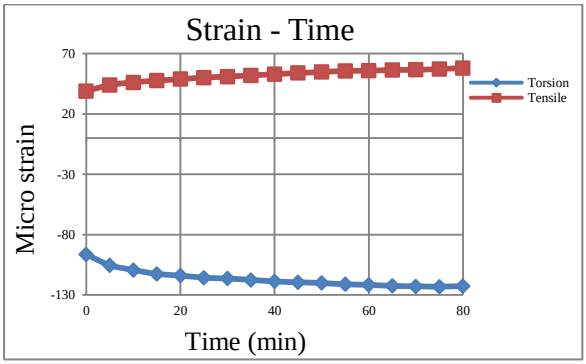

Figure 3.31 Strain-Time curve at SG 1

[Single Tendon-Creep Curve-1.8 kg]

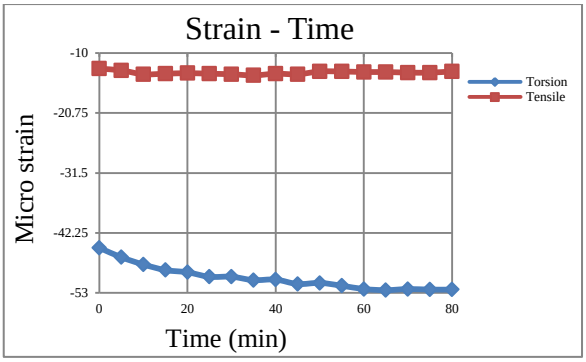

Figure 3.32 Strain-Time curve at SG 2

[Single Tendon-Creep Curve-1.8 kg]

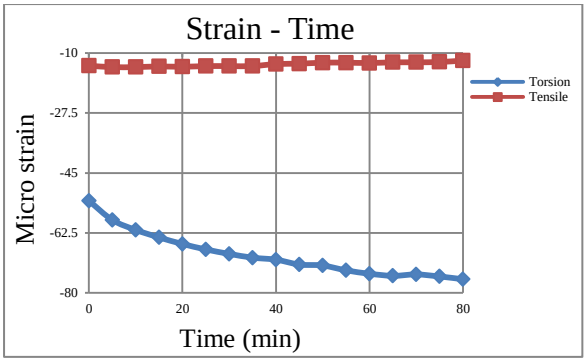

Figure 3.33 Strain-Time curve at SG 3

[Single Tendon-Creep Curve-1.8 kg]

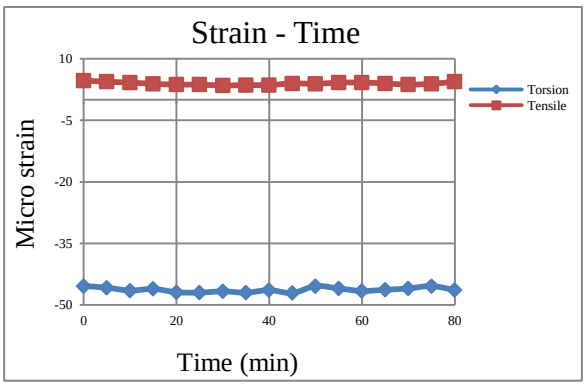

Figure 3.34 Strain-Time curve at SG 4

[Single Tendon-Creep Curve-1.8 kg]

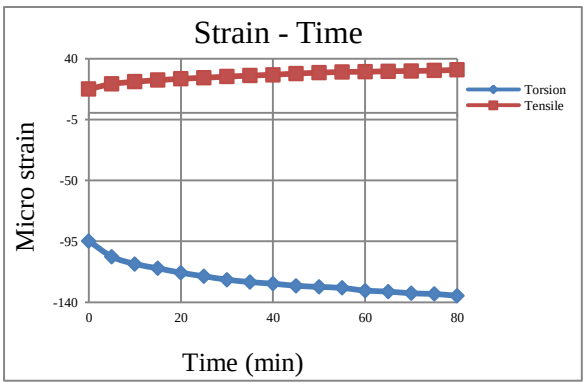

Figure 3.35 Strain-Time curve at SG 5

[Single Tendon-Creep Curve-1.8 kg]

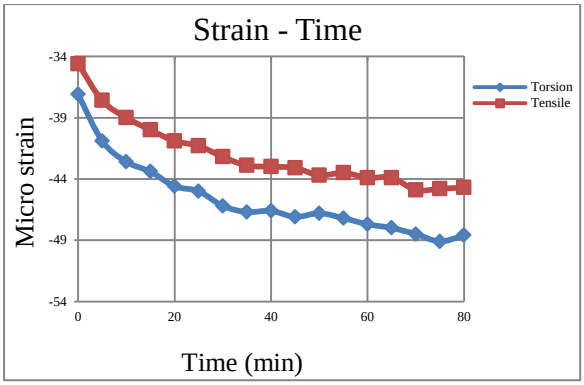

Figure 3.36 Strain-Time curve at SG 6

[Single Tendon-Creep Curve-1.8 kg]

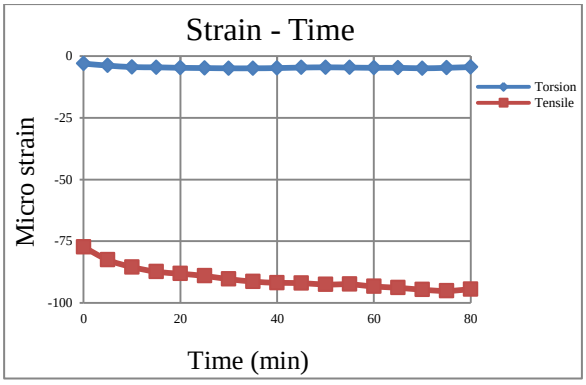

Figure 3.37 Strain-Time curve at SG 7

[Single Tendon-Creep Curve-1.8 kg]

3.7 Bending

The aim of this test is to investigate the non-linear behaviour caused by interlayer slip during the bending test. The results of the experiments are plotted in bending-moment curvature diagrams. The first step is to find the specimen yield point for the maximum load at middle in order to make sure that during the experiment the materials of flexible riser remain elastic with no plastic deformation. The moment at point A for the beam shown in figure 3.38 can be calculated using the following formulations:

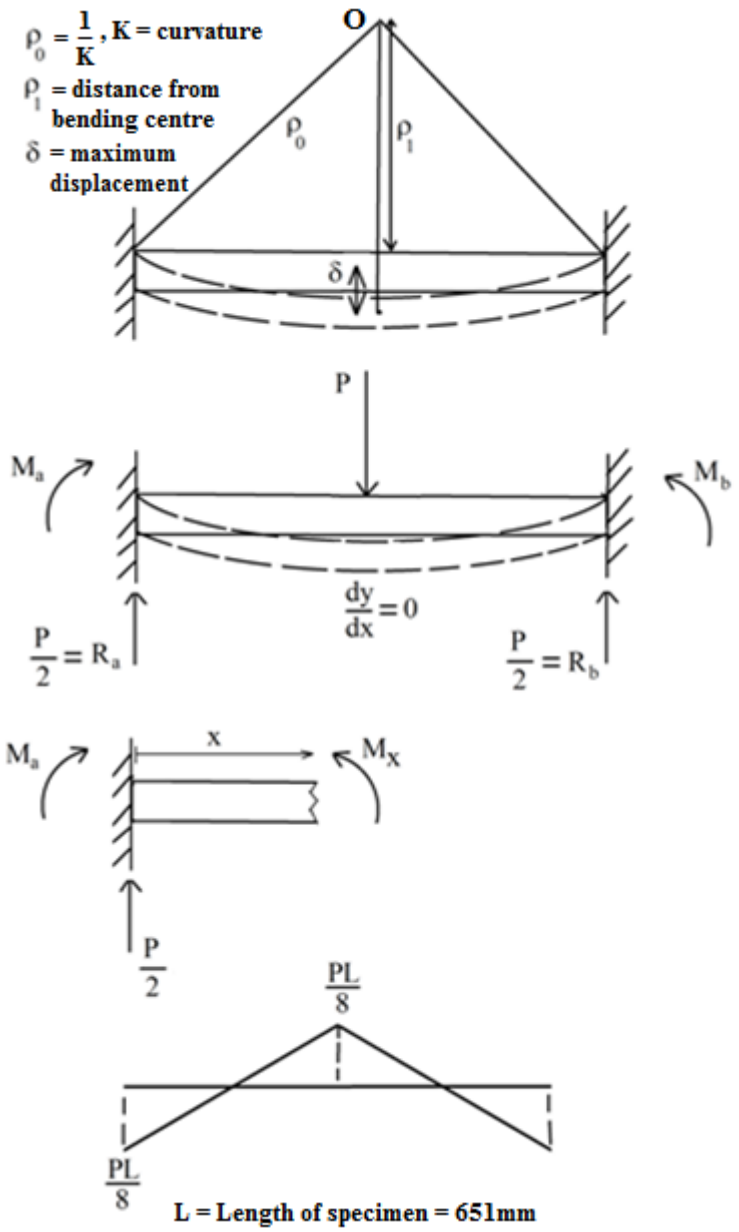

Figure 3.38 Moment as function of length and middle load

$$M_a = \frac{PL}{8} \tag{3.2}$$

For bending, we know that $\sigma = \frac{My}{I}$, (3.3)

Where M is bending moment, y is the distance between bending neutral axis and bended surfaces = inner radius of inner tube: $y = 47\text{mm} = 0.047\text{m}$,

"I" is area moment inertia, calculated from:

$$I = \frac{\pi}{64}\left[{d_o}^4 - {d_i}^4\right] = \frac{\pi}{64}\left[(0.1)^4 - (0.94)^4\right] \approx 1.0762 \times 10^{-6}\text{m}^4.$$

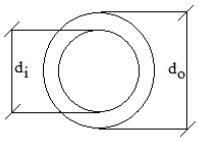

Knowing that yield stress is 60MPa from CES[1] selector software, yield moment and load are:

$$M_y = \sigma_y \times \frac{I}{y} = 60 \times 10^6 \times \frac{1.0762 \times 10^{-6}}{0.047} = 1373.8723\ \text{Nm}$$

$$P_y = 8 \times \frac{M_y}{L} = \frac{8 \times 1373.87}{0.651} = 16883.195\text{N} \approx 16.88\ \text{kN}$$

In order to study the inter-layer non-linear effects without reaching yield point, the maximum load used for bending test was 13kN, which was lower than 16.88kN. The value of curvature for bending can be calculated from:

$$K = \frac{\frac{d^2y}{dx^2}}{[1+(\frac{dy}{dx})^2]^{\frac{3}{2}}} \tag{3.4}$$

In order to use equation 3.4 for measuring curvature at each load increment, nine displacement transducers were placed under the specimen. However, the displacements of two points at the end of each side were ignored because of the negligible small values. So

(1) Cambridge material selector software

effectively, seven displacement transducers were used for the analysis. The space between the displacement transducer was 65.1 mm (figure 3.39).

The accuracy of displacement measurement is one hundredth of millimetre. On direction of helical tendon, five strain gauges were installed with the accuracy of a micro-strain (figure 3.40). The bending load is increased and decreased in 105 steps with the load increment of 250N (figure 3.41).

Each displacement transducer was installed on a variable sized metallic base. The maximum load value could not exceed 13kN in practice. This was because at this load *the lowest part of outer tube touched the top surface of one base*; thus, more loading was practically impossible.

For controlling oil and letting the air to exit easily while pressure oil is induced inside the inner-tube, two valves were designed which are shown in figure 3.42. The air notch had to be drilled in higher position to evacuate more air at the same time as oil was pressured in (left side of figure 3.42). As demonstrated in the right side of the figure 3.42, in oder to observe and control the oil pressure, a pressure gauge and a valve (black) placed respectively between the end-cap and one-way oil valve. A one way valve designed to dispatch oil-pump easily. Bed is positioned on INSTRON loading machine with three M20 bolts in middle.

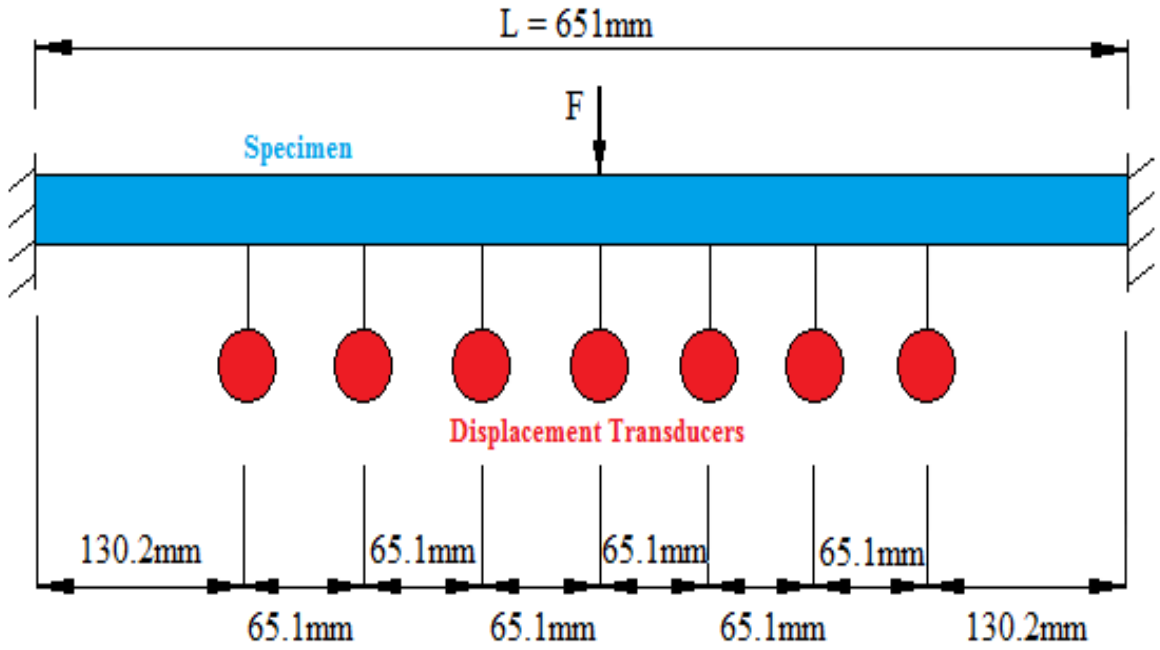

Figure 3.39 Specimen for bending test: displacement transducers positions

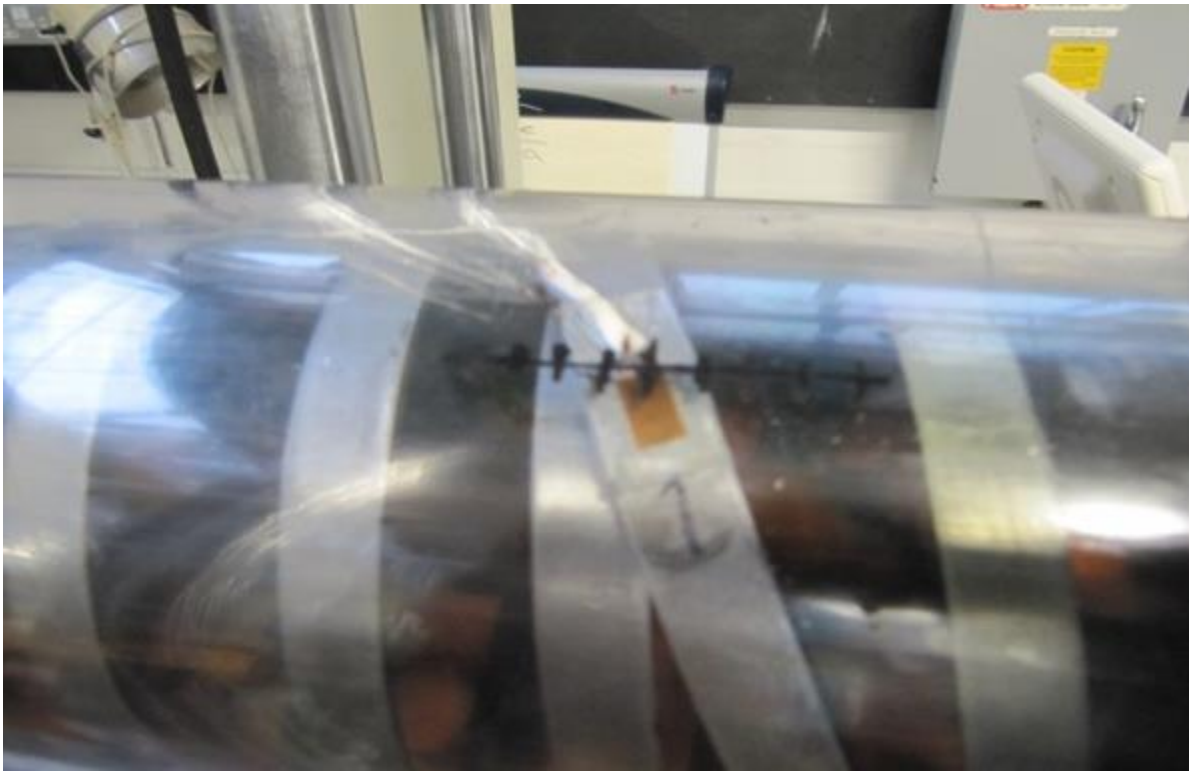

Figure 3.40 Strain gauge of the helical tendon

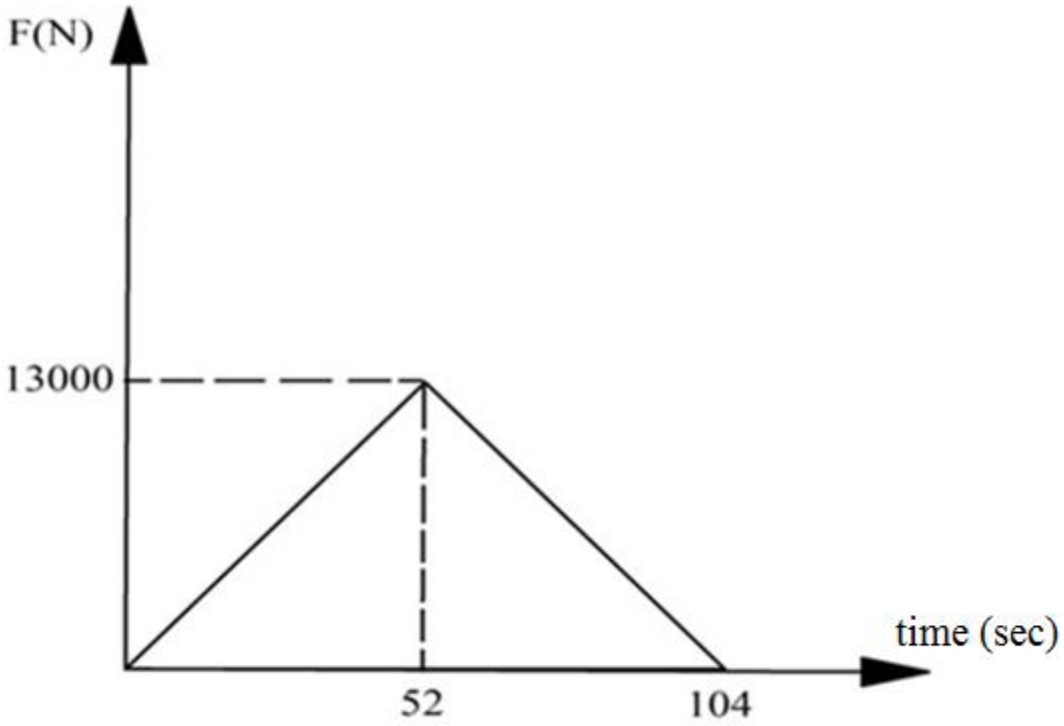

Figure 3.41 Schematic view of load increments versus time

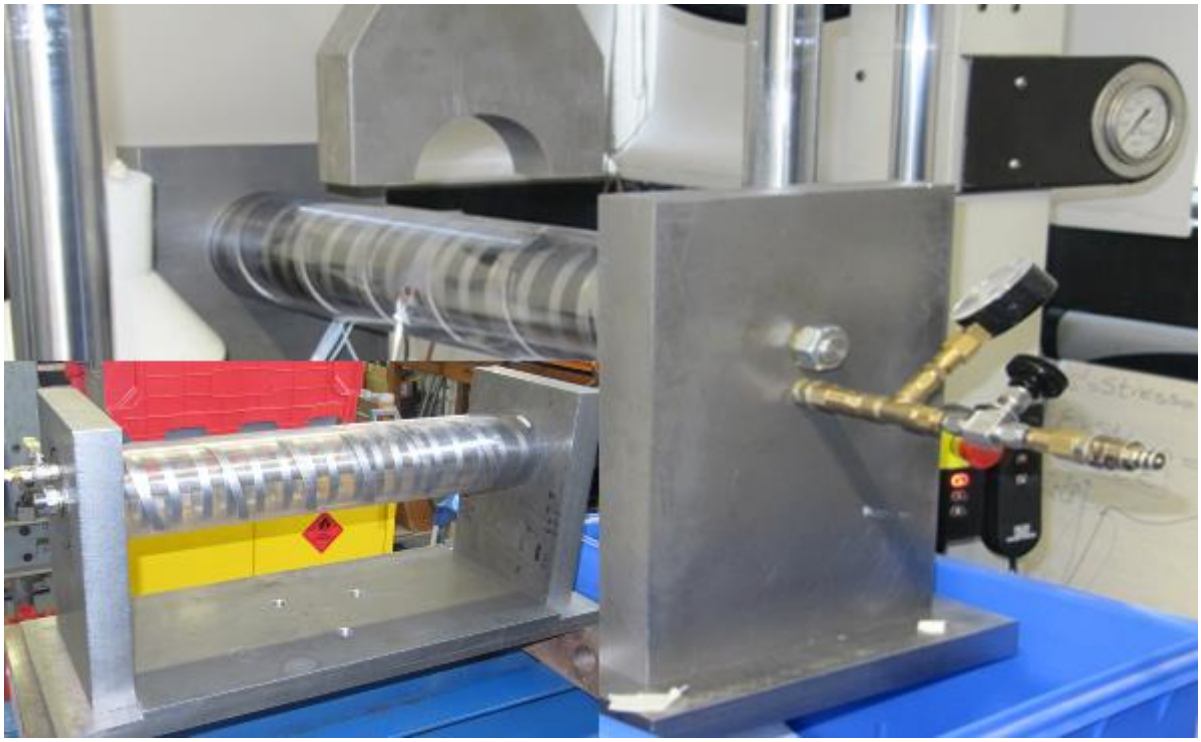

Figure 3.42 Specimen for bending test: air valve on the left, and oil components on the right

The calculation of curvature for each load is done in three steps:

a. First, for each load, the seven deformation values shown by displacement transducers were transferred to Microsoft Excel software.
b. Then, Excel charts have made from the test data and their approximate second order polynomial trend-line curves with the related equation were calculated by the software.
c. Finally, the first and second diversions of trend-line equations were calculated, and equation 3.4 was used to calculate the curvature in the middle of specimen.

As an example in figure (3.43) these three steps for the calculation of curvature when the load reaches to 5000N has been calculated. In figure 3.43b, the blue dots are the test data, the red curve is the second order polynomial trend-line curve, and the red equation is the trend-line equation.

The results for bending are compared with numerical models in the next chapter. Here only the two cases are shown in figures 3.44 and 3.45.

Load (N)	x[1]	y + dy
5000	0	-60
	130.2	-61.57
	195.3	-62.18
	260.4	-62.44
	325.5	-62.57
	390.6	-62.45
	455.7	-62.19
	520.8	-61.55
	651	-60

a)

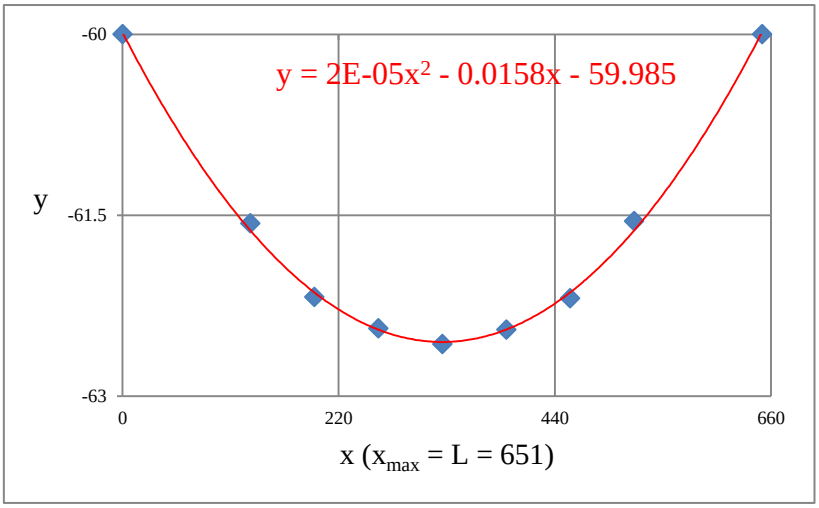

b)

Trend line equation	$\frac{dy}{dx}$	$\frac{d^2y}{dx^2}$	K ($\frac{1}{m}$)
$y = 2 * 10^{-5}x^2 - 0.0158x - 59.985$	$y = 4 * 10^{-5}x - 0.0158$	$y = 4 * 10^{-5}$	0.0399998

c)

Figure 3.43 a) step1: Deformation measurements, b) step2: Resulted chart, c) Final calculation of curvature

(1) maximum value of x = x_{max} = L = 651mm

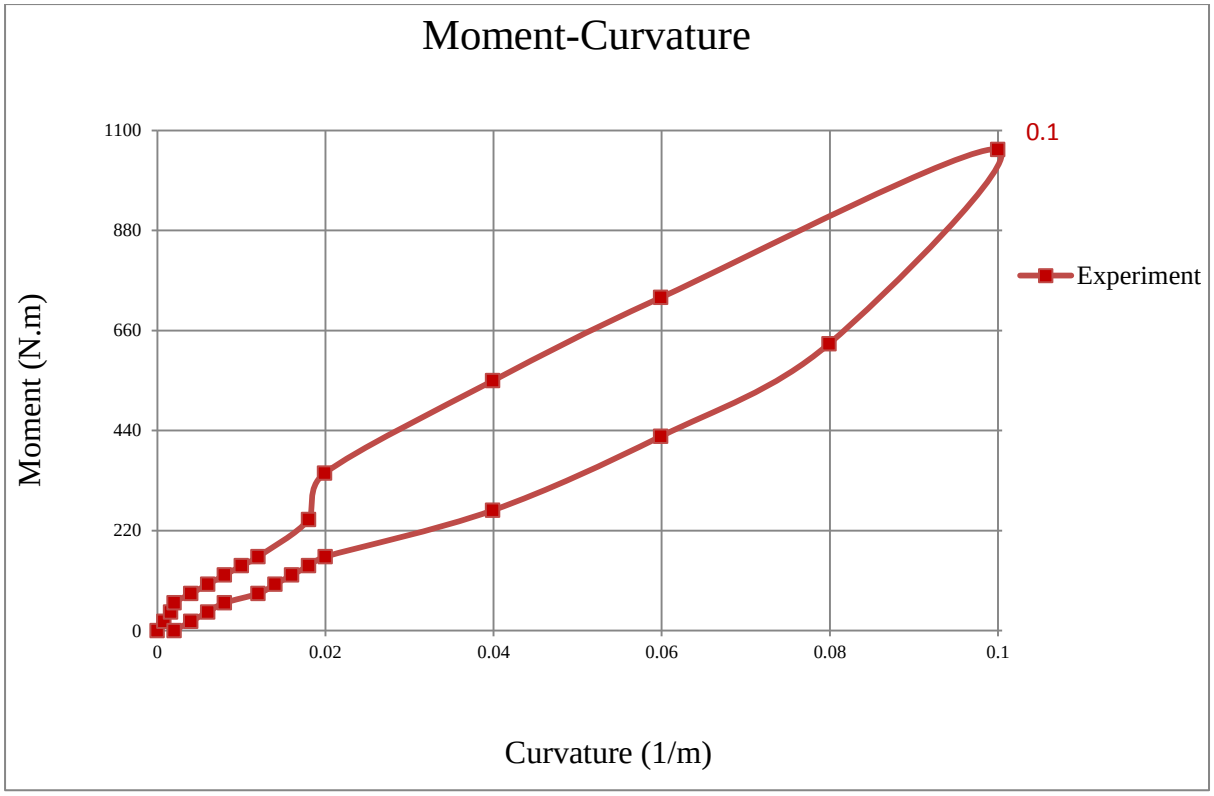

Figure 3.44 Moment Curvature [Bending]

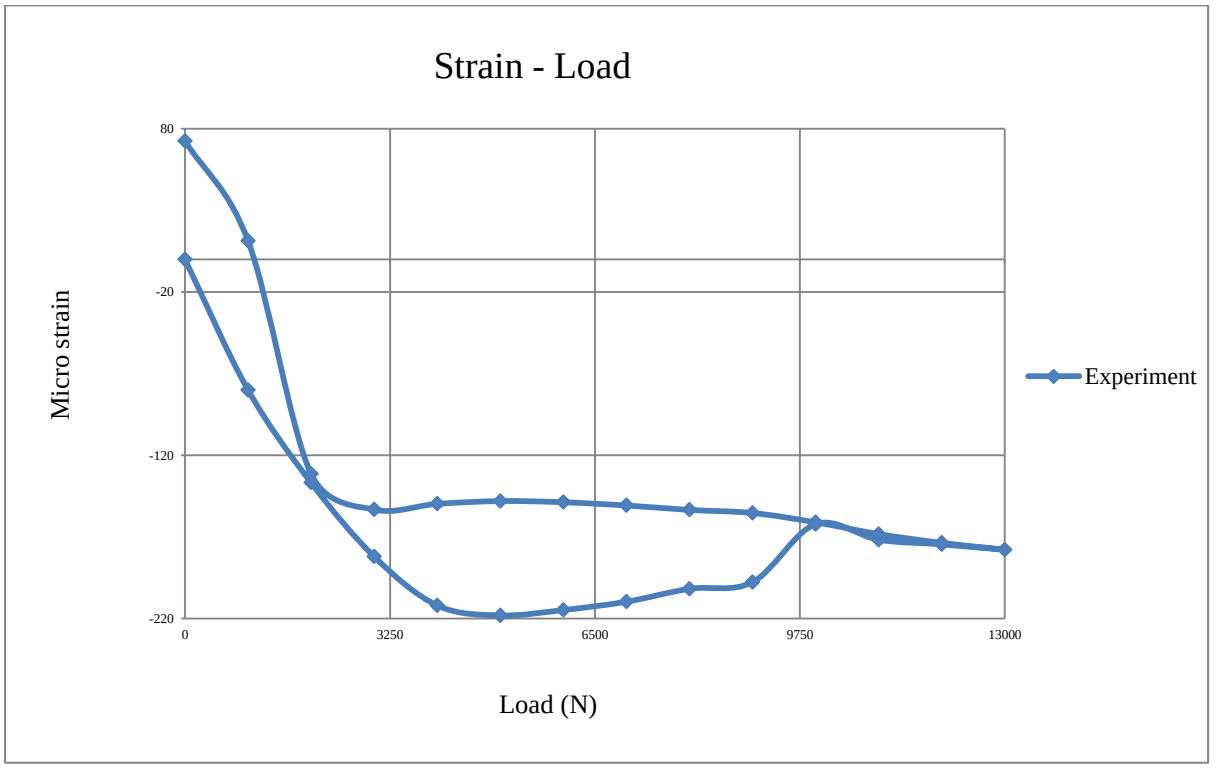

Figure 3.45 Compressive Strain-Load curve at SG 1

3.8 Axial Loading (Compressive)

Many axial loading tests were performed in this study under various conditions shown in tables 3.1 and 3.2. Although there are sixteen different tests, only the results of a few tests are presented in this chapter. The rest are shown in appendix A.

Table 3.3 List of Axial tests (Air Pressure)[1]

Test No.	Layer(s) with strain-gauges	Maximum Load (kN)	Pressure (bar)
01	Inner tube	15	1
02		3	1
03	Outer Tube and Helical Tendon	15	1
04		3	1

Table 3.4 List of Axial tests (Oil Pressure)

Test No.	Layer(s) with strain-gauges	Maximum Load (kN)	Pressure (bar)
05	Inner tube	3	1
06			5
07			10
08			15
09			20
10		No load	1,5,10,12,14,16,18,20
11	Outer Tube and Helical Tendon	3	1
12			5
13			10
14			15
15			20
16		No load	1,5,10,12,14,16,18,20

A large number of wires were attached to strain gauges related to these layers and it was not possible to attach the wires to both strain gauges on the inner and outer tube at the same time. So the tests for every load and pressure were performed twice; first inner tube was measured and then outer tube and helical tendon was studied. To prevent inducing unwanted moment from non axi-symmetric design of bending end-caps, the end-caps design

(1) For all axial tests the increment for 15000N was 500N and for 3000N it was 200N.

become curved for axial tests, which were lighter as well. The prototype assembly for axial loading is shown in figure 3.46. An L shape notch at the bottom and a notch at the top were drilled for oil injecting and air eviction respectively; all oil components of previous tests were used beneath the specimen (figure 3.47). Leakage has been checked before starting the test; the maximum available value of oil pressure, which is twenty bars, was applied continuously for a while. This was a check to make sure that there is no risk to the safety of the people and the loading machine during the experiment (figures 3.46 to 3.48).

Two displacement transducers were used: one for vertical deformation and the other for the buckling changes (figure 3.49). Seven strain gauges were installed on the crucial layers, which are inner-tube, tendon, and outer tube. To measure the strain changes two types of strain gauges one suitable for polymers and one for metal were used (figure 3.50).

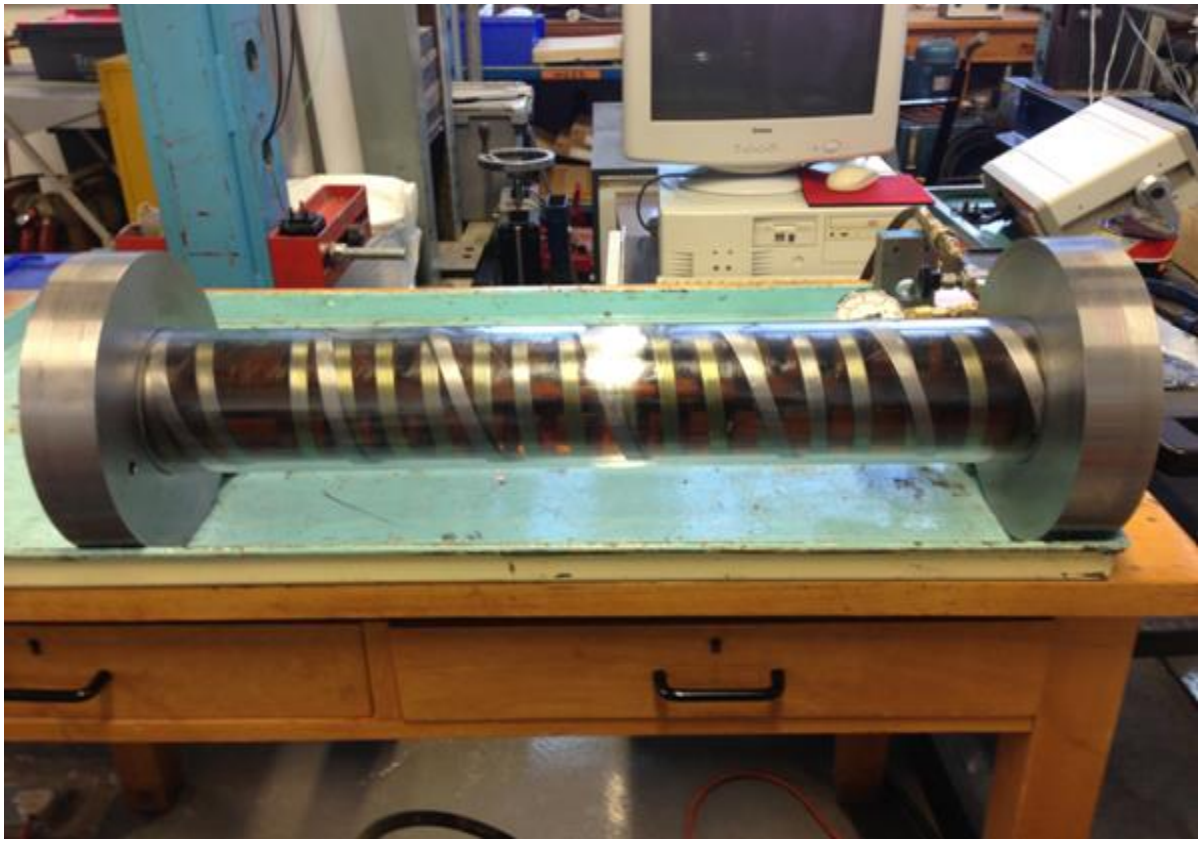

Figure 3.46 Leakage checking at maximum pressure 1 - assembly view

Figure 3.47 Leakage checking at maximum pressure 2 - Pressure gauge at 20bar (maximum)

Figure 3.48 Leakage checking at maximum pressure 3 – Releasing oil

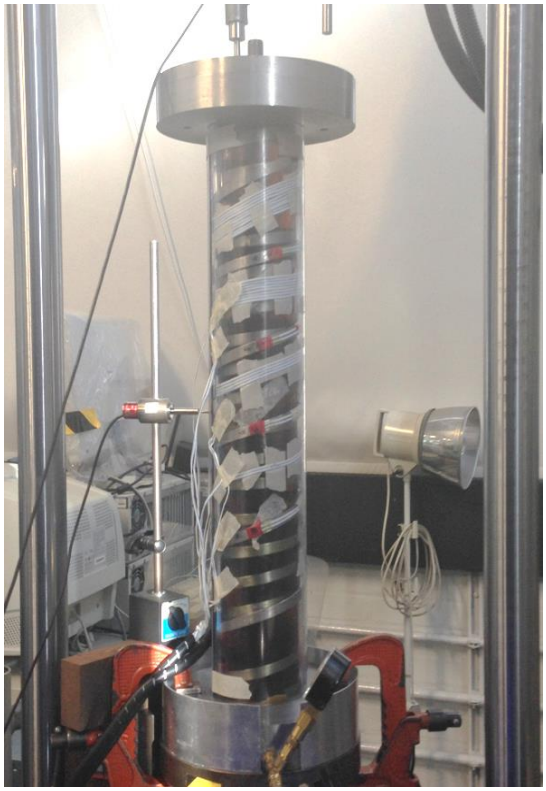

Figure 3.49 Compressive testing for inner tube

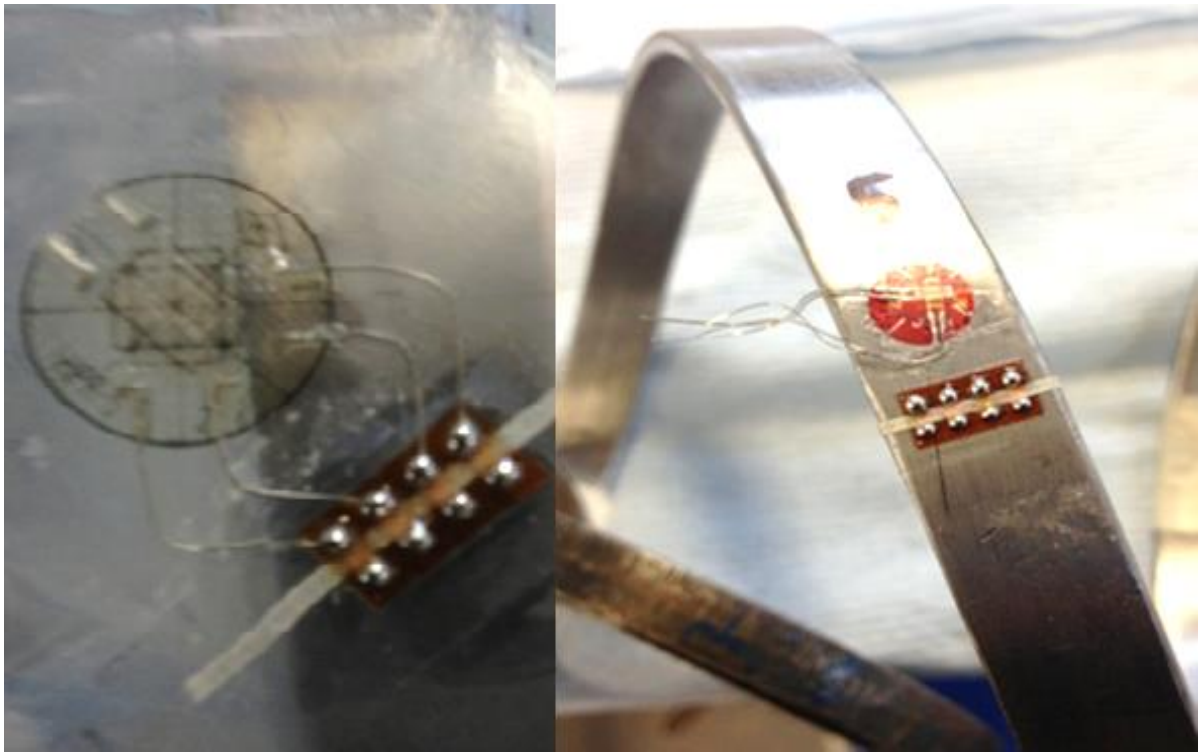

Figure 3.50 Strain gauge for metal tendon (Right) and polymer Tubes (Left)

3.8.1 Pressure Effects with No External Load

The aim of this study was to demonstrate the pure effect of pressure on the deformation and strain changes. The displacement-load relationship has been plotted in figure 3.51. The displacement-load figure shows that there was a strong non-linear behaviour at deformation trend in particular between 10 to 20 bar. During unloading, the residual stresses kept the deformed specimen in similar situation until the value has decreased to the half of maximum pressure, ten bar; at this point the trend had a similar pattern to the previous process. Finally in the end there are residual stresses at specimen. The figure demonstrates that even small internal pressure value, may activate the interlayer behaviour of flexible pipe.

In figures 3.52 to 3.65 the strain changes versus pressure are demonstrated. In two cases figure 3.52 and 3.58 due to a problem in the strain gauges it was not possible to measure strains. For helical tendon, the induced torsion results had less residual strains comparing to compression; this means, the pressure had less effects on helix at torsion direction comparing to compressive direction. Except gauge number seven, the trend of compression indicate residual strains at the end. For torsion trends, except gauge number six, there are residual strains. The torsion trends are not similar in terms of direction as each gauge local position is different. For outer tube, similar to previous part, the compressive residual strains were larger than the results of buckling. The figures have shown that the trends are similar for buckling and compression.

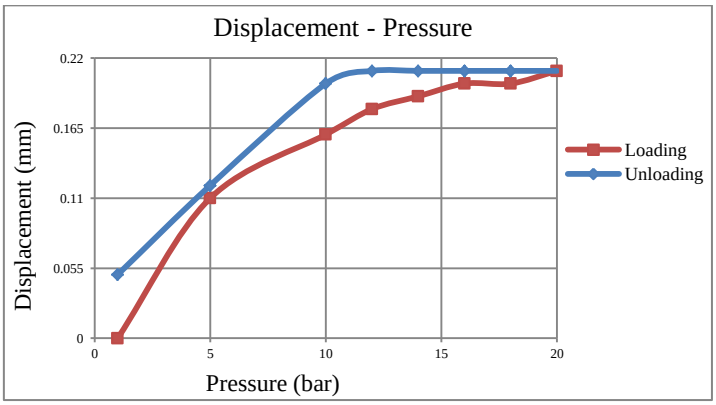

Figure 3.51 Displacement-Pressure curves [Axial-Outer Tube and Helical Tendon-pure pressure effects]

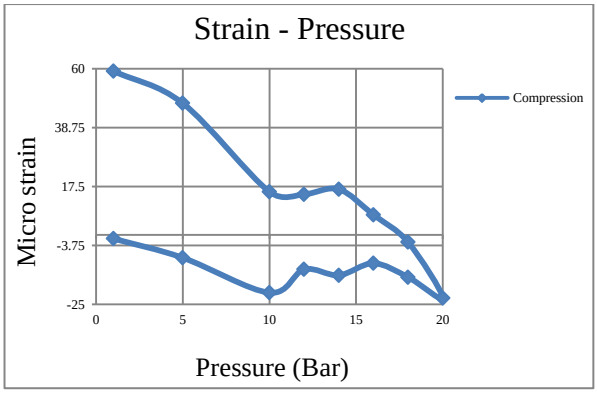

Figure 3.52 Strain-Pressure curves at SG 1

[Axial-Helical Tendon-pure pressure effects]

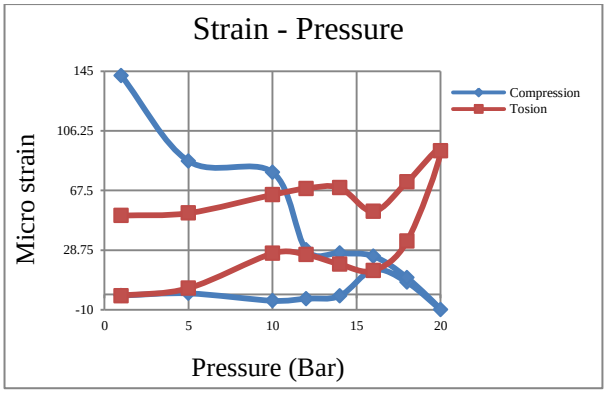

Figure 3.53 Strain-Pressure curves at SG 2

[Axial-Helical Tendon-pure pressure effects]

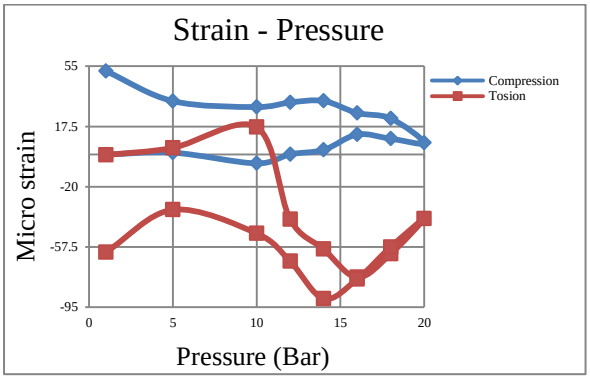

Figure 3.54 Strain-Pressure curves at SG 3

[Axial-Helical Tendon-pure pressure effects]

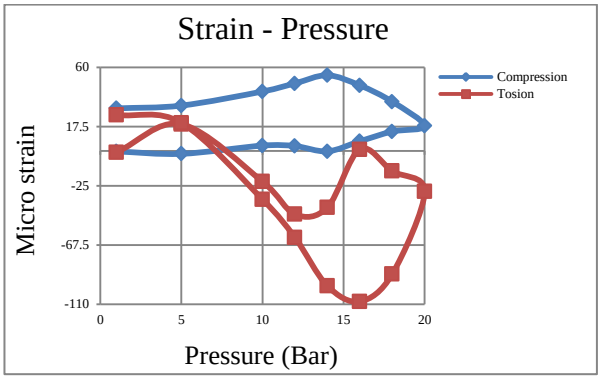

Figure 3.55 Strain-Pressure curves at SG 4

[Axial-Helical Tendon-pure pressure effects]

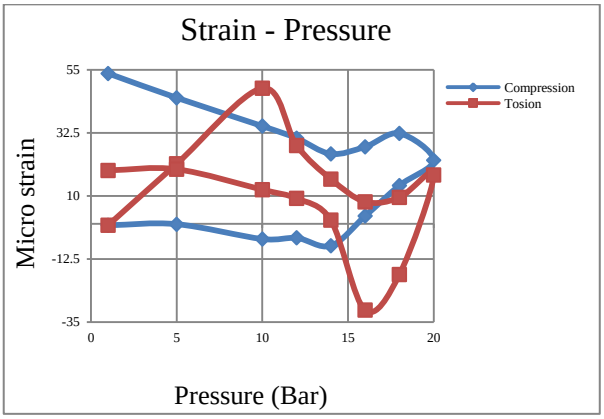

Figure 3.56 Strain-Pressure curves at SG 5

[Axial-Helical Tendon-pure pressure effects]

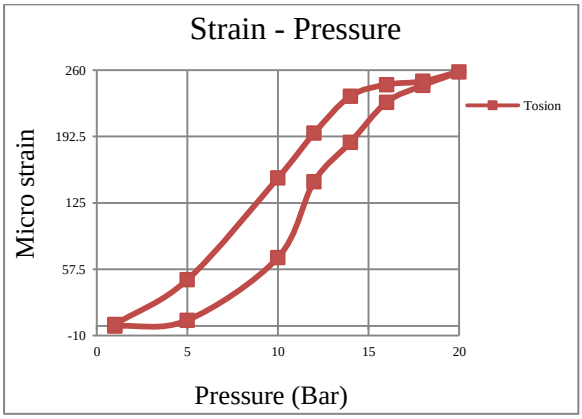

Figure 3.57 Strain-Pressure curves at SG 6

[Axial-Helical Tendon-pure pressure effects]

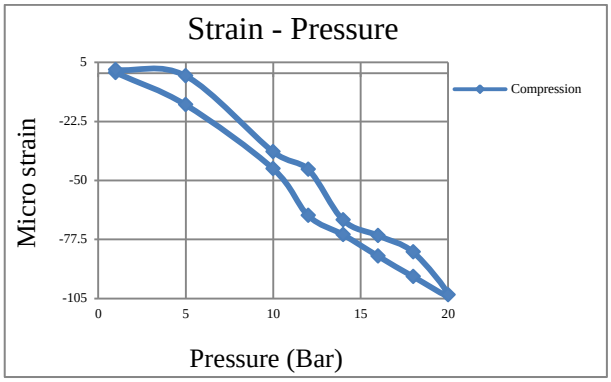

Figure 3.58 Strain-Pressure curves at SG 7

[Axial-Helical Tendon-pure pressure effects]

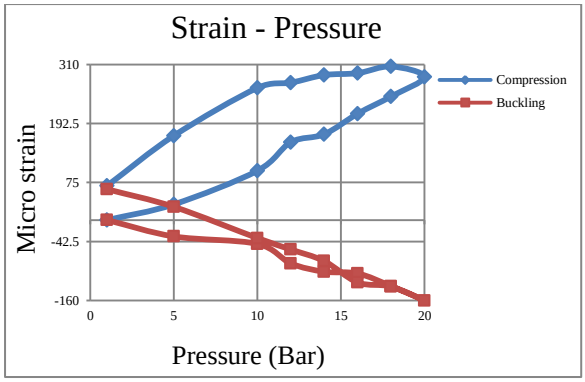

Figure 3.59 Strain-Pressure curves at SG 1

[Axial-Outer Tube-pure pressure effects]

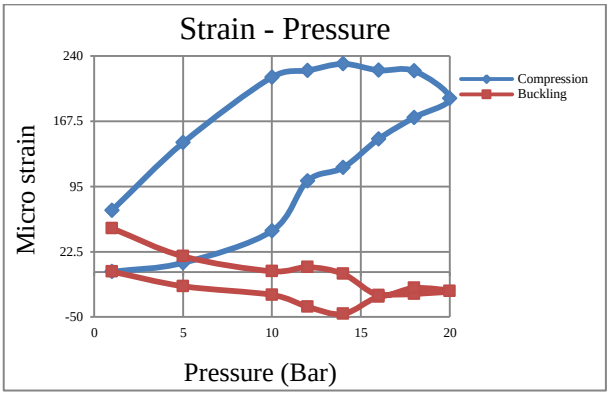

Figure 3.60 Strain-Pressure curves at SG 2

[Axial-Outer Tube-pure pressure effects]

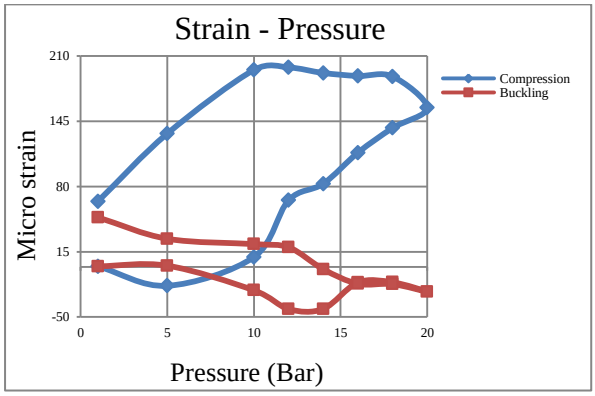

Figure 3.61 Strain-Pressure curves at SG 3

[Axial-Outer Tube-pure pressure effects]

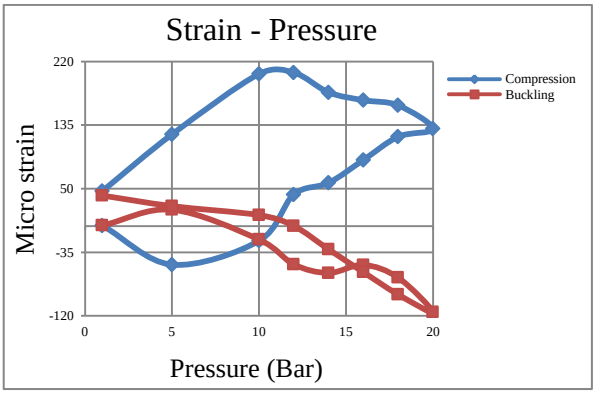

Figure 3.62 Strain-Pressure curves at SG 4

[Axial-Outer Tube-pure pressure effects]

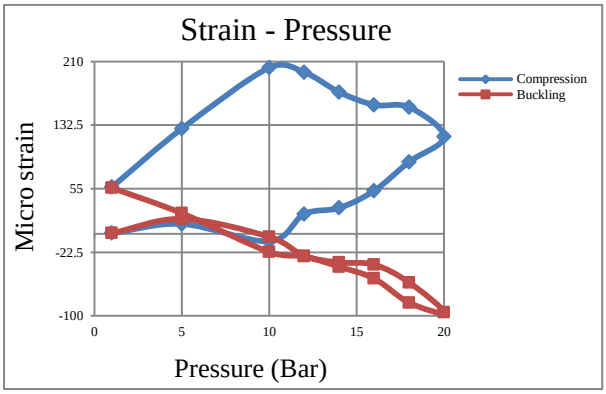

Figure 3.63 Strain-Pressure curves at SG 5

[Axial-Outer Tube-pure pressure effects]

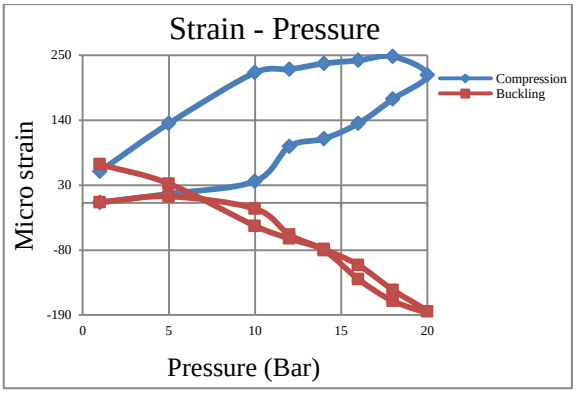

Figure 3.64 Strain-Pressure curves at SG 6

[Axial-Outer Tube-pure pressure effects]

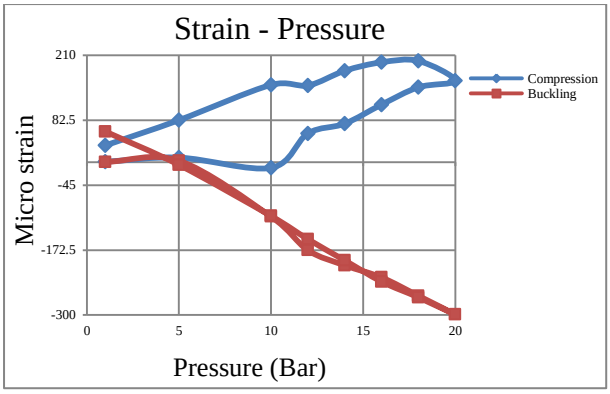

Figure 3.65 Strain-Pressure curves at SG 7

[Axial-Outer Tube-pure pressure effects]

3.8.2 Pressure Effects on Displacement-Load Diagrams

The effects of pressure on the displacement were studied through a similar axial loading/unloading test with various pressure values.

In this study, the inner tube and the helical tendon with the outer tube under both high and low pressure were examined. As shown in figures (3.66) to (3.69), when the oil pressure is increased, the displacement of the specimen is decreased. It seems that oil reacts as a resistant against the compression when the pressure increases. It is interesting to note that when oil is not used there are residual strains.

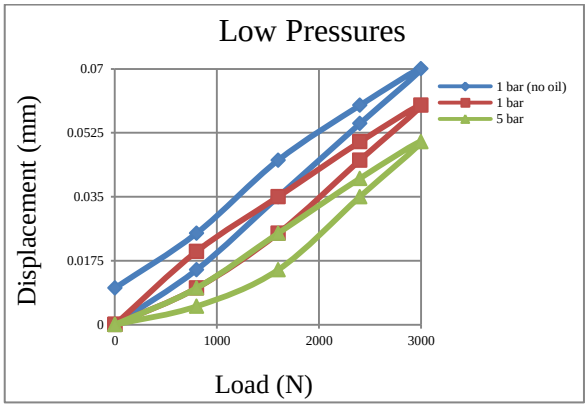

Figure 3.66 Pressure effect on Load-Displacement

[Axial-Inner Tube]

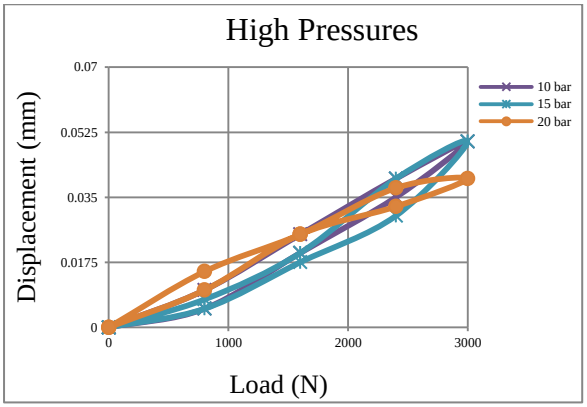

Figure 3.67 Pressure effect on Load-Displacement

[Axial-Inner Tube]

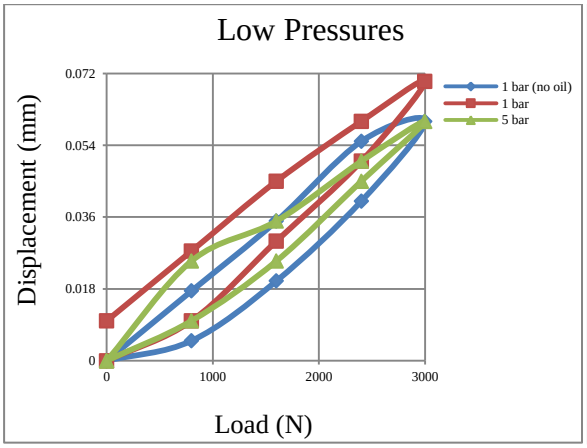

Figure 3.68 Pressure effect on Load-Displacement [Axial-Outer Tube and Helical Tendon]

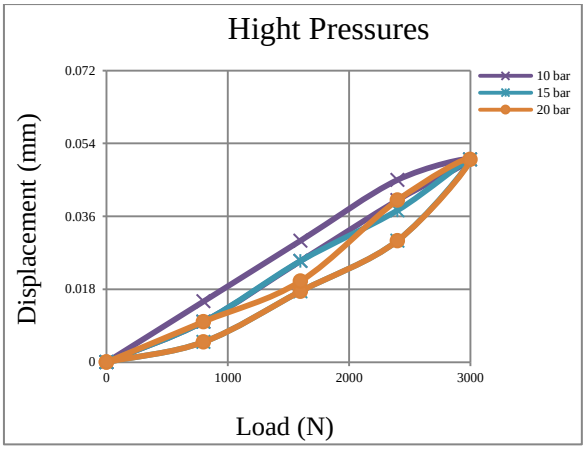

Figure 3.69 Pressure effect on Load-Displacement [Axial-Outer Tube and Helical Tendon]

3.8.3 Effect of External Axial Load (No Internal Pressure)

In this study, compression loading and unloading tests on the model with no internal pressure were investigated. In figure 3.70, the displacement versus load diagram is demonstrated. The results of this figure show the hysteresis of displacement-load relationship. It can be seen that there is non-linearity in displacement-load relationship caused by interlayer behaviour of flexible pipe (as the material of structure is elastic).

Strain-load relationships for each of three layers have illustrated in figures 3.71 to 3.91. For tubes at direction perpendicular to compression there is buckling whilst for tendon layer there is signs of torsion of helix. Although the values are different, the obtained results of tubes have similar behaviour; the residual strains have observed for buckling but not for the compression test. The values of compression at peak were much larger than buckling which proved the safety of specimen under the selected maximum load. For the helical tendon the residual strain values of torsion are larger than that of compression.

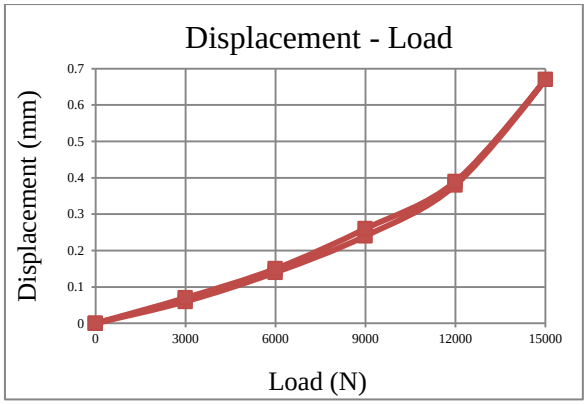

Figure 3.70 Displacement-Load curve [Axial-no-oil-15kN max]

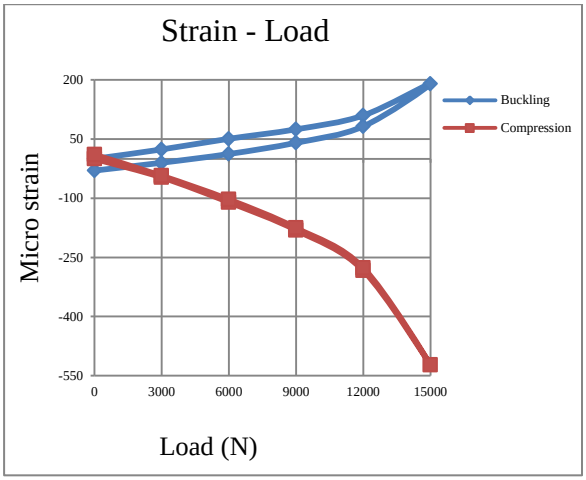

Figure 3.71 Strain-Load curve at SG 1

[Axial-Inner Tube-no oil-15kN max]

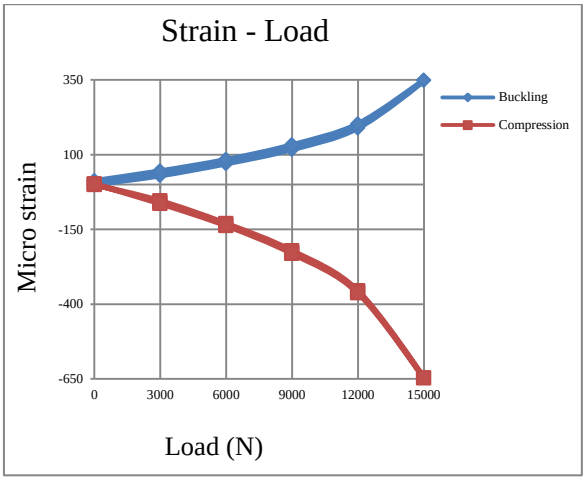

Figure 3.72 Strain-Load curve at SG 2

[Axial-Inner Tube-no oil-15kN max]

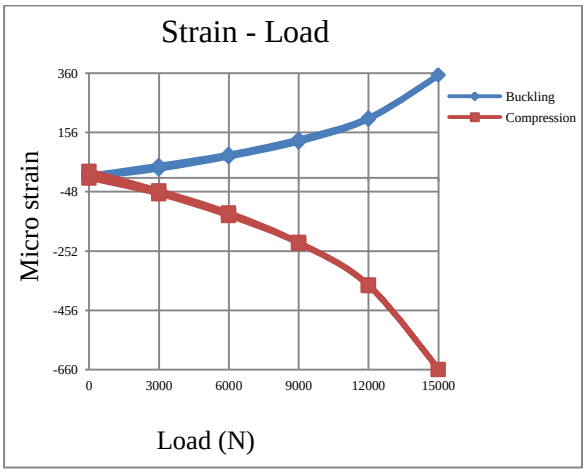

Figure 3.73 Strain-Load curve at SG 3

[Axial-Inner Tube-no oil-15kN max]

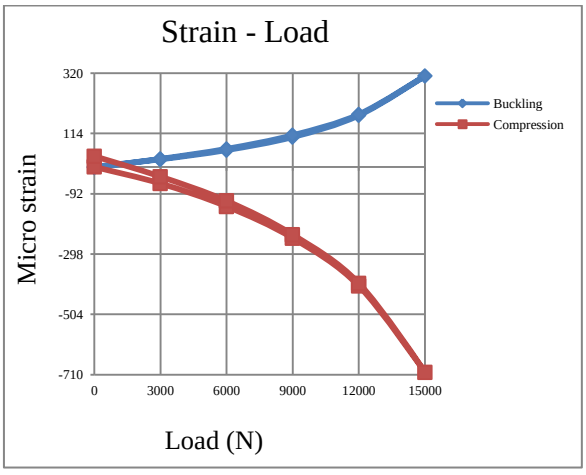

Figure 3.74 Strain-Load curve at SG 4

[Axial-Inner Tube-no oil-15kN max]

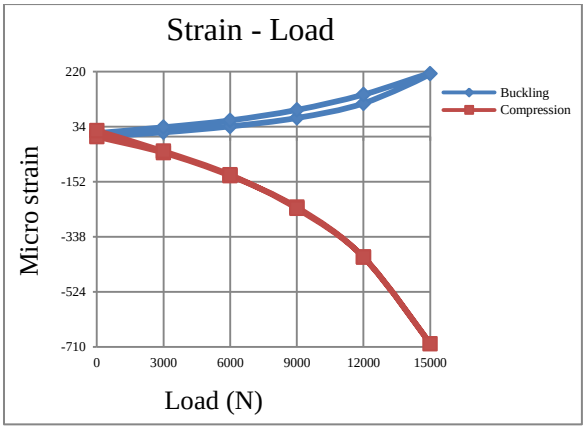

Figure 3.75 Strain-Load curve at SG 5

[Axial-Inner Tube-no oil-15kN max]

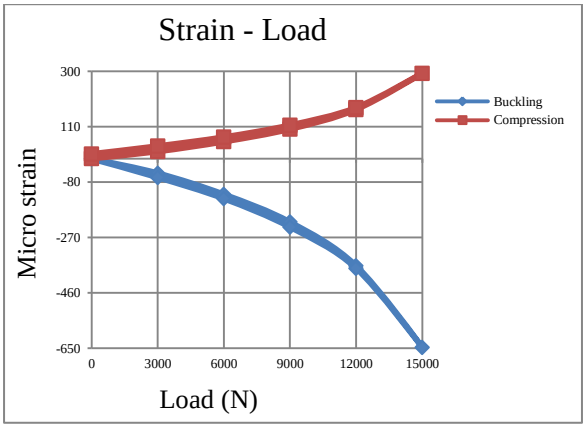

Figure 3.76 Strain-Load curve at SG 6

[Axial-Inner Tube-no oil-15kN max]

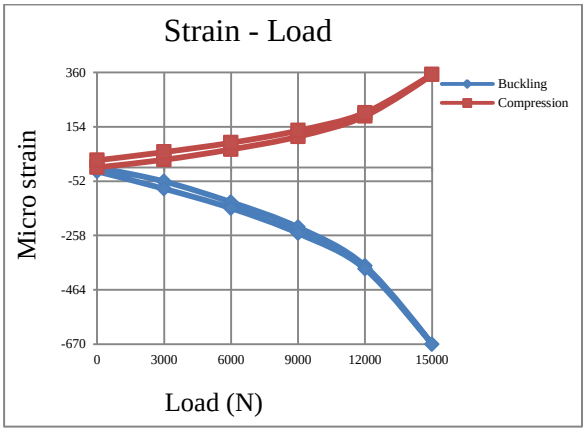

Figure 3.77 Strain-Load curve at SG 7

[Axial-Inner Tube-no oil-15kN max]

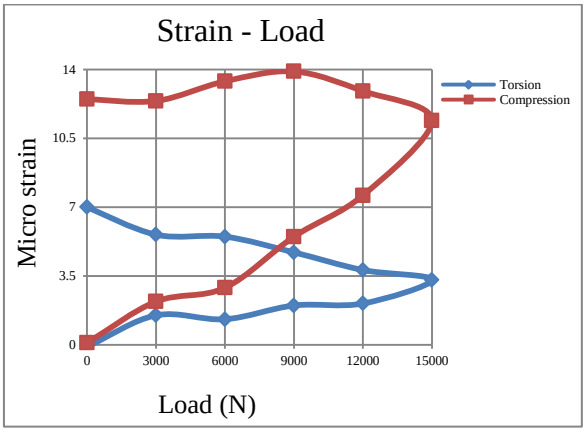

Figure 3.78 Strain-Load curve at SG 1

[Axial-Helical Tendon-no oil-15kN max]

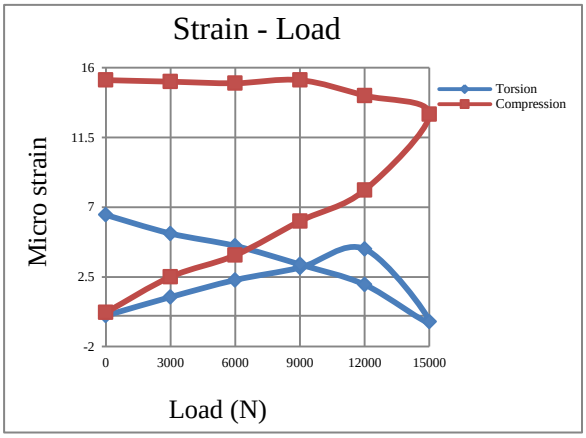

Figure 3.79 Strain-Load curve at SG 2

[Axial-Helical Tendon-no oil-15kN max]

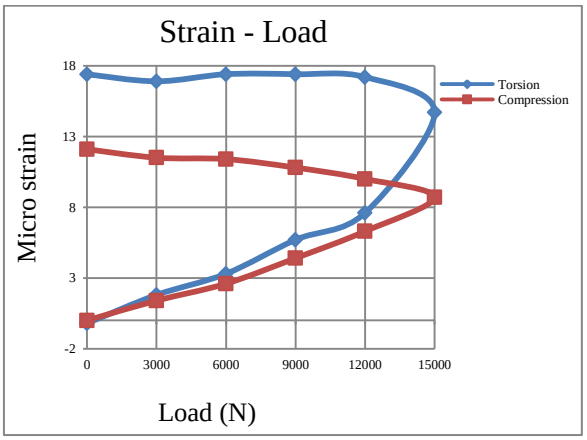

Figure 3.80 Strain-Load curve at SG 3

[Axial-Helical Tendon-no oil-15kN max]

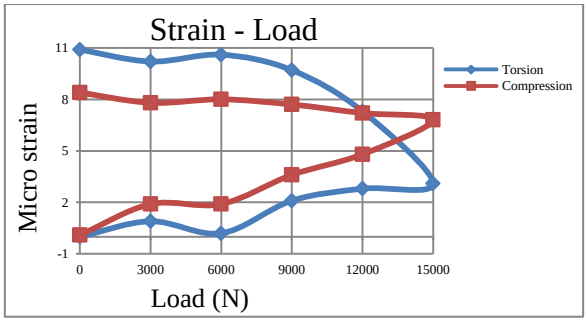

Figure 3.81 Strain-Load curve at SG 4

[Axial-Helical Tendon-no oil-15kN max]

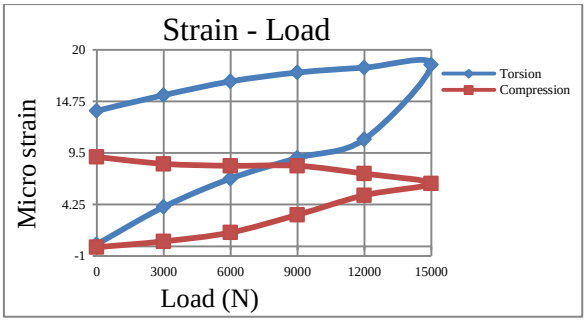

Figure 3.82 Strain-Load curve at SG 5

[Axial-Helical Tendon-no oil-15kN max]

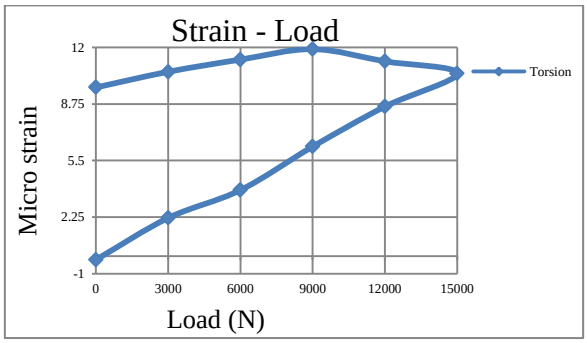

Figure 3.83 Strain-Load curve at SG 6

[Axial-Helical Tendon-no oil-15kN max]

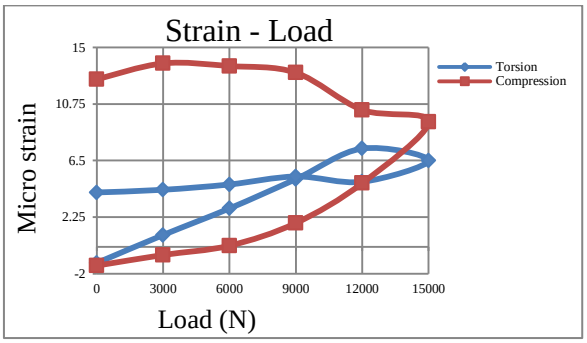

Figure 3.84 Strain-Load curve at SG 7

[Axial-Helical Tendon-no oil-15kN max]

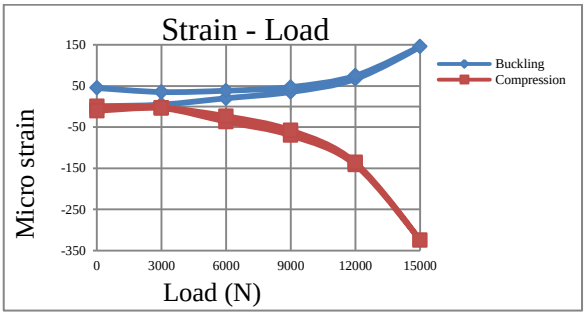

Figure 3.85 Strain-Load curve at SG 1

[Axial-Outer Tube-no oil-15kN max]

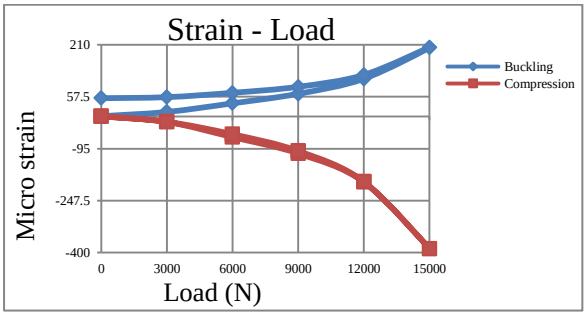

Figure 3.86 strain-Load curve at SG 2

[Axial-Outer Tube-no oil-15kN max]

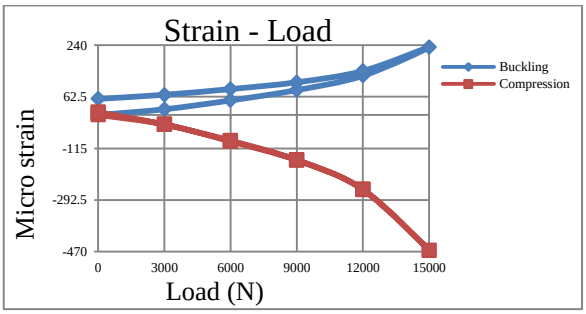

Figure 5.87 Strain-Load curve at SG 3

[Axial-Outer Tube-no oil-15kN max]

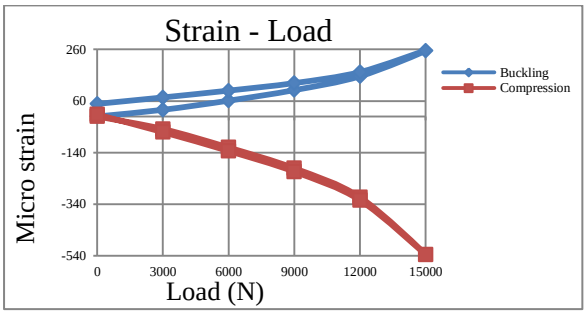

Figure 5.88 Strain-Load curve at SG 4

[Axial-Outer Tube-no oil-15kN max]

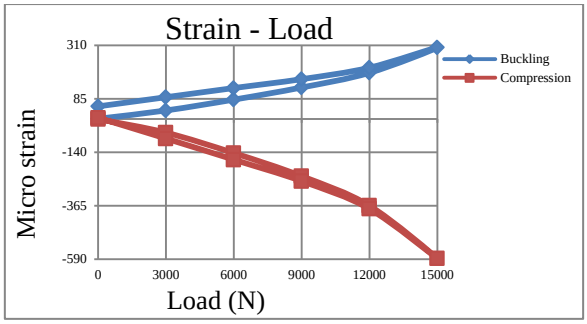

Figure 5.89 Strain-Load curve at SG 5

[Axial-Outer Tube-no oil-15kN max]

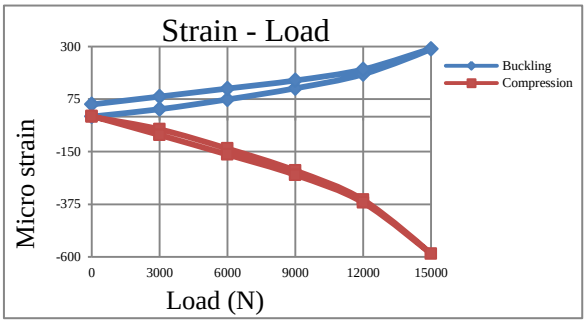

Figure 5.90 Strain-Load curve at SG 6

[Axial-Outer Tube-no oil-15kN max]

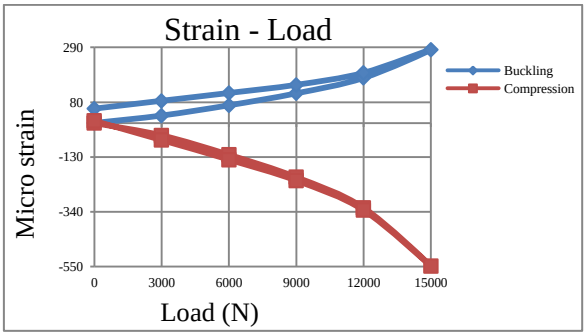

Figure 5.91 Strain-Load curve at SG 7

[Axial-Outer Tube-no oil-15kN max]

3.9 Conclusion

Several experiments on a prototype of flexible pipe were conducted to investigate its non-linear behaviour caused by interlayer slip during bending and axial loading tests. The effect of static loads on the deformation and strain changes of a single helical tendon layer was also investigated. A strong non-linear behaviour in both the bending and the axial load tests were observed. The experimental results can be used as a benchmark solution to investigate the accuracy of various FE based models for analysing flexible pipes.

Chapter 4:

Numerical Modelling

4.1 Introduction

Many types of commercial software are available for analysing flexible pipes, such as ABAQUS, Adina, ALGORA, ANSA, ANSYS, LS DYNA, LUSAS, and NASTRAN. In some software extra patches or subroutines can be developed to solve specific problems or obtaining faster solutions e.g. Patran for NASTRAN, Workbench for ANSYS, and Zencrack for ABAQUS. In this chapter, two finite elements (FE) models, one for a tendon and the other for a flexible pipe, are described. The tendon model is analysed using the *ABAQUS* software while the numerical analysis of flexible pipe is based on the *ANSYS Workbench*. The capabilities of these FE based software are validated against corresponding experimental data.

4.2 Geometry of Models

The models were designed using Solidworks CAD software (figure 4.1) and then imported to the FEA software for numerical modelling (figure 4.2). For static dead-loading a single helical tendon layer was modelled, the ABAQUS model is shown in figure 4.3. The cross sections of steel carcass and tendon were rectangular with the dimensions of 3x12 mm^2. Details of the dimensions and arrangement of the layers are given in Table 4.1. Material properties are reported in Table 4.2.

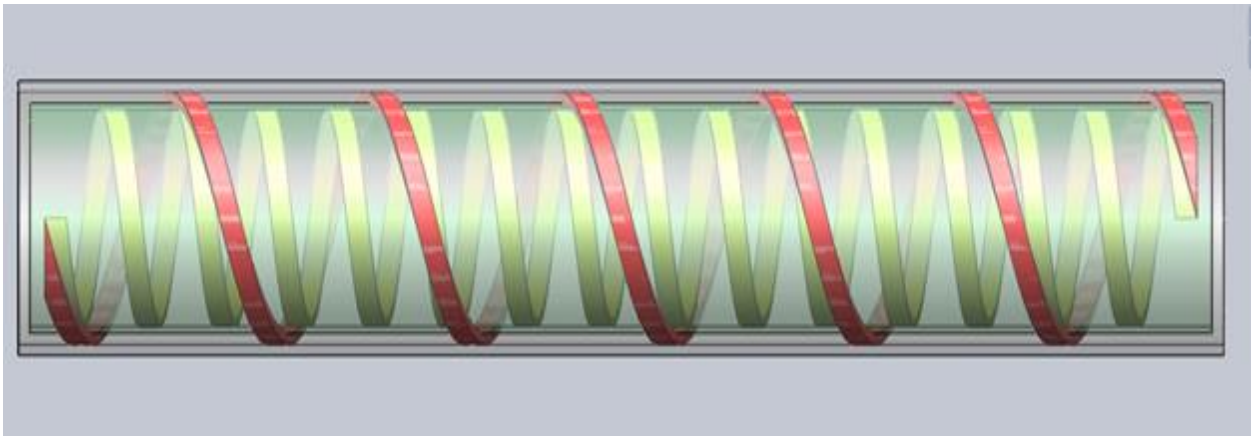

Figure 4.1 Prototype layers

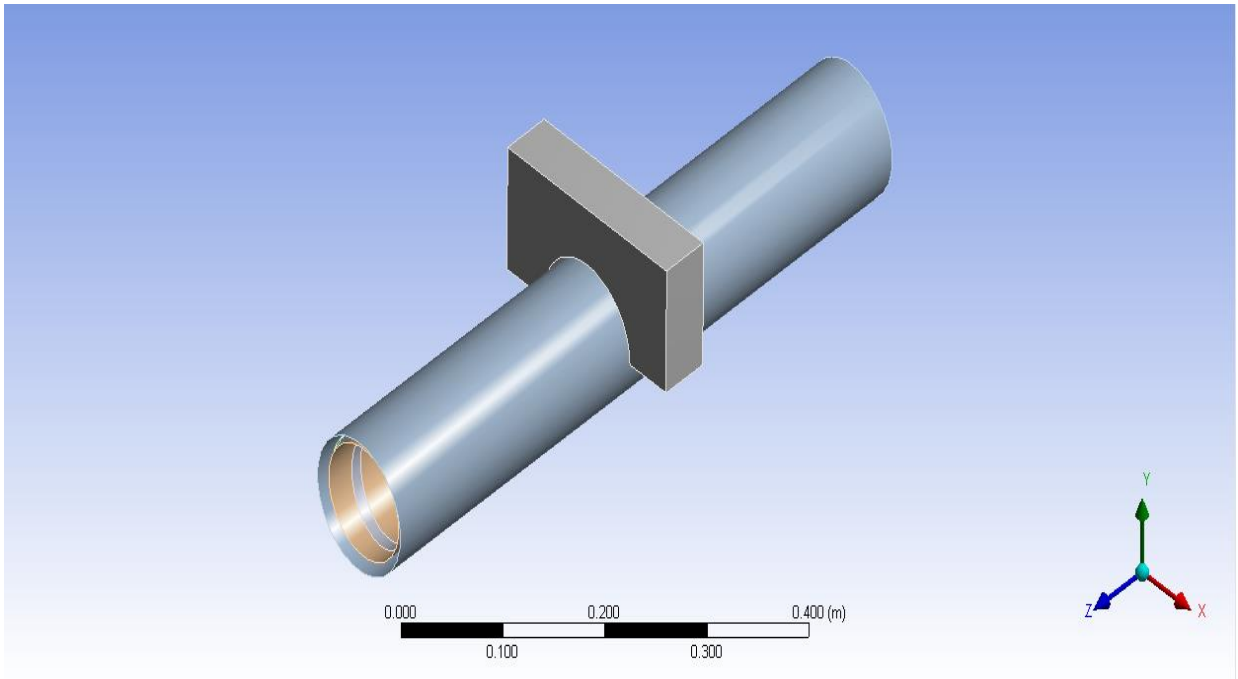

Figure 4.2 Workbench model of prototype for Bending

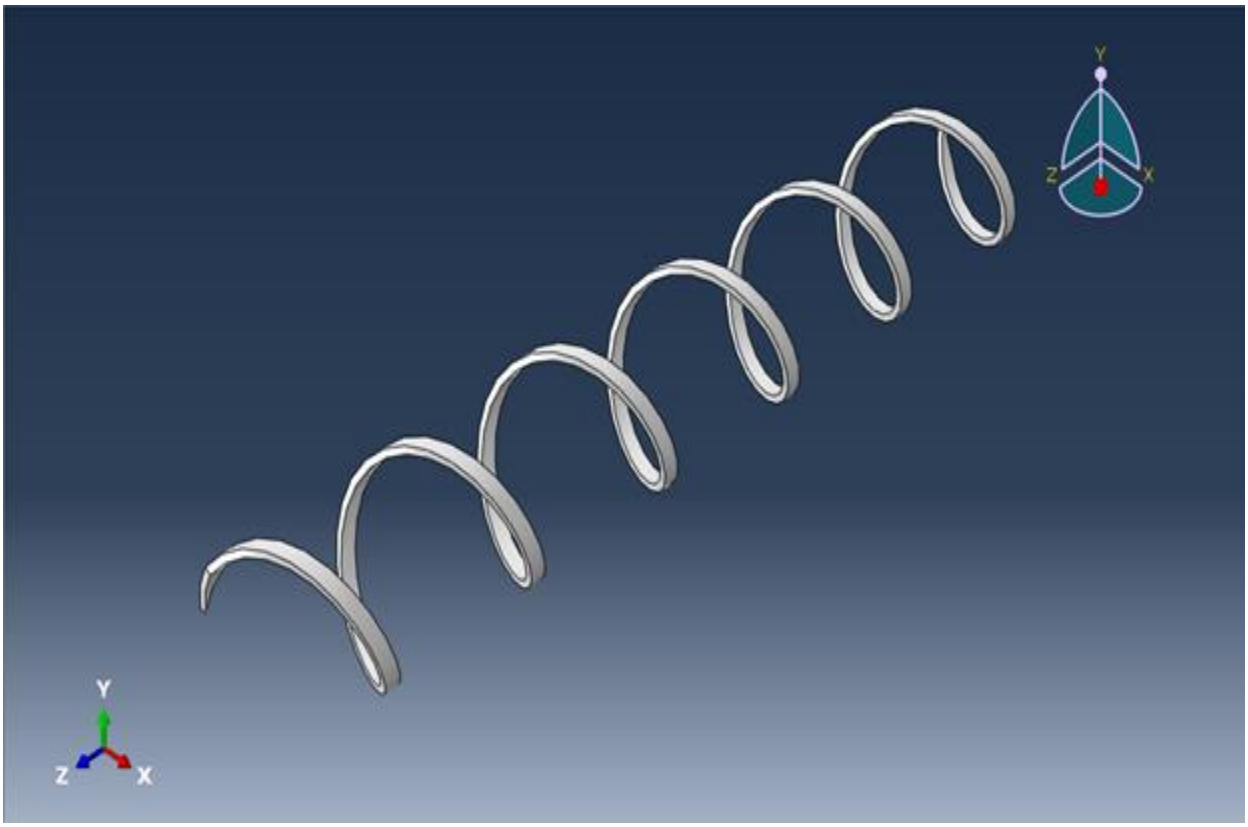

Figure 4.3 Single Tendon model

4.3 Meshing and Element Selection[1]

Because of geometry, in ANSYS Workbench an eight-node structural element, SOLID185, for solid load component was used. The element was non-layered type used full integration and pure displacement (figure 4.4). For riser layers, a four-node shell element SHELL181 with full integration was used. In this element there are two assumptions (figure 4.5):

- Normals to the centre-plane after deforming are straight, yet they do not have to remain perpendicular to centre-plane.
- Every Integration points set of any layer in radial direction are similar in terms of element (or material) orientation.

To keep the load component in a vertical direction for either loading or unloading processes, there is a need of a frictionless support. So, new surface element SURF154, a three dimensional structural surface with four nodes (figure 4.6) were used. For Contact, ANSYS Workbench used two elements CONTA174 and Target170, which are explained in the next section. In total, 6500 elements were used in the meshing process for the riser model in ANSYS.

The tendon was assumed solid and an eight node linear brick shaped C3D8R element with reduced integration and hourglass control was selected in ABAQUS. The node numbering and the integration point for this element are demonstrated in figure 4.7. Only 150 elements were required for modelling the tendon in ABAQUS. In figure 4.8, the developed mesh for the riser in ANSYS Workbench is shown while in figure 4.9 the mesh for tendon layer in ABAQUS is given.

(1) As demonstrated by ANSYS Inc. (2012) and Dassault Systems (2013).

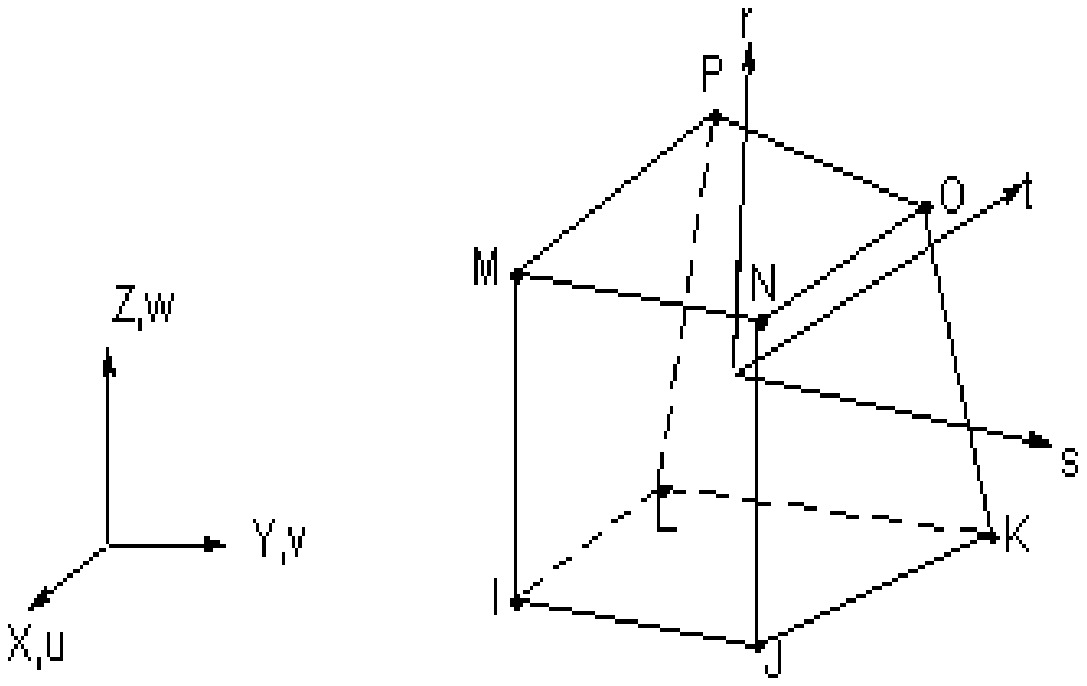

Figure 4.4 SOLID 185 for loading component at Bending (ANSYS Inc., 2012)

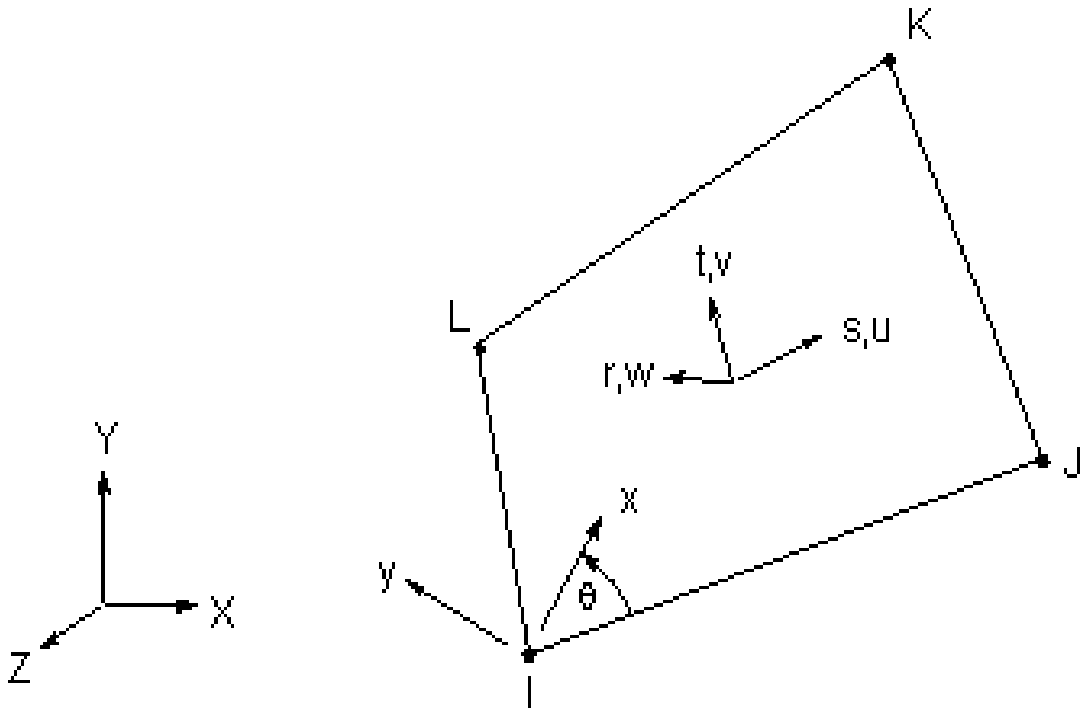

Figure 4.5 SHELL 181 for prototype layers at Bending (ANSYS Inc., 2012)

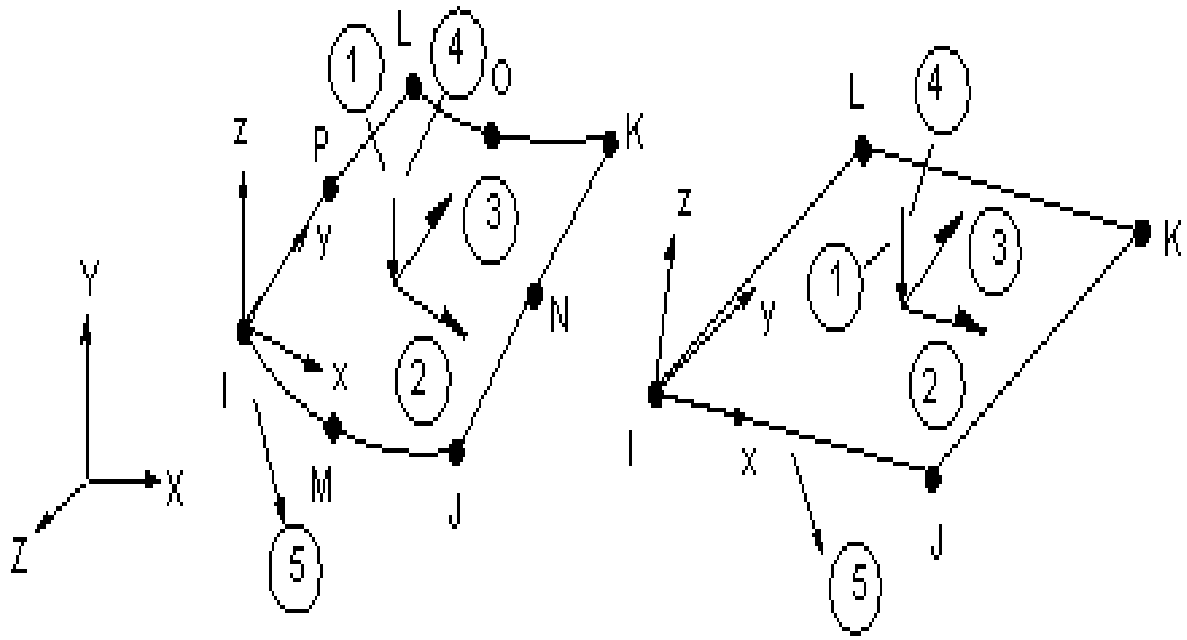

Figure 4.6 SURF 154 [Bending] (ANSYS Inc., 2012)

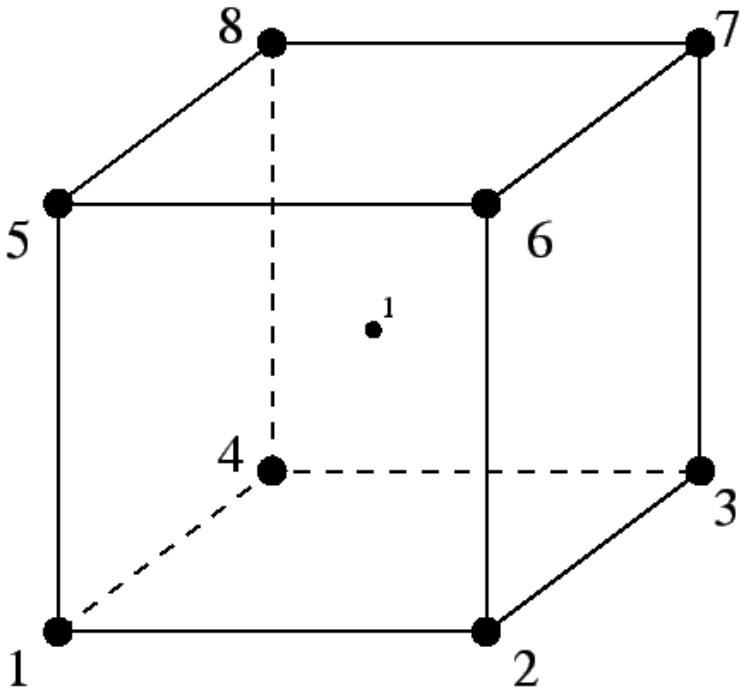

Figure 4.7: C3D8R Node Numbering and 1x1x1 integration point scheme [Static dead loading] (Dhondt, 2011)

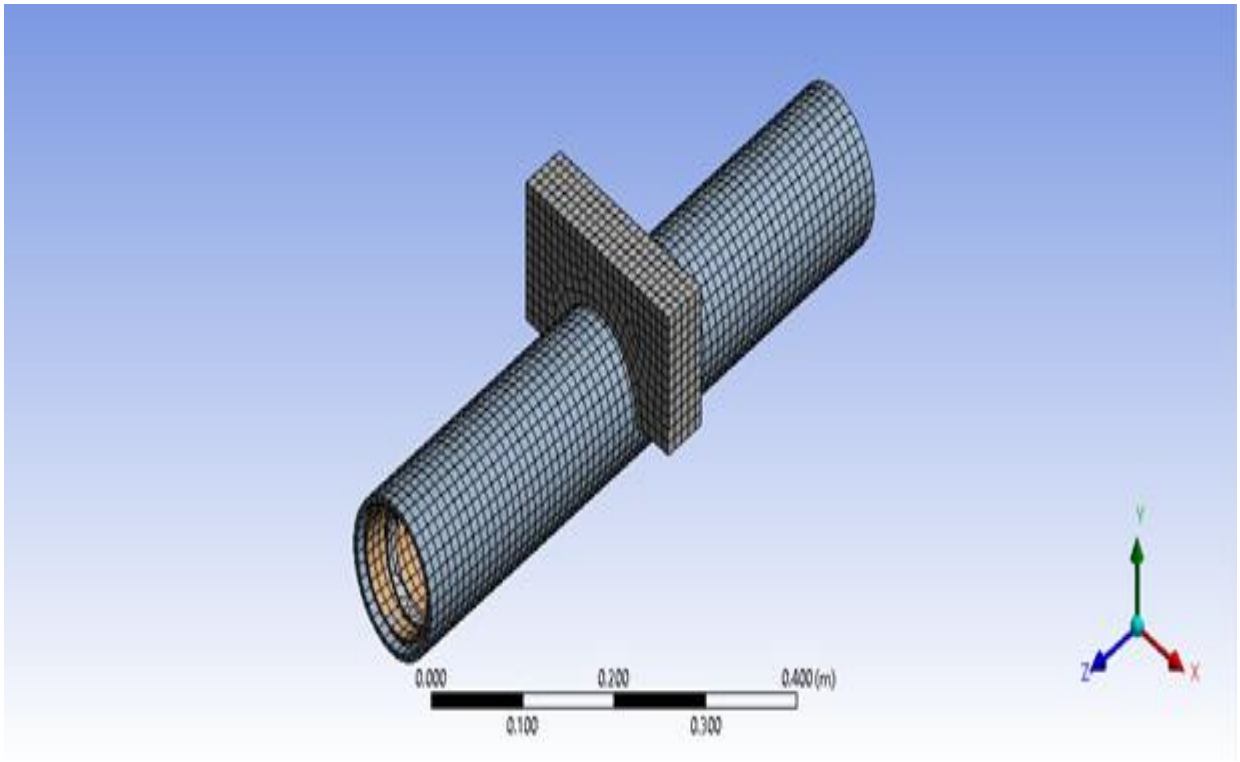

Figure 4.8 Meshing [Bending]

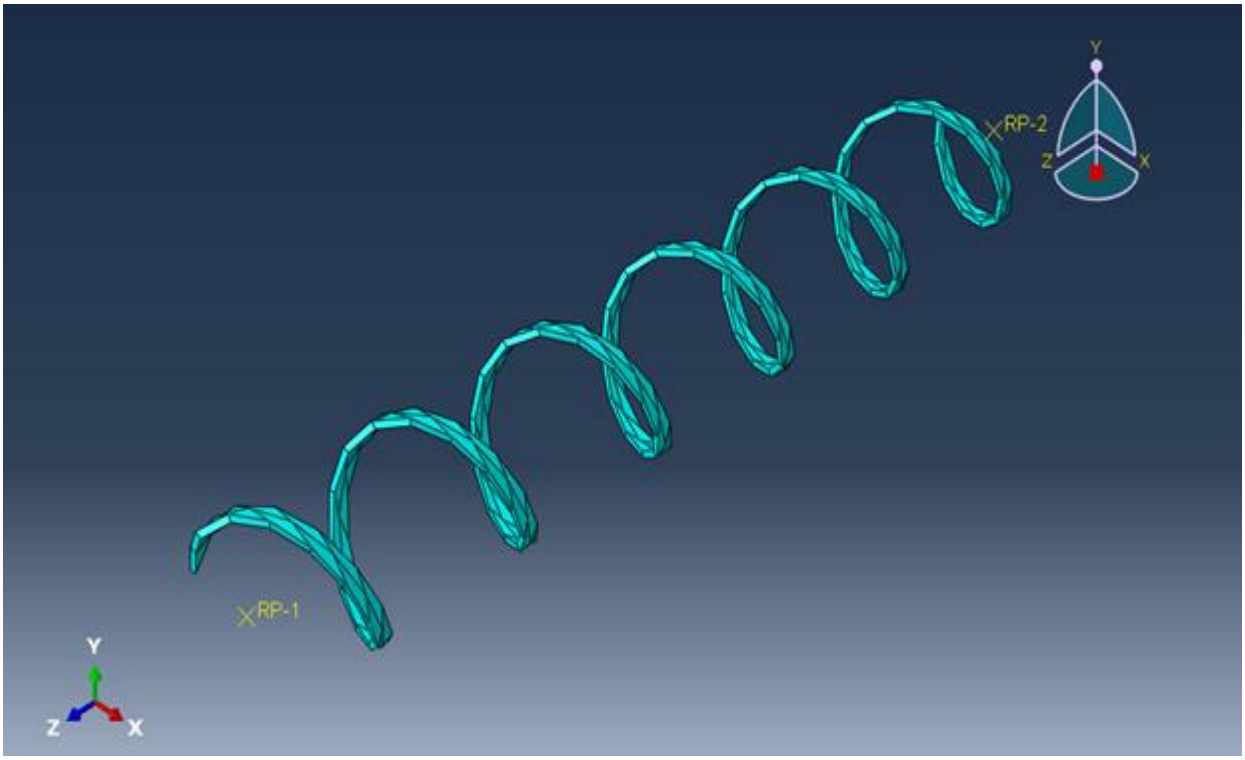

Figure 4.9 Meshing [Static dead loading]

4.4 Contact

There is a three dimensional surface to surface contact between layers and also between outer tube and loading part. So, a contact modelling technique is required to take into account the contact effects. Penalty method with Gauss integration points was used to model contact in ANSYS Workbench. Coefficient of friction between layers is assumed as 0.2. For contact modelling two types of elements have to be defined *contact* and *target*. These elements, defined automatically by ANSYS, are CONTA174 (shown in figure 4.10) and target 170 in figures 4.11 and 4.12. As shown in figure 4.13, deformable solid materials are normally defined as contact whereas rigid bodies are defined as targets. In the riser model, tubes were considered as contact, while helical carcass, helical tendon, and load part modelled as target. In figure 4.14, contact modelling between outer tube and helical tendon is demonstrated.

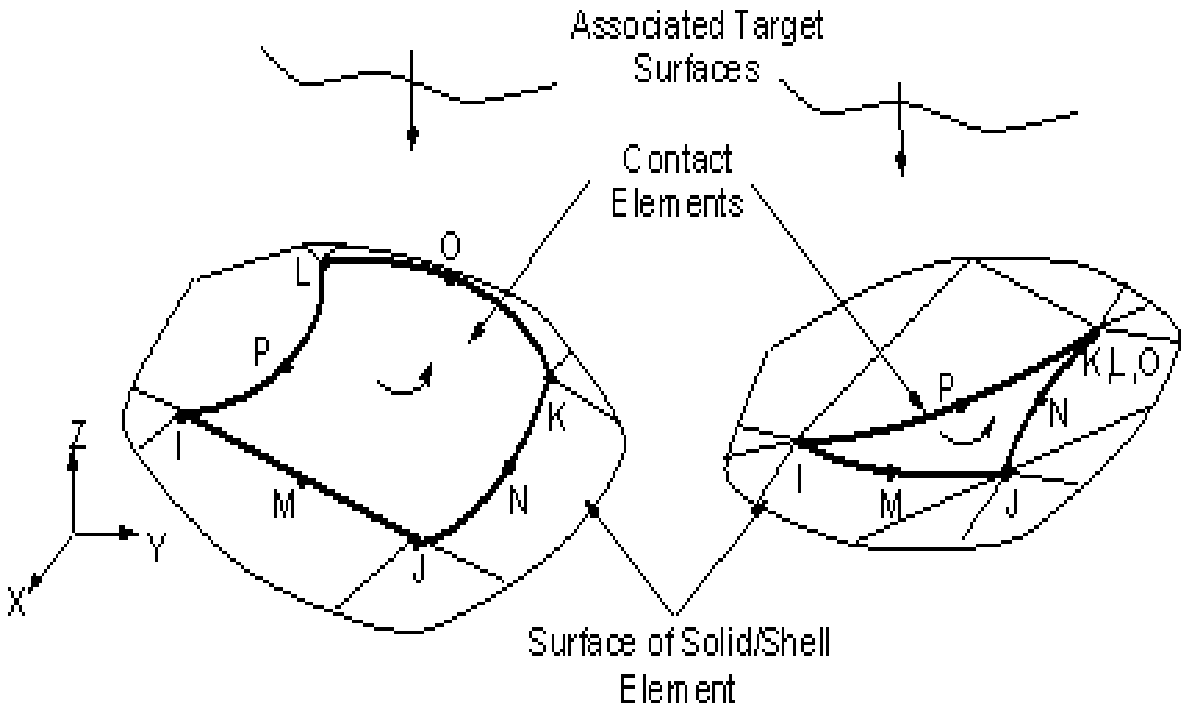

Figure 4.10 CONTA174 [Bending] (ANSYS Inc., 2012)

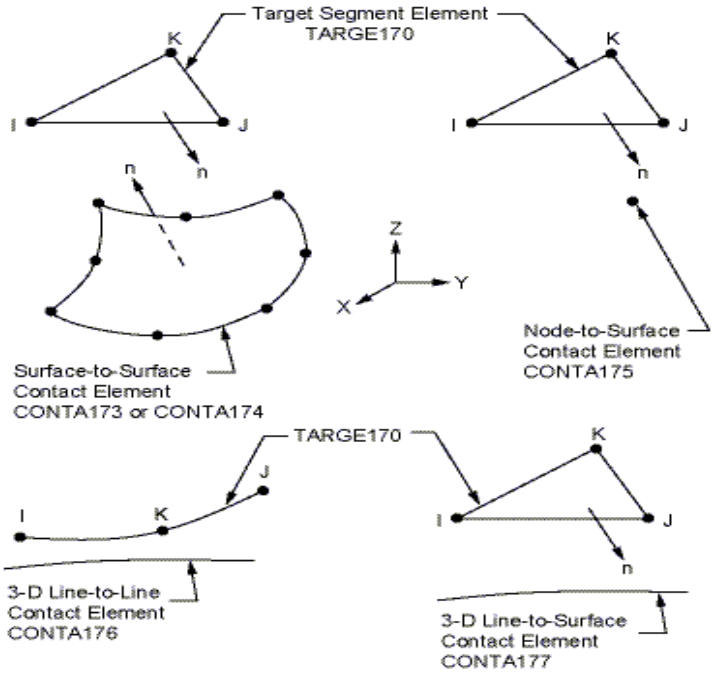

Figure 4.11 Target170 [Bending] (ANSYS Inc., 2012)

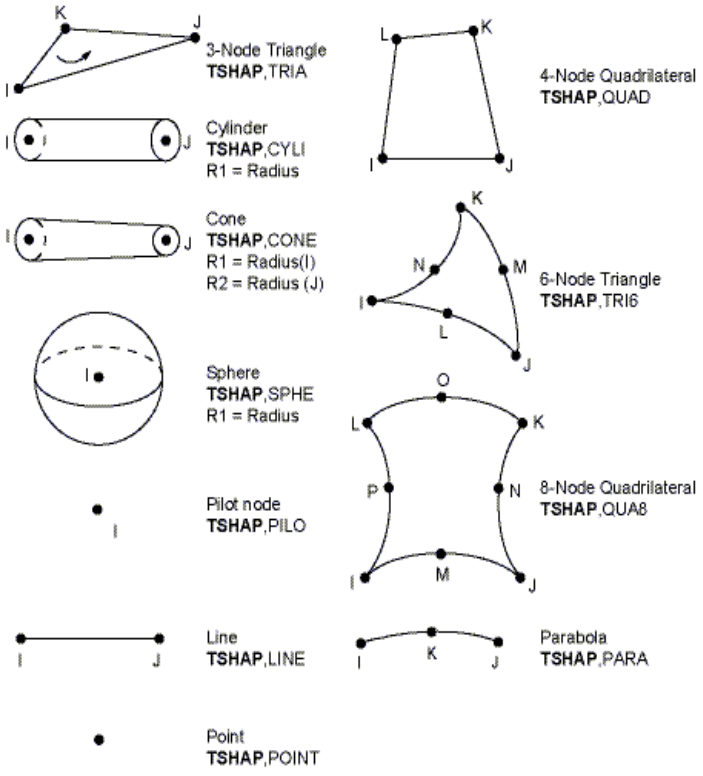

Figure 4.12 Target170 Segment types [Bending] (ANSYS Inc., 2012)

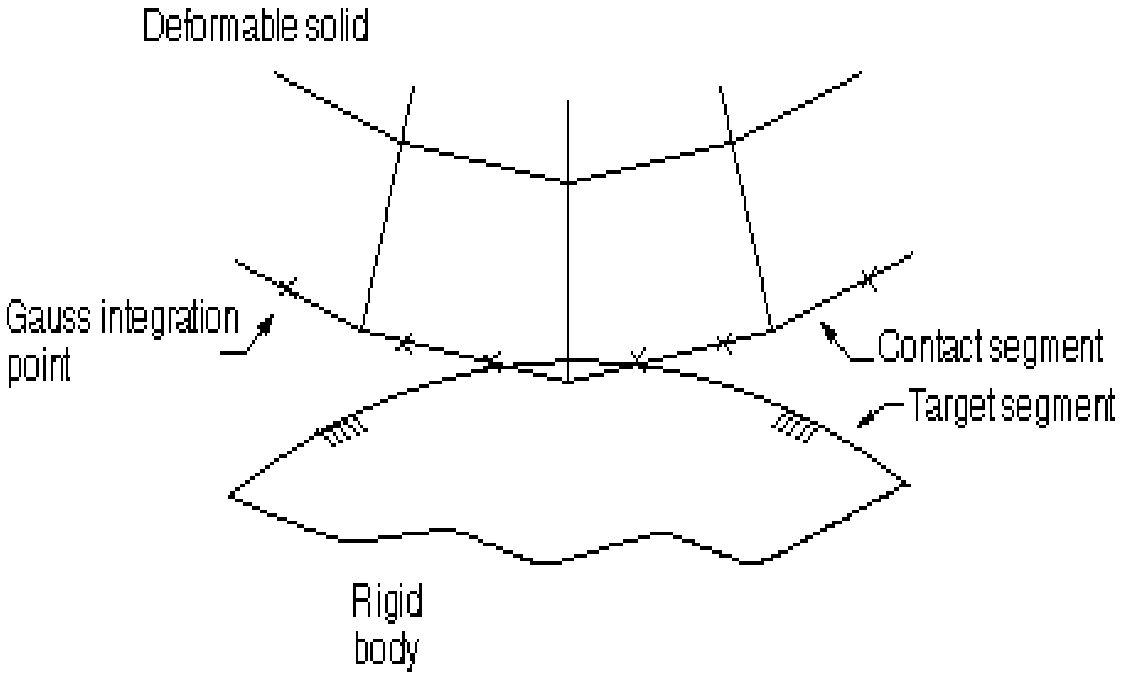

Figure 4.13 Contact detection point at Gauss point [Bending] (ANSYS Inc., 2012)

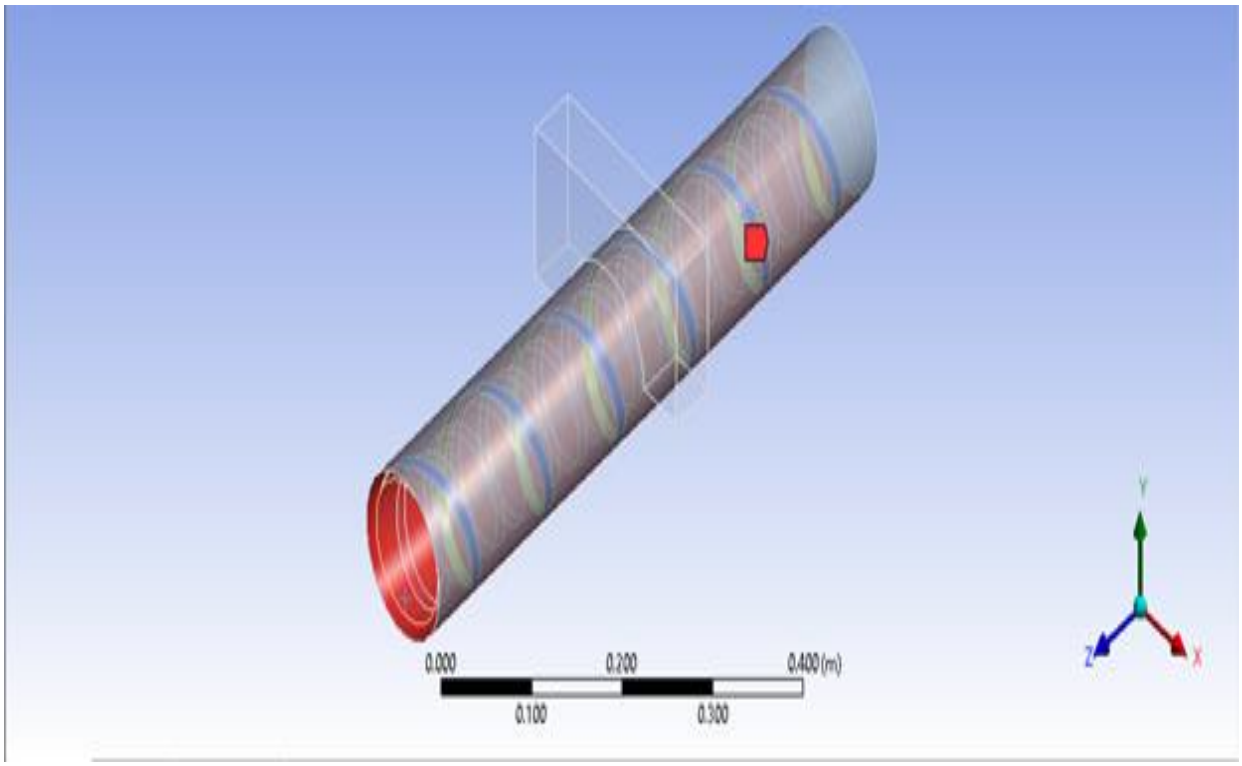

Figure 4.14 Contact modelling [Bending]

4.5 Load, Boundary Conditions, and Remained Controls

A uniform displacement boundary condition is used to analyse the tendon in ABAQUS. In this boundary condition all points on the one end section remain in plane throughout the analysis. An axial force is applied on the other end which gradually increases to 29kN. The boundary conditions and loading reference points was positioned at centre line of helix at the both ends (figures 4.15 and 4.16).

Figure 4.15 Schematic view of the Single Helical Tendon study

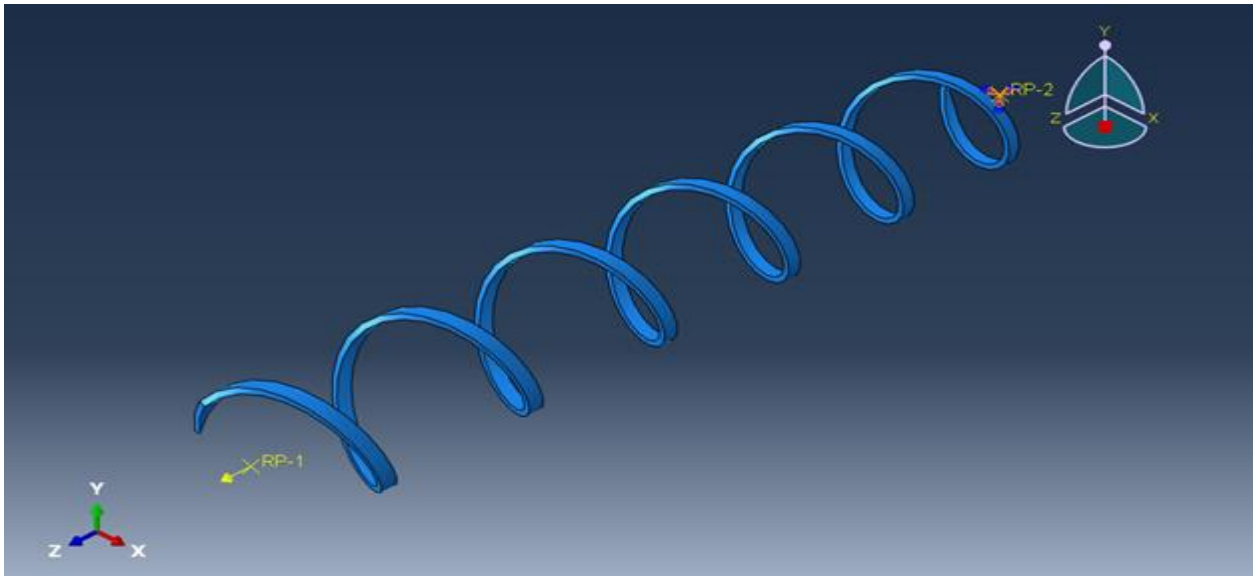

Figure 4.16 ABAQUS modelled load and boundary conditions using Reference Points [Static dead loading]

For the analysing of the riser in ANSYS, a loading force was applied at the support which is increased by 250N increment value to reach 13000N (figure 4.17). For unloading test analysis this value decreased to zero with the same increment. To model this process, tabular method was used in ANSYS Workbench. To keep load part in its position, a frictionless support was modelled through four surfaces surrounding the load component (blue surfaces in figure 4.18). For boundary conditions, one side of the riser modelled as fixed support whilst the other side can slide freely (see D, E, F, and G signs in figure 4.18). The numerical modelling of bending was assumed as non-linear problem because the interlayer effect of pipe structure is non-linear.

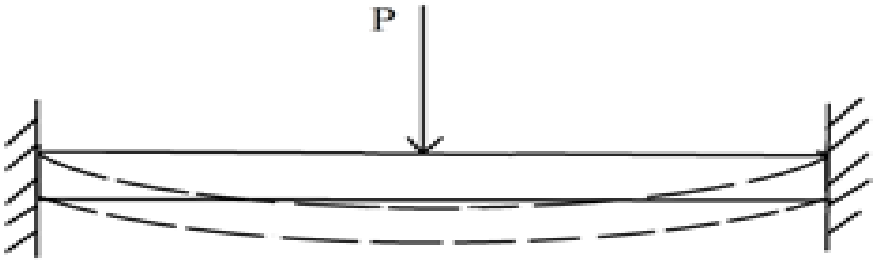

Figure 4.17 Schematic view of bending

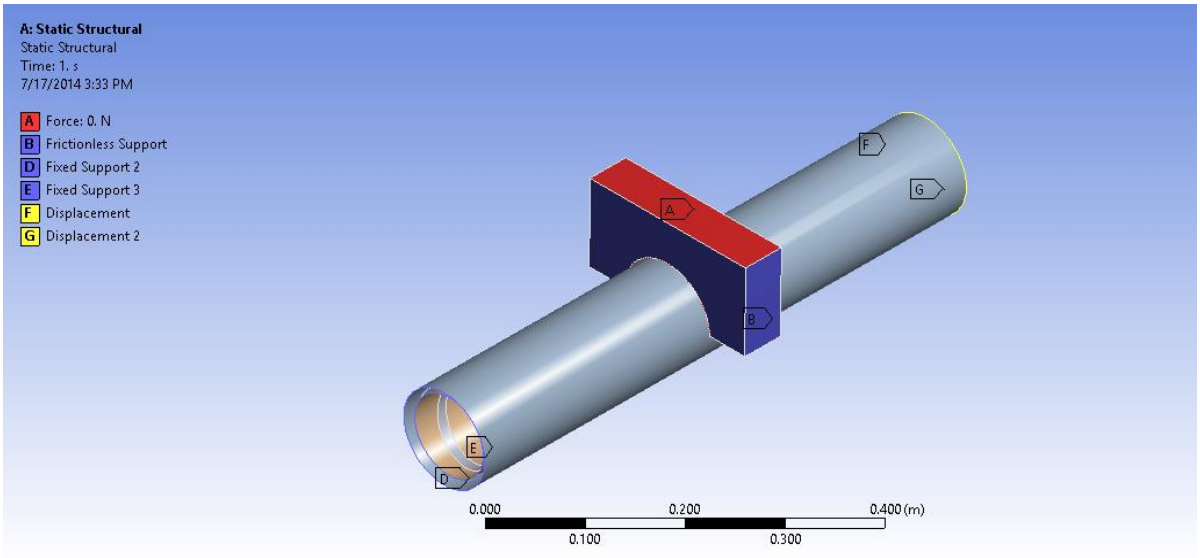

Figure 4.18 ANSYS modelled load, frictionless support, and boundary conditions [Bending]

4.6 Solution Methods

The solution model used in ANSYS and ABAQUS are briefly explained here (ANSYS Inc., 2012):

- **Full Integration**, also called $\overline{\mathrm{B}}$ method or selective reduced integration, this method prevents volumetric mesh locking in incompressible models. Volumetric strain at the Gauss integration point is replaced with the average volumetric strain of elements. The crucial problem of this way is restrictions in bending problems, where shear locking could not be ignored. Using the enhanced strain formulation in these conditions is strongly recommended.

- **Reduced Integration**, similar to previous method, in this method the volumetric mesh locking in incompressible models is banned. Although this method is much more accurate in terms of efficiency than full integration method, the accuracy of the respond is influenced by energy used for hourglass control.

- **Enhanced Strain Formulation**, shear locking for bending and volumetric locking in incompressible models are prevented in this method. The formulation introduces thirteen internal DOFs; nine of them are used to overcome shear locking at bending conditions. In some FE computer programs such as ANSYS these DOFs are made by the software and are not accessible by the users. Because of extra DOFs, static considerations, and low efficiency (lower than full integration), this method is roughly selected in the FE models.

- **Simplified Enhanced Strain Formulation**, similar to previous method, shear locking is prevented. The number of DOFs is reduced in this method. This means, the number of DOFs preventing volumetric locking are decreased; thus, the simplified formulation

cannot be used for incompressive materials in most of the models. This method is much better than previous one because of its lower degrees of freedom, yet full integration method is better than both of them.

- **Lagrange Multiplier Method in Contact Elements**, in this method, the given internal energy term is completed through a constraints set which was applied by a Lagrange multiplier and integrated over its volume, leads to an augmented form. For more details of this method please refer to appendix C.

For modelling bending in ANSYS, Full Integration method was used. The numerical solution method used in ABAQUS is Reduced Integration method.

4.7 Results and Discussion

4.7.1 Static Dead Loading

The fatigue failures of tendons in flexible risers are quite common. So, it is important to examine the predictive ability of FE methods for this layer compared with experimental results. A schematic model of residual displacements in tendon layer under axial load, predicted by ABAQUS software, is given in the figure 4.19.

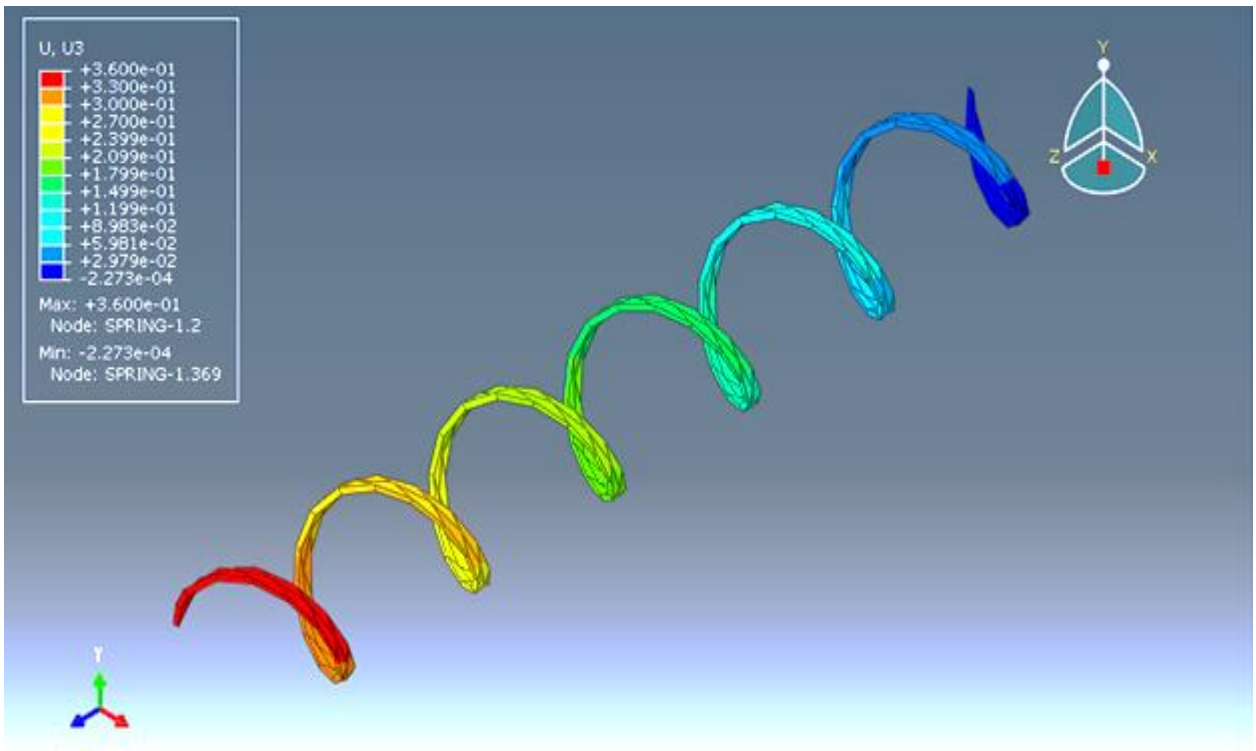

Figure 4.19 Deformation at last second [Static dead loading]

In all results an initial load equivalent to the lighter hanger weight (17.1605N) used in the experiment is applied. The load is then increased from 17.16N to 29N. The displacement-load relationship and corresponding experimental data is shown in figure 4.20. The strain-load results in figures 4.21 to 4.27 are plotted. Both the numerical results and experimental data show the residual strains with very little difference. The small difference in values is

resulted from the loading machine or numerical errors. It seems that the first four gauges on front side (gauges numbers one to four) have a symmetric reaction for unloading condition while this behaviour is not shown in the three other gauges. At this side, gauge number five has a similar trend to gauges number one and four, gauges number seven has a higher tensile changes, as it is close to the weights; the effects of both gauge numbers five and seven are neutralized in gauge number six, which demonstrates less difference in strain changes between tensile and torsion directions.

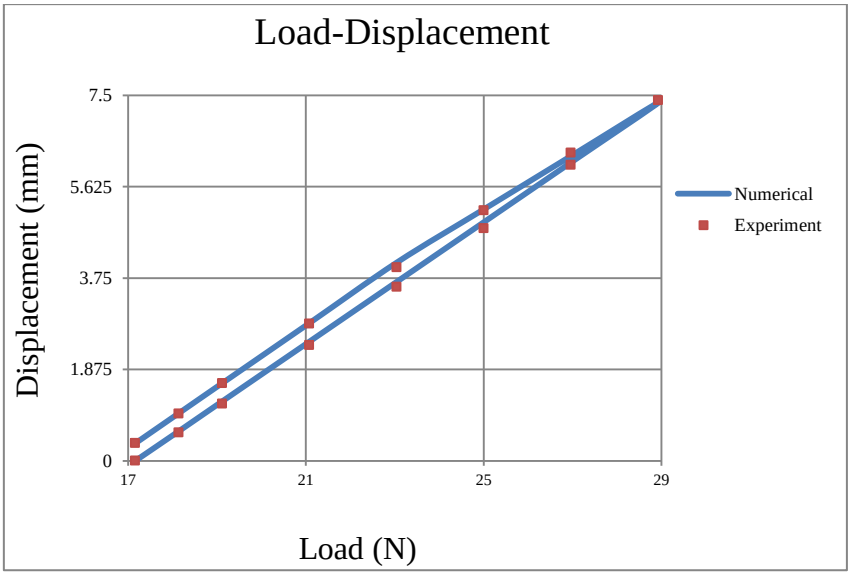

Figure 4.20 Displacement-Load curve

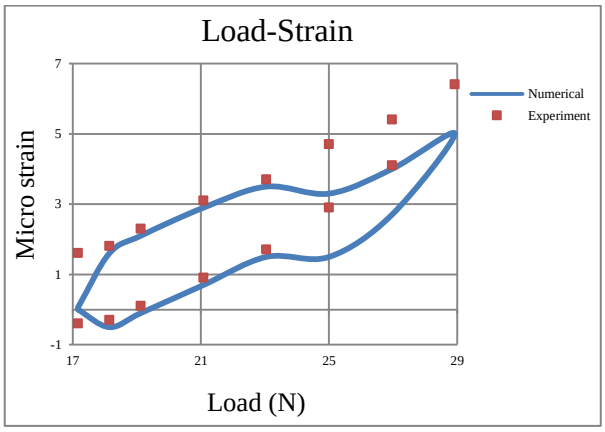

Figure 4.21.a Tensile Strain-Load curve at SG 1

[Single Tendon-Static dead loading]

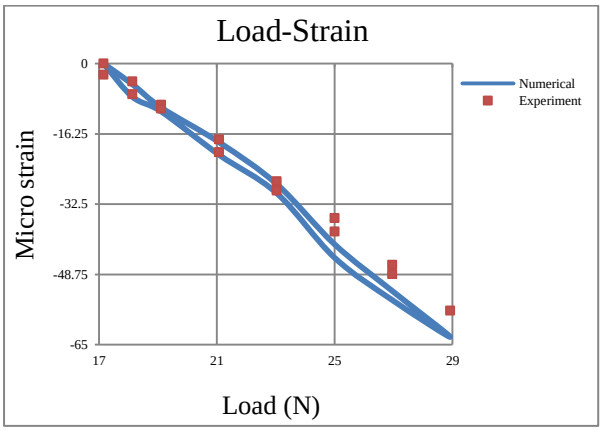

Figure 4.21.b Torsional Strain-Load curve at SG 1

[Single Tendon-Static dead loading]

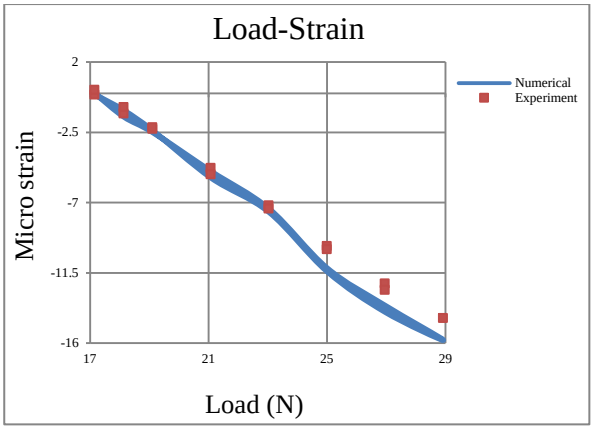

Figure 4.22.a Tensile Strain-Load curve at SG 2

[Single Tendon-Static dead loading]

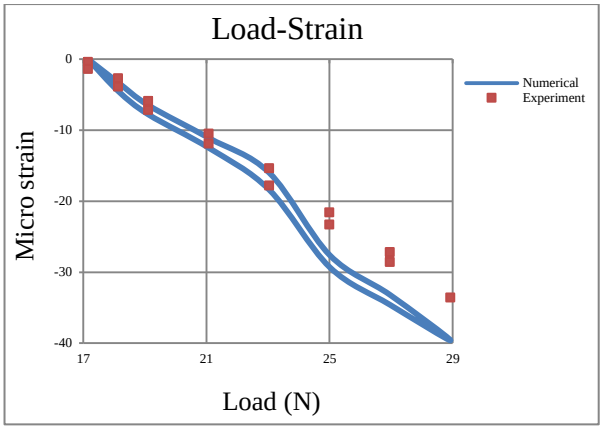

Figure 4.22.b Torsional Strain-Load curve at SG 2

[Single Tendon-Static dead loading]

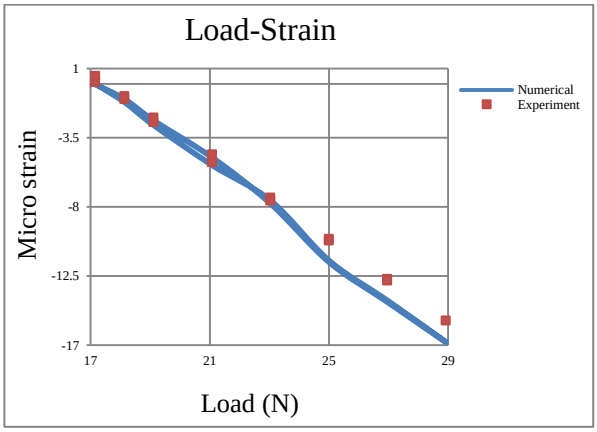

Figure 4.23.a Tensile Strain-Load curve at SG 3

[Single Tendon-Static dead loading]

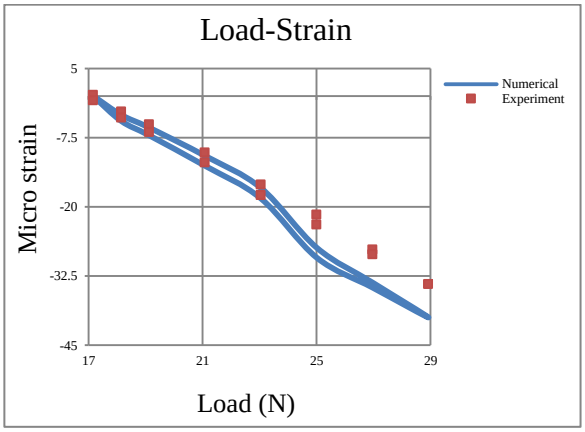

Figure 4.23.b Torsional Strain-Load curve at SG 3

[Single Tendon-Static dead loading]

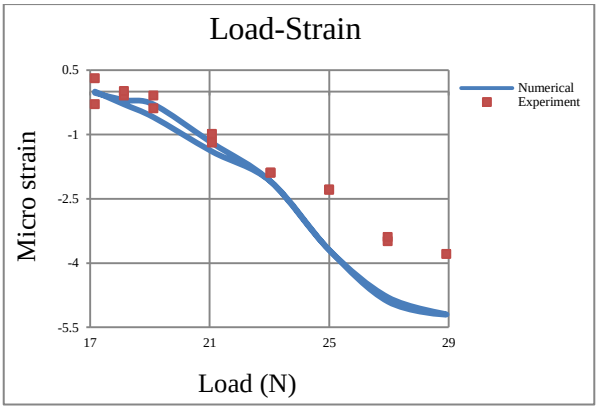

Figure 4.24.a Tensile Strain-Load curve at SG 4

[Single Tendon-Static dead loading]

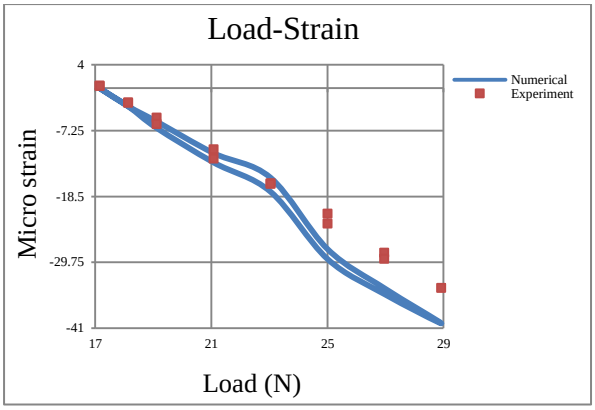

Figure 4.24.b Torsional Strain-Load curve at SG 4

[Single Tendon-Static dead loading]

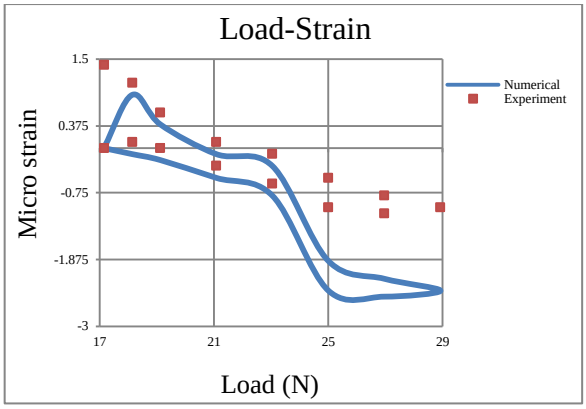

Figure 4.25.a Tensile Strain-Load curve at SG 5

[Single Tendon-Static dead loading]

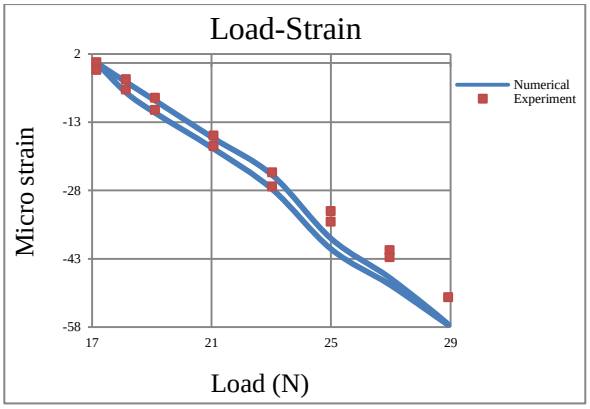

Figure 4.25.b Torsional Strain-Load curve at SG 5

[Single Tendon-Static dead loading]

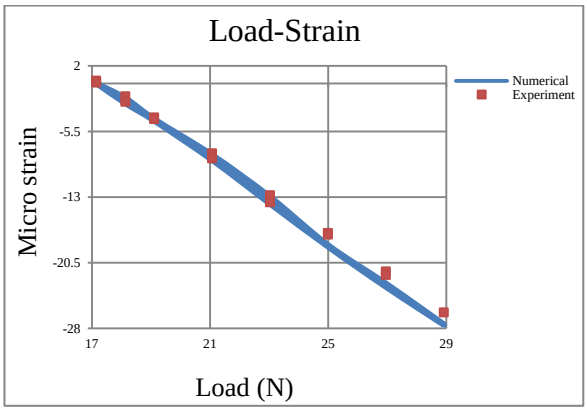

Figure 4.26.a Tensile Strain-Load curve at SG 6

[Single Tendon-Static dead loading]

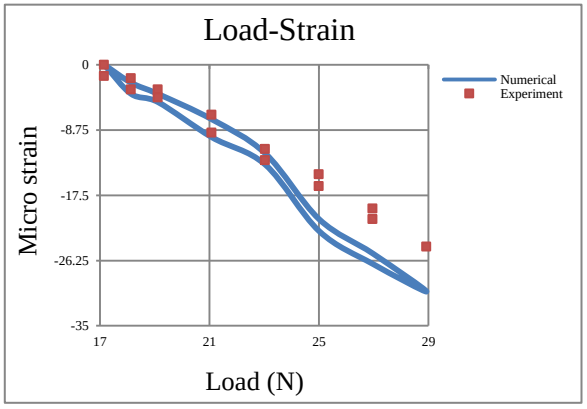

Figure 4.26.b Torsional Strain-Load curve at SG 6

[Single Tendon-Static dead loading]

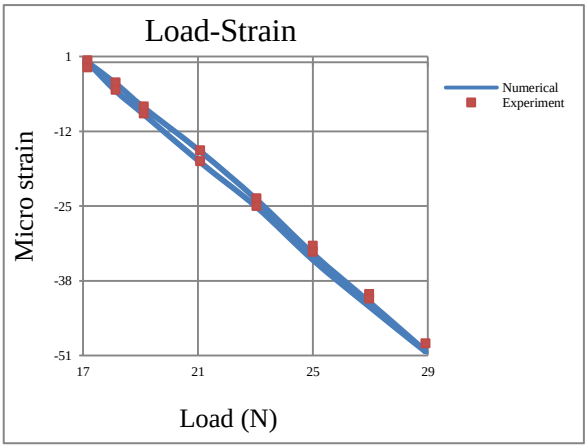

Figure 4.27.a Tensile Strain-Load curve at SG 7

[Single Tendon-Static dead loading]

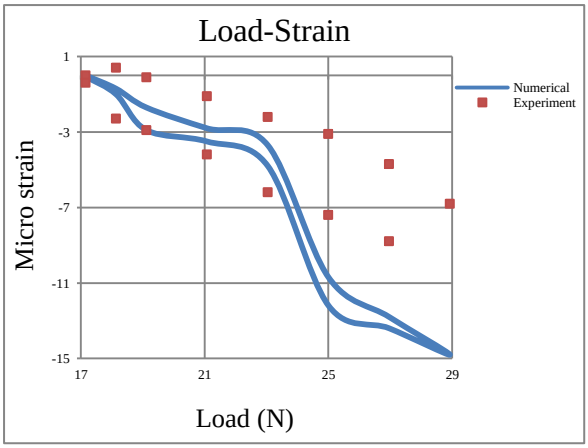

Figure 4.27.b Torsional Strain-Load curve at SG 7

[Single Tendon-Static dead loading]

4.7.2 Bending Simulation

The pipe model was tested under bending by applying load at the middle (figure 4.28).

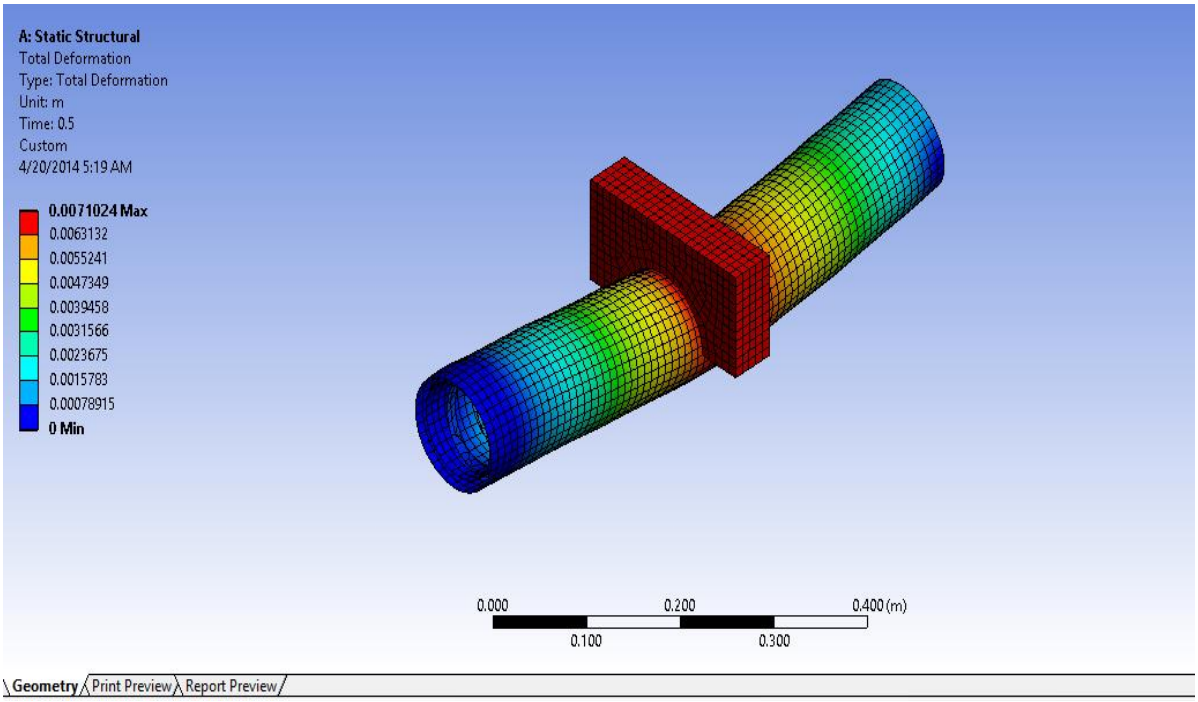

Figure 4.28 Deformed prototype (total direction) [Bending]

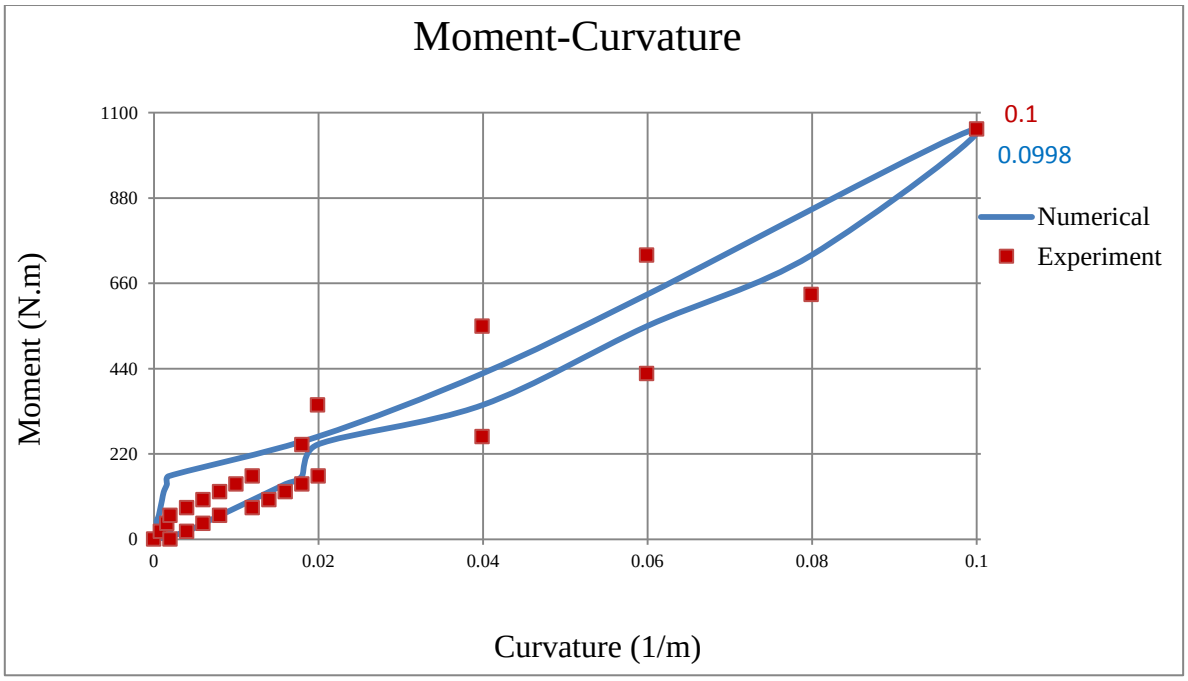

Figure 4.29 Moment Curvature [Bending]

When the external load is small a linear behaviour is shown in the resulting curvature. This is because, there is no slip between specimen layers and therefore, the trend of Moment-Curvature is linear. By applying more loads, external bending load overcomes the layers frictions and interlayer slip occurs and the non-linear behaviour in bending-moment curvature is appeared. There is no material non-linearity as the maximum load used is much less than the load required for the specimen yield point. So, the non-linear trend shown in figure 4.29 has only caused by interlayer behaviour of the structure. Although the values of the numerical analysis and experimental specimen are not exactly the same, the trend captured by the numerical model is very close to the experimental results. In figures 4.30 to 4.33 the strain-load diagrams of helical tendon for both torsional and compressive directions are demonstrated. Similar to figure 4.29, the trends of strain load diagrams are linear at the beginning and have steeper shape, and then it becomes non-linear because of interlayer effects.

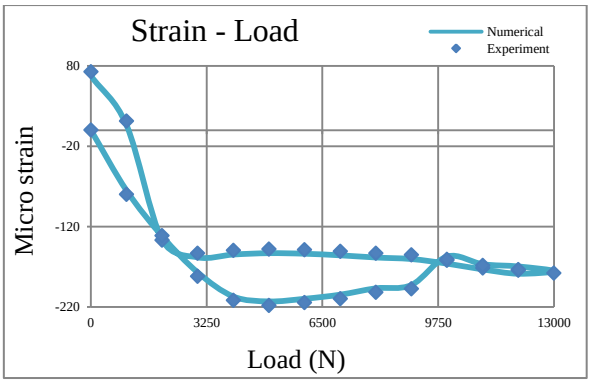

Figure 4.30.a Compressive Strain-Load curves at SG 1

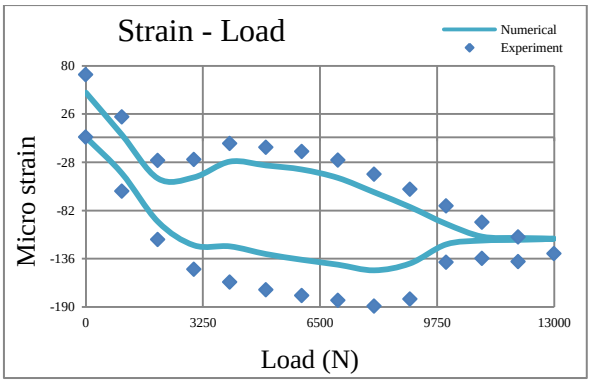

Figure 4.30.b Torsional Strain-Load curves at SG 1

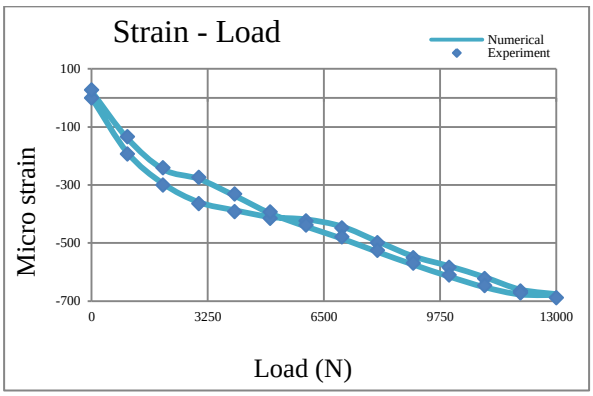

Figure 4.31.a Compressive Strain-Load curves at SG 2

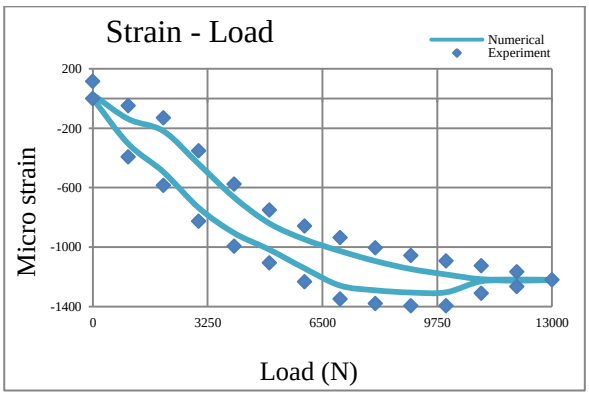

Figure 4.31.b Torsional Strain-Load curves at SG 2

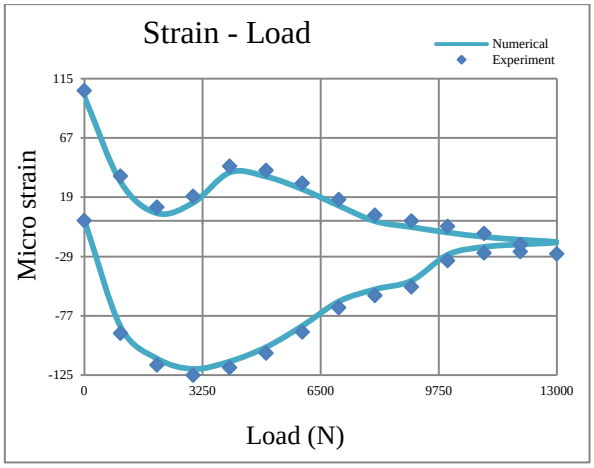

Figure 4.32.a Compressive Strain-Load curves at SG 3

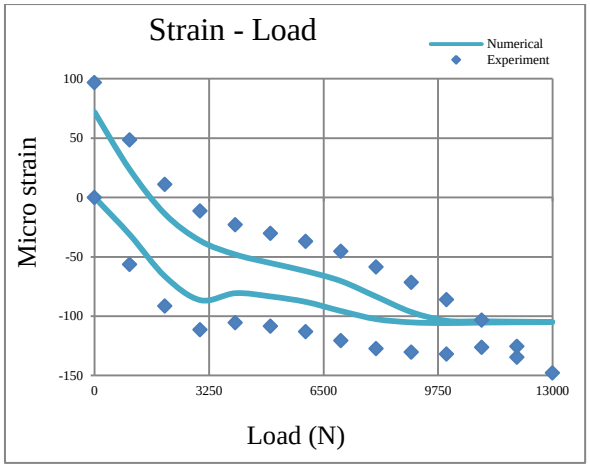

Figure 4.32b Torsional Strain-Load curves at SG 3

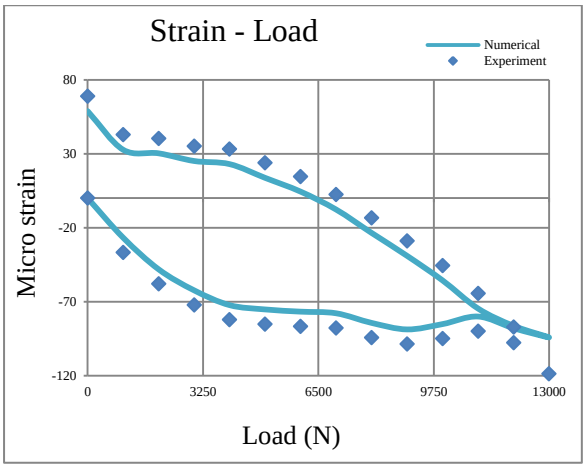

Figure 4.33.a Compressive Strain-Load curves at SG 5

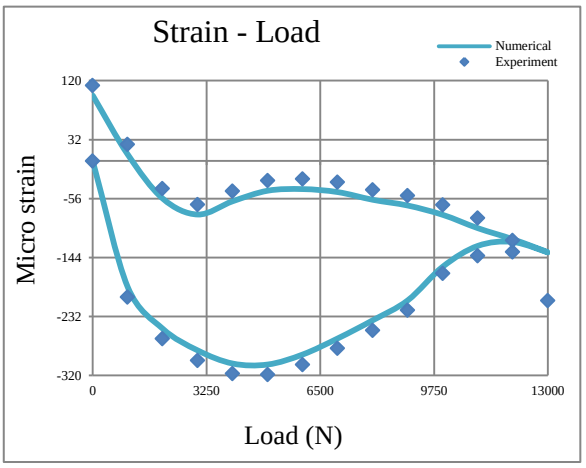

Figure 4.33.b Torsional Strain-Load curves at SG 5

4.8 Conclusion

The capabilities of the FE software for analysing flexible pipes are validated using experimental data. The investigation of a single tendon under axial load using a numerical model shows residual strains similar to the experimental data. The maximum error of numerical results in comparison with experimental data is 14%. Both the numerical model and experimental data show a non-linear behaviour in bending-moment curvature for flexible pipe under bending moment. The results highlight the need for non-linear FE methods for analysing flexible pipes.

Chapter 5:

Conclusion and Recommendations for Future Work

5.1 Conclusions

The two main objectives of this research have been successfully accomplished. One is the successful experiments of the prototype of a flexible pipe which has led to the understanding of the complex non-linear structural behaviour of flexible risers. The other is the validations of two non-linear finite element based programmes for analysing flexible pipes which has demonstrated the capability of finite element based methods in capturing the structural non-linearity observed in the experiments.

5.1.1 Experiments on the Flexible Pipe

Several experiments on a model of flexible pipe were conducted. First, a test was conducted on a single helical tendon layer. This is a significant test because the failure in helical wires is a major concern in flexible risers and analysing their behaviour is essential to understand their failure mechanism. The effects of static loads on the deformation and strain changes of a single helical tendon layer were investigated. Significant residual strains were observed when the tendon is under pure axial loading. Also, the creep behaviour of the tendon was examined and tendon creep curves were evaluated for each stain gauge.

The prototype of a flexible pipe was tested by applying variable bending loads to investigate the bending moment-curvature relationship. The prototype had a helical armour layers as a carcass in an actual riser, a helical tendon layer, and two tubes as outer sheath and anti-wear layers. It was shown that for small loads there is a linear behaviour between bending moment and curvature as there is no slip between specimen layers. However, by increasing the bending load, interlayer slip occurs and the non-linear behaviour in bending-moment curvature is observed. To make sure that no material non-linearity is present in the analysis, the maximum load used is much less than the load required for the specimen yield point. Also, the behaviour of the prototype of flexible pipe under axial loading was studied and the effect of internal pressure was tested. The displacement-load behaviour shows that there

was a strong non-linear behaviour in deformation trend in particular between 10 to 20 bar. Besides, the residual strains have been observed for buckling but not for the compression test.

5.1.2 Non-linear Finite Elements Methods

The predictive ability of FE methods compared with experimental results is examined for a model of a single tendon layer under axial load. Solid elements used to model the tendon with an eight node linear brick shaped element. The reduced integration method and hourglass control options was selected in ABAQUS software. Only one hundred and fifty elements were required for modelling the tendon in ABAQUS. An implicit solution procedure with fixed boundary conditions imposed at control nodes was used. The numerical results show residual strains with a pattern very similar to the experimental data. A very small difference exists between the numerical and experimental results, which is due to the loading machine and numerical errors.

A detailed finite element model of a flexible pipe has also been developed. This model is based on solid elements and takes into account contact interactions between all components in the pipe. In this model, the most recent developments in contact modelling such as application of a penalty method for enforcing normal contact constraints were used. The model uses an implicit solution procedure and fixed boundary conditions imposed with a control nodes. The pipe models were tested under bending by applying load at the middle of the pipe. Similar to the experimental data, numerical model predicts non-linear behaviour in bending-moment curvature for flexible pipe under bending moment. The results highlight the need for non-linear FE methods for analysing flexible pipes.

5.2 Recommendations for Future Work

The following three areas are identified as a potential of this work:

5.2.1 Enhancing of the Prototype

The experiment in this study was carried out on a prototype consists of a helical armour layer, a helical tendon layer, and two tubes as outer sheath and anti-wear layers. A typical unbounded flexible riser consists of about 6 to 20 layers with different material, performances and cross-sections. The tensile armour wires and the pressure sheaths are used in all unbounded flexible pipes. However, most flexible designs use additional layers to reduce gas permeability, provide thermal insulation or to increase flexibility. So, it is recommended to use a prototype with more number of layers. Also in this study only one helical armour or helical tendon is used which can be increase to about 30 for each layer. The role of tensile armour in the structural integrity of flexible risers are quite important as this layer is providing strength in longitudinal direction and gives support to the weight of all the layers and transferring that to end termination point on the structure or vessel. The tensile armour is also transferring some of the longitudinal load into an inward radial force analogous to the external pressure.

5.2.2 Further Numerical Investigations

A number of experiments were conducted in this study. However, only two sets of experiments are used to examine the capabilities of numerical methods for prediction of strain. Further numerical analysis can be performed to investigate the accuracy of FE software in predicting the behaviour of pipes in creep circumstances for various loads. Also the behaviour of the prototype under axial testing and the effects of internal pressure can be analysed numerically. The numerical results used for comparison would need to include

results for the stresses in the tensile wires, local bending stresses in the wires, as well as bending moment-curvature data under different values of internal pressure.

5.2.3 Multi-scale Approach

The numerical and experimental data presented in this work can be used to develop methodologies for large scale modelling of flexible pipes. One method is the development of constitutive models based on the framework of beam models. The relationship between generalised stresses and strains in the beam can be developed based on the analogy between frictional slipping between different layers of a flexible riser and frictional slipping between micro-planes of a continuum medium in non-associative elasto-plasticity. So, a linear elastic relationship can be used for the initial response in which no-slip occurs and a non-associative rule with linear kinematic hardening to model the full-slip phase, Bahtui (2008). Alternatively computational homogenisation procedures currently in widespread use for the modelling of composite materials can be developed for multi-scale modelling of flexible risers. These methods allow the large-scale dynamics of large installed pipes to be related to the behaviour of its internal components which was examined in this study, Edmans (2012).

Bibliography

Advanced Technology Program, 2004, *Composites Manufacturing Technologies: Applications in Automotive, Petroleum, and Civil Infrastructure Industries Economic Study of a Cluster of ATP-Funded Projects*

ANSYS Inc., 2012, ANSYS 13 help viewer [Computer Programme].

API Specification 17J, 2002, *Specification for Unbonded Flexible Pipe,* American Petroleum Institute

Bahtui, A., Bahai, H., Alfano, G., 2009. Numerical derivation of constitutive models for unbonded flexible risers, *International Journal of Mechanical Sciences*, 51, pp. 295-304

Bahtui, A., 2008. *Development of a Constitutive Model to Simulate Unbonded Flexible Riser Pipe Elements.* Ph.D. thesis, Department of mechanical engineering, Brunel University, London, UK

Bai, Q., Bai, Y., 2010. *Subsea Engineering Handbook*, London: Gulf Professional Publishing / Elsevier

Bauchau, O.A., Craig, J.I., 2009. *Structural Analysis*, Dordrecht: Springer, pp: 173-221

Beden, S. M., Abdullah, S., Ariffin, A. K., 2009. Review of Fatigue Crack Propagation Models for Metallic Components, *European Journal of Scientific Research*, 28 (3), pp.364-397

Byer, O., Lazebnik, F., Smeltze, D., 2010, *Methods for Euclidean Geometry*, USA: Mathematical Association of America, p. 210

Carpinteria, A., Paggi, M., 2007, Are the Paris' Law Parameters Dependent on each other? *Frattura ed Integrità Strutturale*, 2, pp. 10-16

Clarke, T., Jacques, R., Bisognin, A., Camerini, C., Damasceno, S., Strohaecker, T. 2011, Monitoring the structural integrity of a flexible riser during a full-scale fatigue test, *Engineering Structures*, 33, pp.1181–1186

Clements, R.A., Jamal, N., Sheldrake, T., 2006, Riser Strategies: Fatigue Testing and Analysis Methodologies for Flexible Risers. In: Offshore Technology Conference, Houston, USA, 1-4 May 2006. Offshore Technology Conference

Custódio, A.B., Vaz, M.A., 2002. A nonlinear formulation for the axisymmetric response of umbilical cables and flexible pipes, Applied Ocean Research 24, pp. 21-29

Dassault Systems Simulia Corp., 2013, ABAQUS Analysis User's Guide [Computer Programme].

Dhondt, G., 2011, Eight-node brick element with reduced integration (C3D8R and F3D8R), MIT University, Massachusetts, US

Edmans, B., 2012. *Non-linear Finite Element Analysis of Flexible Pipes for Deep-water Applications.* Ph.D. thesis, Department of mechanical engineering, Brunel University, London, UK

Féret, J.J., Bournazel, C.L., 1987. Calculation of stresses and slip in structural layers of unbonded flexible pipes. Journal of Offshore Mechanics and Arctic Engineering 109, pp. 263-269.

Fernández, L. Troyano (2003). *Bridge Engineering: A Global Perspective*. London: Thomas Telford. 514

Felippa, C.A., Chung, J.S., 1981. Nonlinear static analysis of deep ocean mining pipe, Transactions of the ASME: Journal of Energy Resources Technology 103, pp. 11-25

Harte, A.M., McNamara, J.F., 1993. Modeling procedures for the stress analysis of flexible pipe cross-sections. Journal of Offshore Mechanics and Arctic Engineering 115, pp. 46-51

Huang, N. C., 1978. Finite Extension of an Elastic Strand with a Central Core, *Journal of Applied Mechanics*, 45, pp. 852-858

Illinois Tool Works Inc., 2008, *8800 Servohydraulic Testing Systems*

Illinois Tool Works Inc., 2012, *8801 Servohydraulic Fatigue Testing System Up to 100kN*

Kebadze, E., Kraincanic, I., 2001, Slip initiation and progression in helical armouring layers of unbonded flexible pipes and its effect on pipe bending behavior, *The Journal of Strain Analysis for Engineering Design,*36(3), pp. 265-275

Knapp, R.H., 1979. Derivation of a new stiffness matrix for helically armoured cables considering tension and torsion. International Journal for Numerical Methods in Engineering 14, pp. 415-529.

Lanteigne, J., 1985, Theoretical estimation of the response of helically armoured cables to tension, torsion and bending, Journal of Applied Mechanics, 52, pp. 423-432

Larsen, C.M, 1992, Flexible riser analysis: comparison of results from computer programs, *Marine Structures*, 5(2-3), pp. 103-119

Le Corre, V., Probyn, I., 2009, Validation of a 3-dimensional finite element analysis model of a deep-water steel tube umbilical in combined tension and cyclic bending, in: Proceedings of the International Conference on Offshore Mechanics and Arctic Engineering, Honolulu, Hawaii

Leroy, J.M., Estrier, P., 2001, Calculation of stresses and slips in helical layers of dynamically bent flexible pipes. Oil and Gas Science and Technology - Rev. IFP 56, pp. 545-554

Leroy, J.M., Estrier, P., et al, T.P., 2010, Stress assessment in armour layers of flexible risers, in: Proceedings of the ASME 2010 29th International Conference on Offshore, Ocean and Arctic Engineering. OMAE2010-20932

Love, A.E.H., 1927, *A Treatise on the Mathematical Theory of Elasticity*, Dover, New York, 4th edition.

Løseth, K., 2011, *Response of Flexible Risers in Bend Stiffener Area*, M.Sc. NTNU Norwegian University of Science and Technology

MacFarlane, C.J., 1989. Flexible riser pipes: problems and unknowns, *Engineering Structures*, 11(4), pp. 281–289

McIver, D.B., 1995, A method for modelling the detailed component and overall structural behaviour of flexible pipe sections. Engineering Structures 17, pp. 254-266

Norouzi, S. 2012, Simulation of Bending in Off-shore Flexible Risers: Deformation of Tendon Layers. In: Brunel University, *ResCon (Annual Research Conference).* London, UK, 19 June 2012. London: Brunel University.

Out, J.M.M., von Morgen, B.J., 1997, Slippage of helical reinforcing on a bent cylinder, Engineering Structures 19, pp. 507-515

PSA, 2013. *Un-bonded Flexible Risers - Recent Field Experience and Actions for Increased* Robustness, Norway: PSA

Prasad, B.B., 2009. *Fundamentals of Soil Dynamics and Earthquake Engineering*, Delhi: PHI Learning, pp. 178-179

Rial, D., Kebir, H., Wintrebert, E., Roelandt, J. M., 2013, Multi-axial fatigue analysis of a metal flexible pipe, *Materials and Design*, 54 (2014), pp. 796–804

Risa, A., 2011, Finite element analysis of marine umbilical, Master's thesis, Department of Marine Structures, NTNU, Trondheim, Norway

Shetty, M. N., 2013. *Dislocations and Mechanical Behaviour of Materials*, India: Prentice Hall of India Pvt. Ltd pp. 496-498

Solartron Instruments Ltd., 1993, *Scorpio Data Acquisition System USER MANUAL*

Sævik, S., 1993, A finite element model for predicting stresses and slip in flexible pipe armouring tendons, *Computers and Structures*, 46(2), pp. 219-230

Sævik, S., 2010, Comparison between theoretical and experimental flexible pipe bending stresses, in: Proceedings of the ASME 2010 29th International Conference on Offshore, Ocean and Arctic Engineering, OMAE2010-20352

Sævik, S., 2011, Theoretical and experimental studies of stresses in flexible pipes, *Computers and Structures*, 89, pp. 2273-2291

Tan, Z., Case, M., Sheldrake, T., 2005, Higher Order Effects on Bending of Helical Armor Wire Inside an Unbonded Flexible Pip, In: ASME (American Society of Mechanical Engineers), 24th International Conference on Offshore Mechanics and Arctic Engineering, Halkidiki, Greece, 12-17 June 2005, ASME

Tan, Z., Quiggin, P., Sheldrake, T., 2007, Time domain simulation of the 3D bending hysteresis behaviour of an unbonded flexible riser, in: Proceedings of the 26th International Conference on Offshore Mechanics and Arctic Engineering. OMAE2007-29315

Tong, L.S., Tang, Y.S., ed., 1997. *Boiling Heat Transfer and Two-Phase Flow*, Washington D.C.: Taylor & Francis, pp. 55-56

Vaz, M.A., Rizzo, N.A.S., 2011. A finite element model for flexible pipe armor wire Instability, *Marine Structures*, 24, pp. 275–291

Velinsky, S.A., Anderson, G.L., Costello, G.A., 1984, Wire Rope with Complex Cross Section, *Journal of Engineering Mechanics*, 110, pp. 380-391

Vishay Measurements, n.d. Strain Gauge Installations with M-Bond 200 and AE-10 Adhesive Systems

Witz, J., Tan, Z., 1992, On the Flexural Structural Behaviour of Flexible Risers, Umbilicals and Marine Cable. Marine Structures 5, pp.229-249

Witz, J.A., Tan, Z., 1995, Rotary bending of marine cables and umbilicals, Engineering Structures 17, pp. 267-275

Yue, Q., Lu, Q., Yan, J., Zheng, J., Palmer, A., 2013, Tension behavior prediction of flexible pipelines in shallow water, *Ocean Engineering*, 58, pp. 201–207

Zhao, B., 2013. *Fatigue Analysis of Flexible Riser - Effect of Mean Stress Correction Procedures.* M.Sc., NTNU Norwegian University of Science and Technology

Østergaard, N., Lyckegaard, A., Andreasen, J.H., 2012a. Imperfection analysis of flexible pipe armor wires in compression and bending, *Applied Ocean Research*, 38, pp. 40–47

Østergaard, N., Lyckegaard, A., Andreasen, J.H., 2012b. On modelling of lateral buckling failure in flexible pipe tensile armour layers, *Marine Structures*, 27, pp. 64-81

Appendix A

Axial (Compression)

Test Results

This appendix contains several axial loading tests under various conditions which were performed in this study. These results which can be used as a benchmark for validating FE models are shown in figures AA1 to AA161.

Inner Tube, Max Load= 3000N, Increment= 200N, Pressure= 1bar (No Oil)

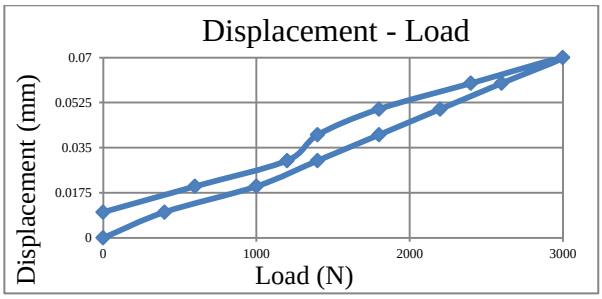

Figure AA1 Displacement-Load curve

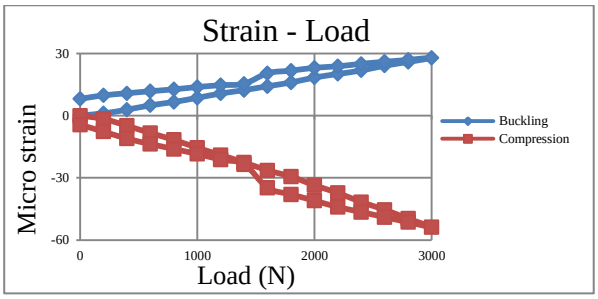

Figure AA2 Strain-Load curve at SG 1

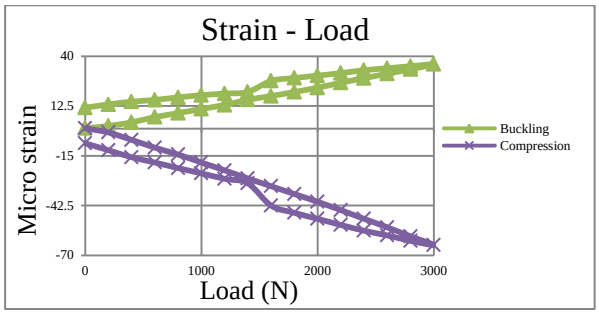

Figure AA3 Strain-Load curve at SG 2

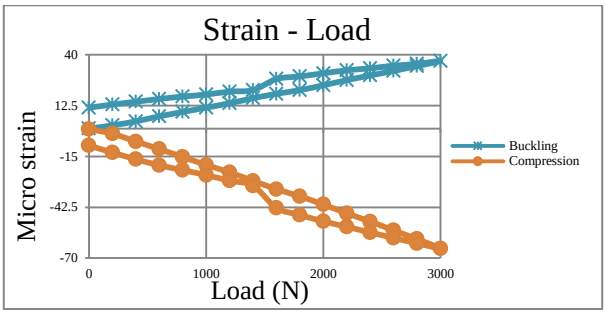

Figure AA4 Strain-Load curve at SG 3

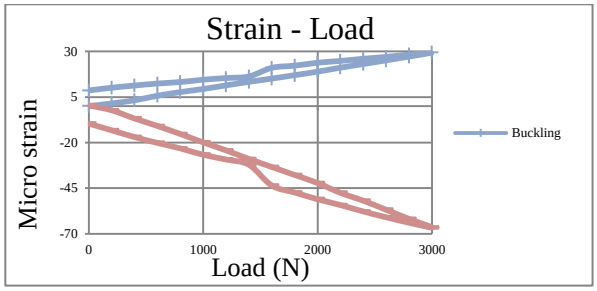

Figure AA5 Strain-Load curve at SG 4

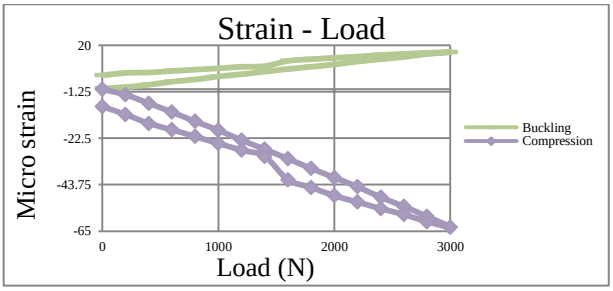

Figure AA6 Strain-Load curve at SG 5

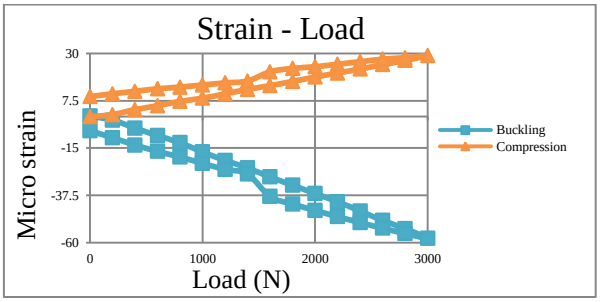

Figure AA7 Strain-Load curve at SG 6

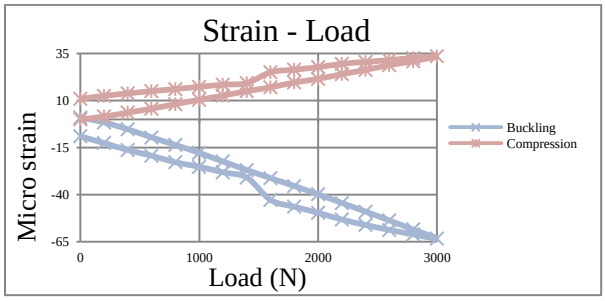

Figure AA8 Strain-Load curve at SG 7

Inner Tube, Max Load= 3000N, Increment= 200N, Pressure= 1bar

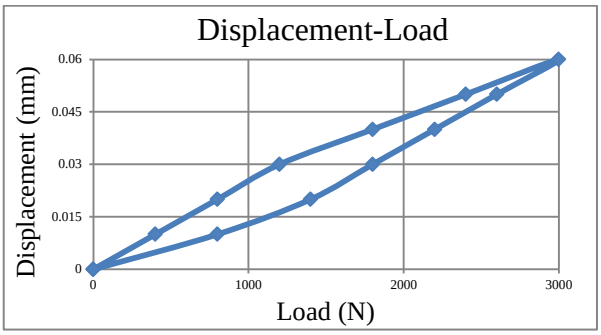

Figure AA9 Displacement-Load curve

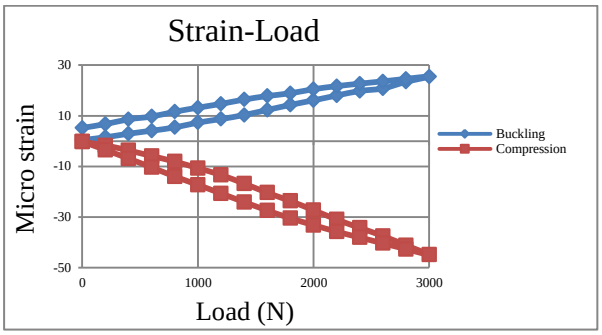

Figure AA10 Strain-Load curve at SG 1

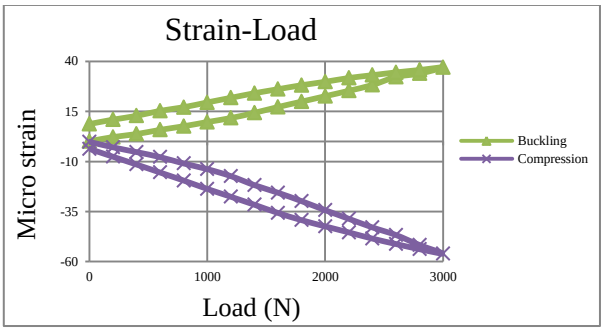

Figure AA11 Strain-Load curve at SG 2

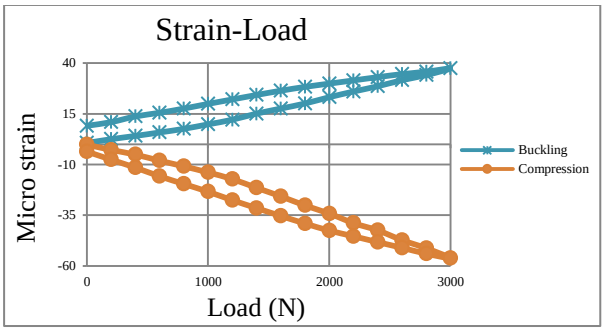

Figure AA12 Strain-Load curve at SG 3

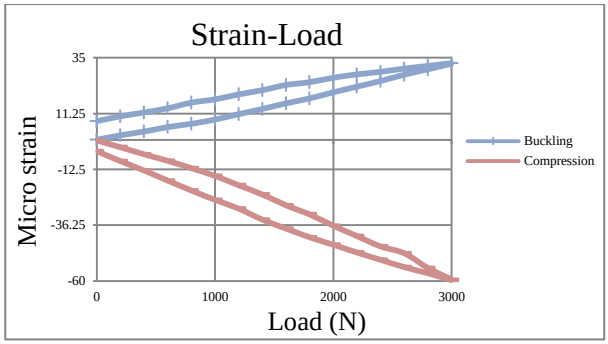

Figure AA13 Strain-Load curve at SG 4

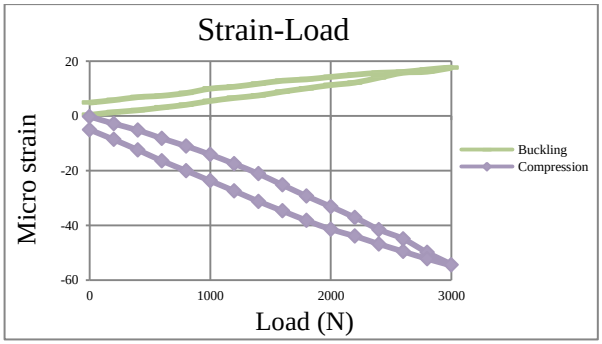

Figure AA14 Strain-Load curve at SG 5

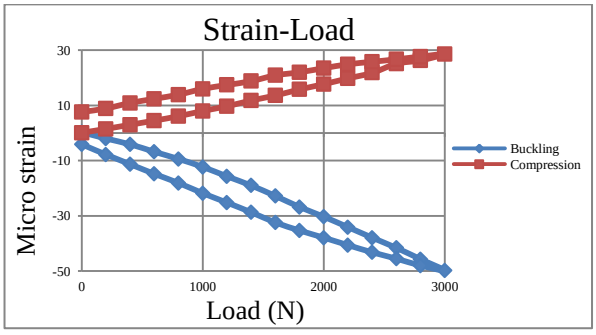

Figure AA15 Strain-Load curve at SG 6

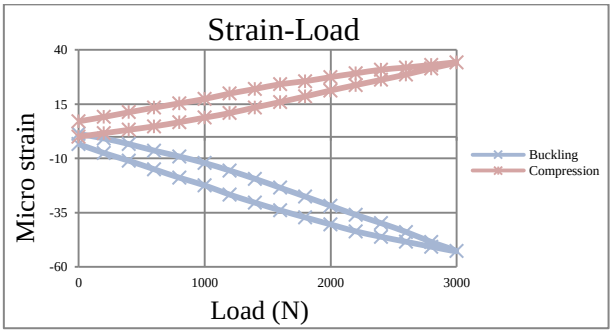

Figure AA16 Strain-Load curve at SG 7

Inner Tube, Max Load= 3000N, Increment= 200N, Pressure= 5bar

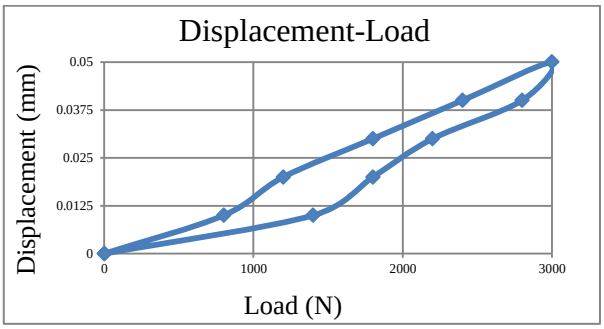

Figure AA17 Displacement-Load curve

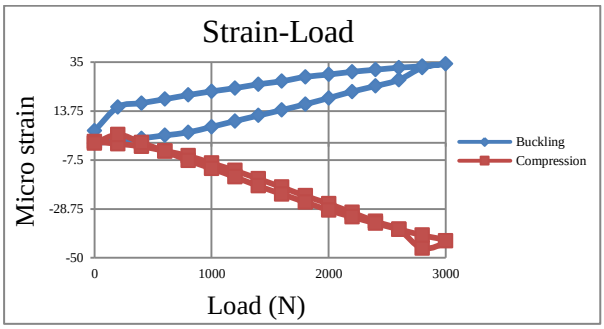

Figure AA18 Strain-Load at SG 1

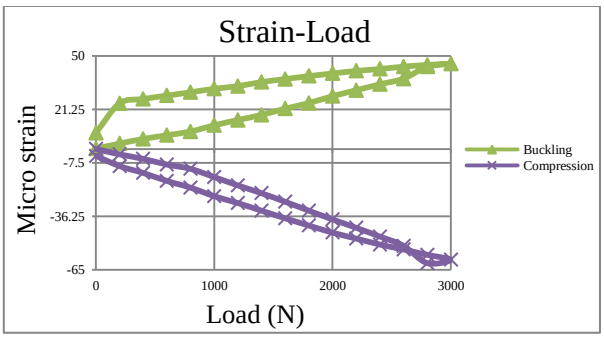

Figure AA19 Strain-Load at SG 2

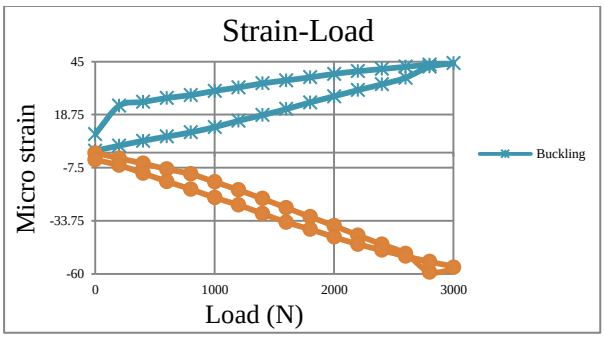

Figure AA20 Strain-Load at SG 3

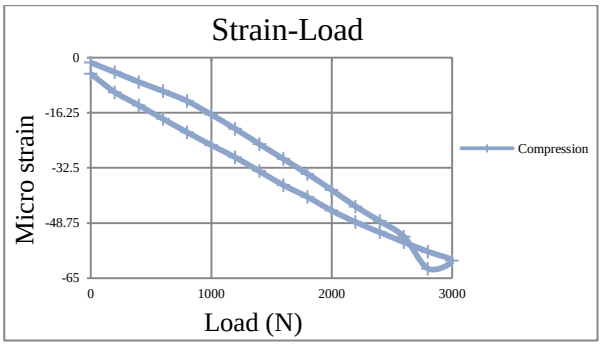

Figure AA21 Strain-Load at SG 4

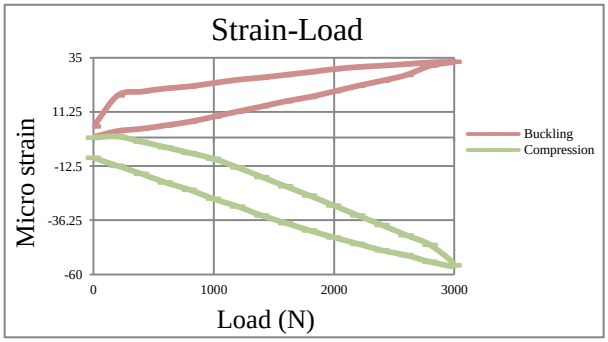

Figure AA22 Strain-Load at SG 5

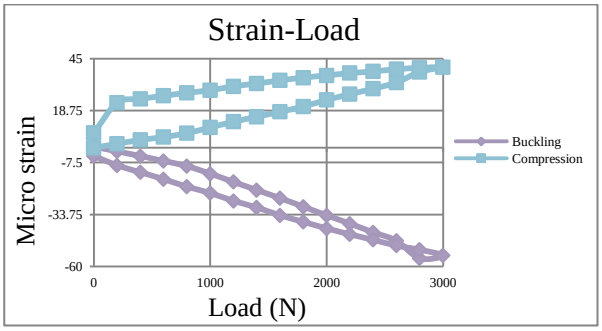

Figure AA23 Strain-Load at SG 6

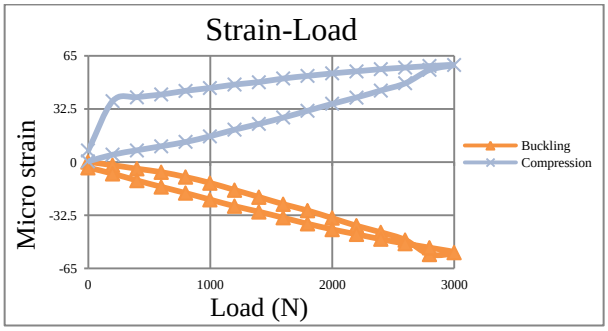

Figure AA24 Strain-Load at SG 7

Inner Tube, Max Load= 3000N, Increment= 200N, Pressure= 10bar

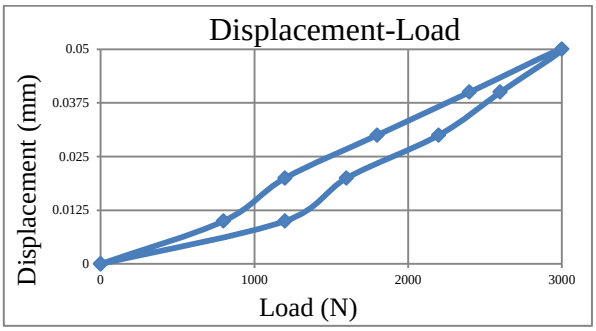

Figure AA25 Displacement-Load curve

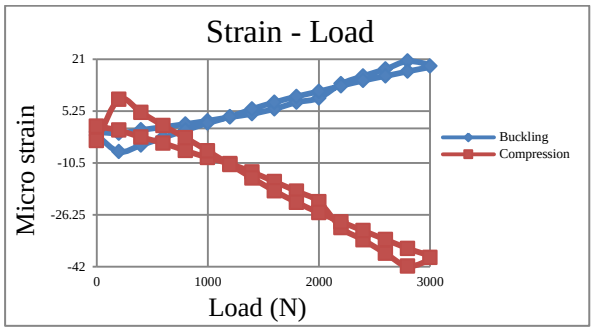

Figure AA26 Strain-Load curve at SG 1

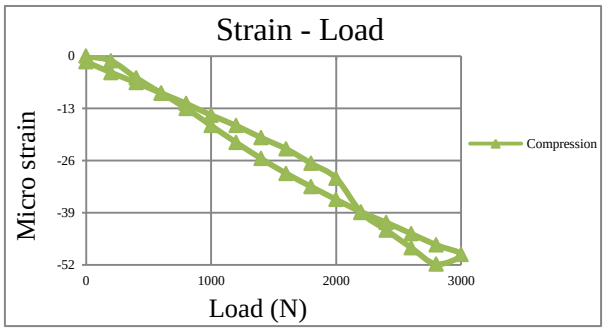

Figure AA27 Strain-Load curve at SG 2

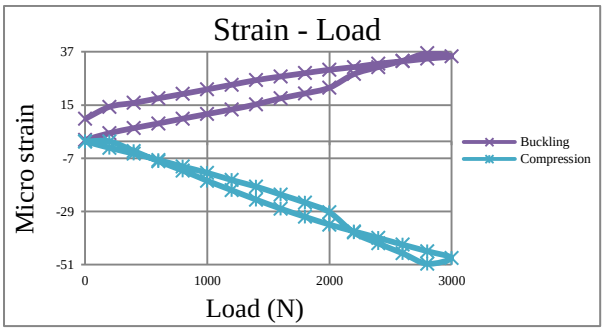

Figure AA28 Strain-Load curve at SG 3

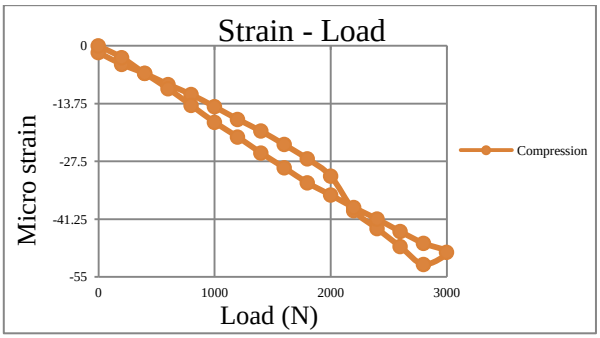

Figure AA29 Strain-Load curve at SG 4

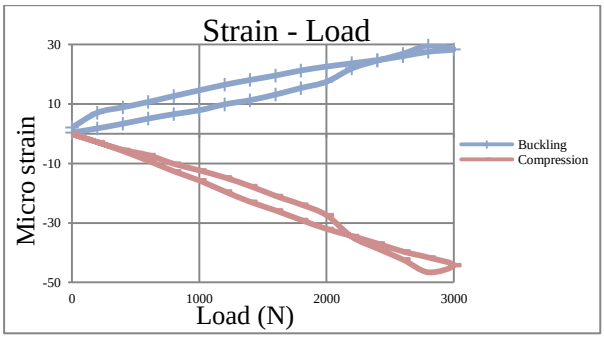

Figure AA30 Strain-Load curve at SG 5

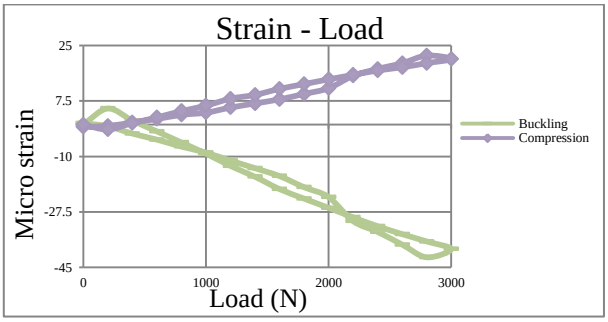

Figure AA31 Strain-Load curve at SG 6

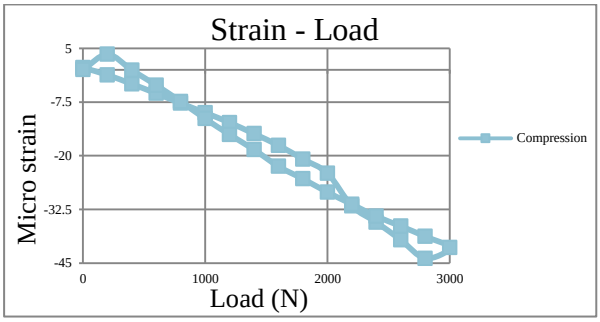

Figure AA32 Strain-Load curve at SG 7

Inner Tube, Max Load= 3000N, Increment= 200N, Pressure= 15bar

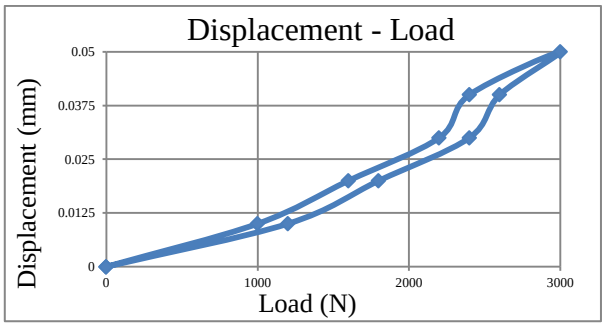

Figure AA33 Displacement-Load curve

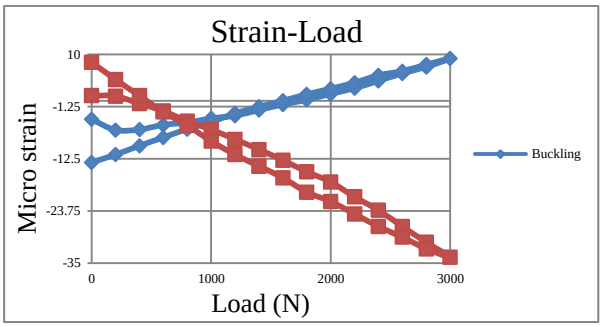

Figure AA34 Strain-Load curve at SG 1

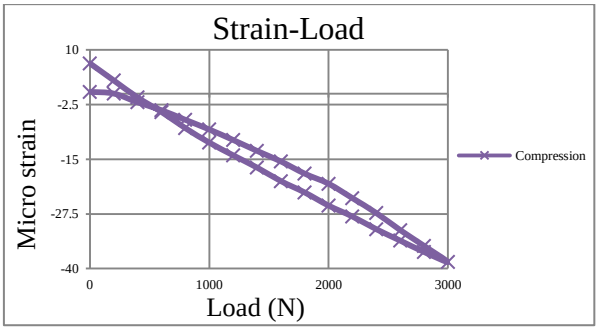

Figure AA35 Strain-Load curve at SG 2

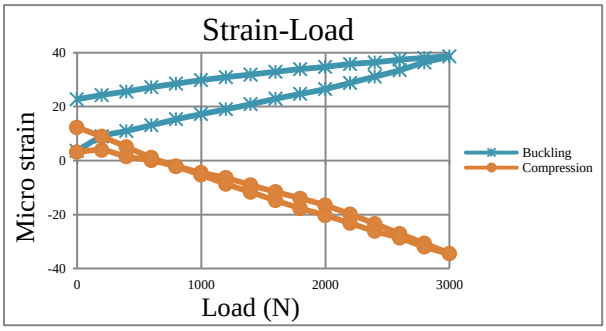

Figure AA36 Strain-Load curve at SG 3

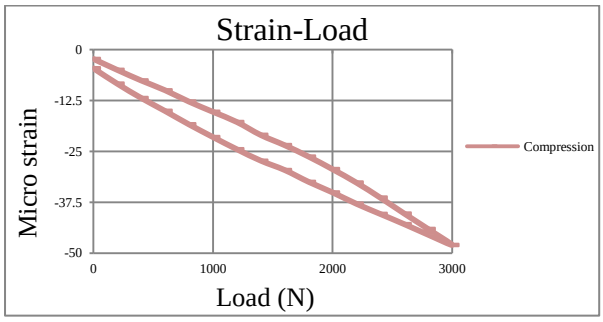

Figure AA37 Strain-Load curve at SG 4

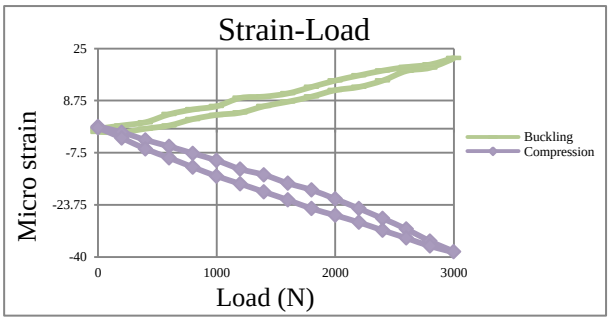

Figure AA38 Strain-Load curve at SG 5

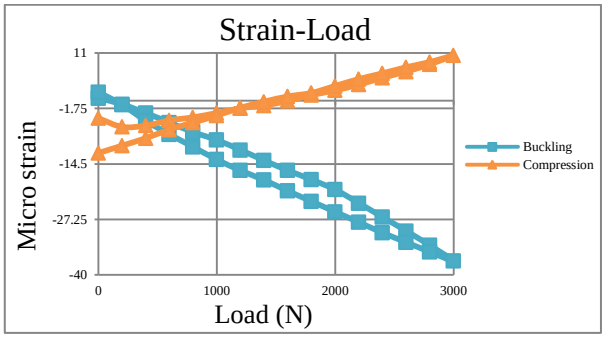

Figure AA39 Strain-Load curve at SG 6

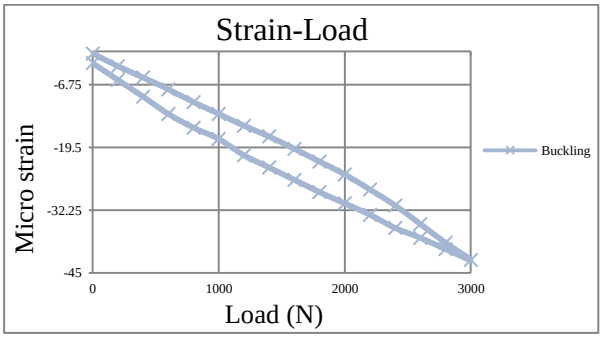

Figure AA40 Strain-Load curve at SG 7

Inner Tube, Max Load= 3000N, Increment= 200N, Pressure= 20bar

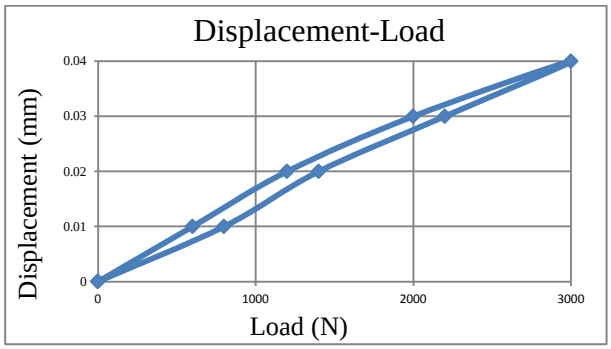

Figure AA41 Displacement-Load curve

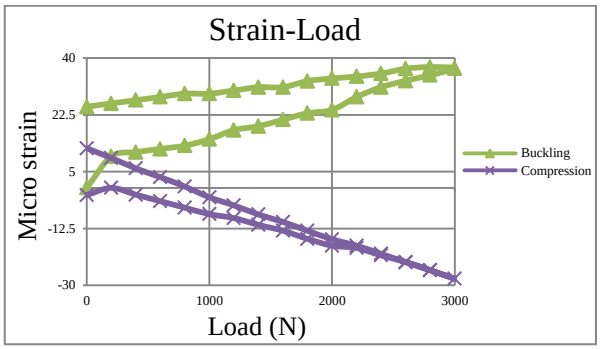

Figure AA42 Strain-Load curve at SG 1

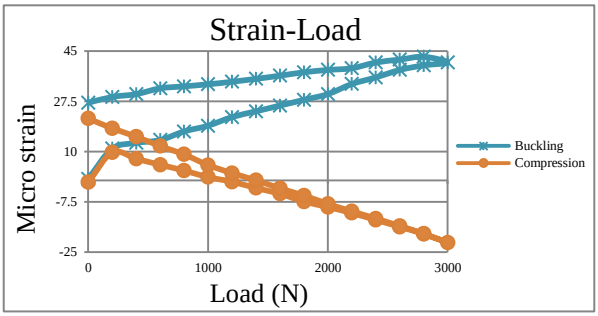

Figure AA43 Strain-Load curve at SG 2

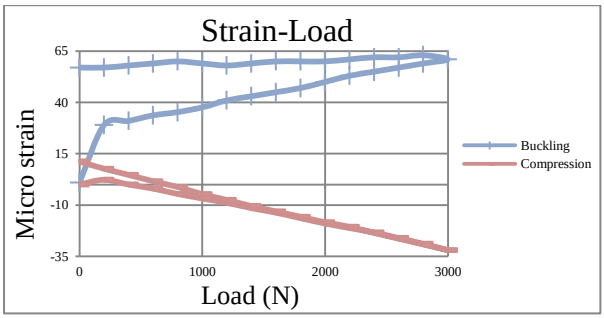

Figure AA44 Strain-Load curve at SG 3

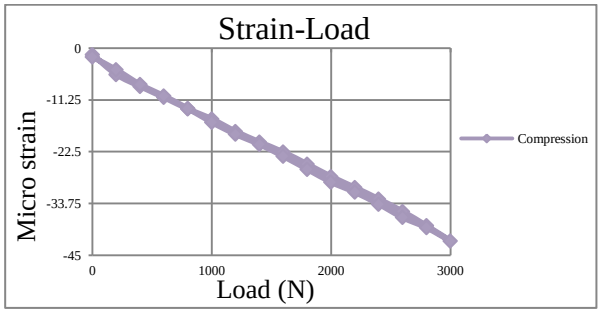

Figure AA45 Strain-Load curve at SG 4

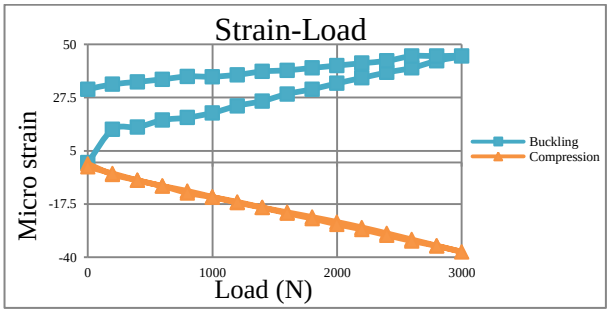

Figure AA46 Strain-Load curve at SG 5

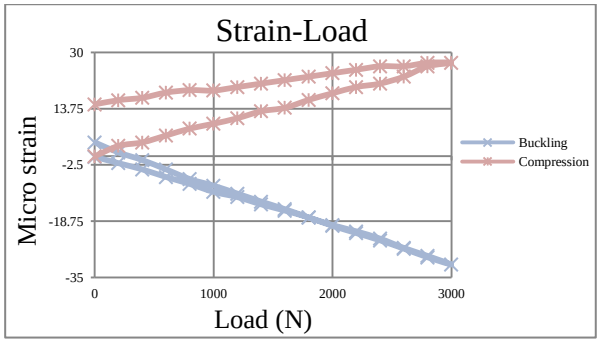

Figure AA47 Strain-Load curve at SG 6

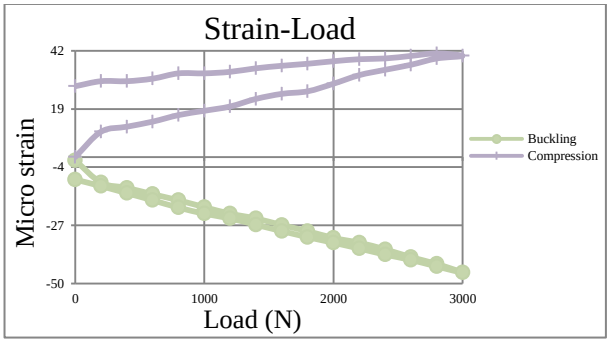

Figure AA48 Strain-Load curve at SG 7

Inner Tube, No Load, Increasing Pressure effects, Max Pressure= 20 bar

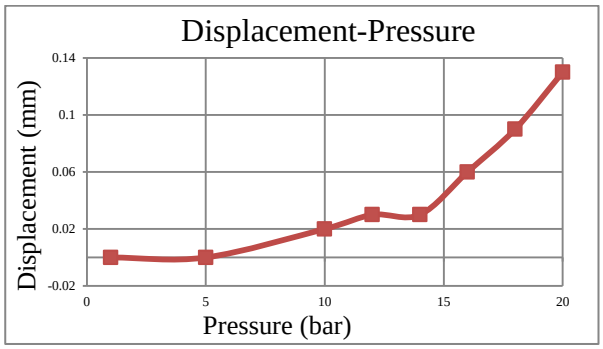

Figure AA49 Displacement-Pressure curve

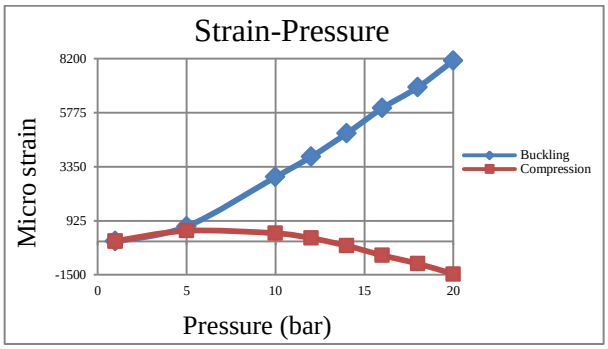

Figure AA50 Strain-Pressure curve at SG 1

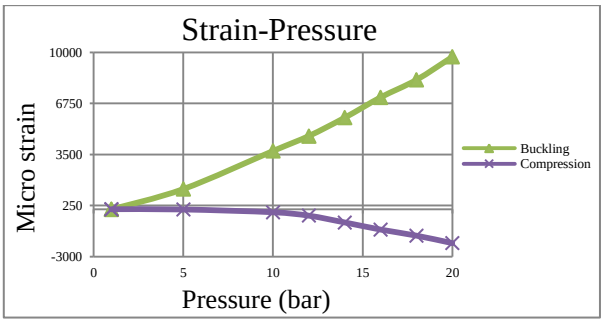

Figure AA51 Strain-Pressure curve at SG 2

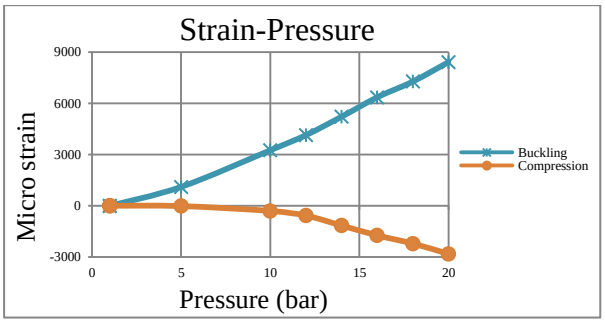

Figure AA52 Strain-Pressure curve at SG 3

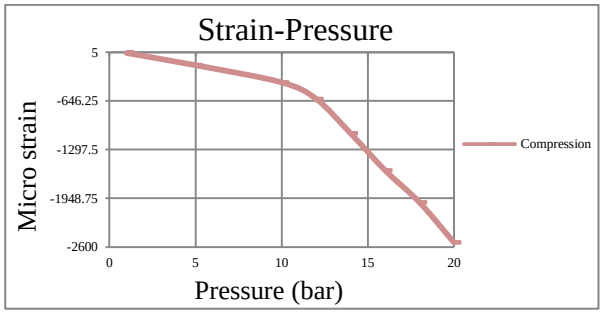

Figure AA53 Strain-Pressure curve at SG 4

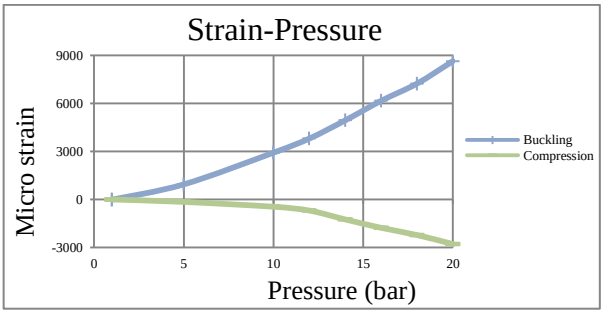

Figure AA54 Strain-Pressure curve at SG 5

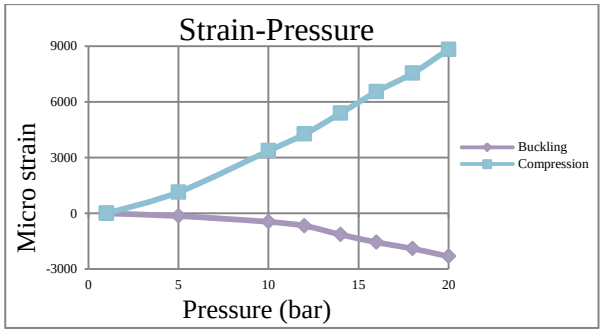

Figure AA55 Strain-Pressure curve at SG 6

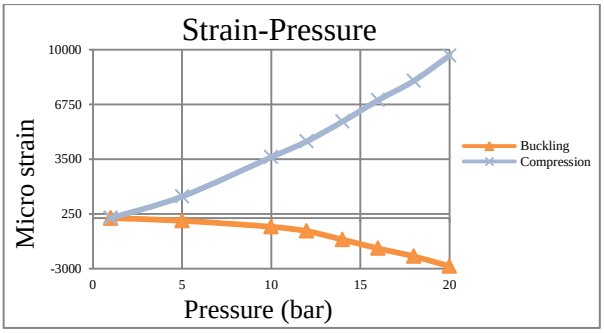

Figure AA56 Strain-Pressure curve at SG 7

Outer Tube and Tendon, Max Load= 3000N, Increment= 200N, Pressure= 1bar (No Oil)

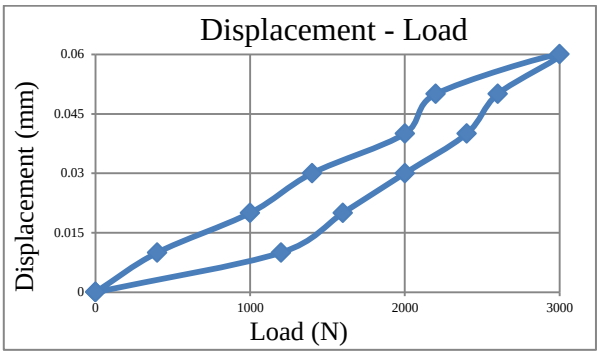

Figure AA57 Displacement-Load curve (Tendon and Outer Tube)

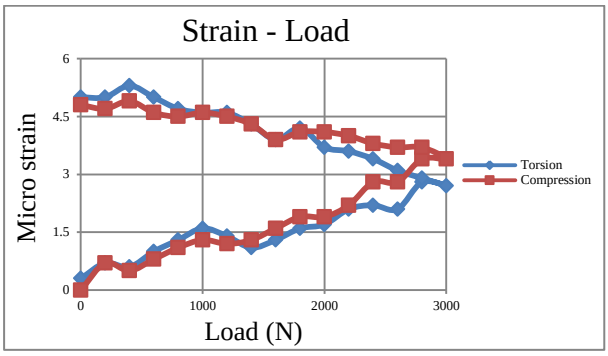

Figure AA58 Strain-Load curve at SG 1 (Tendon)

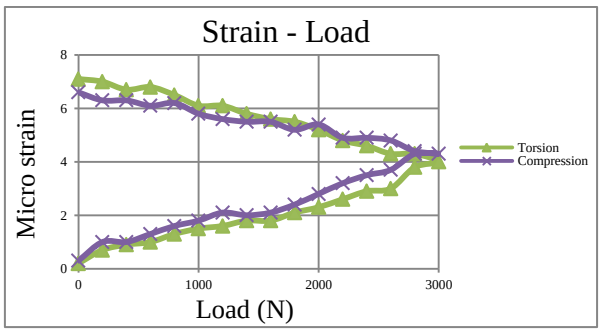

Figure AA59 Strain-Load curve at SG 2 (Tendon)

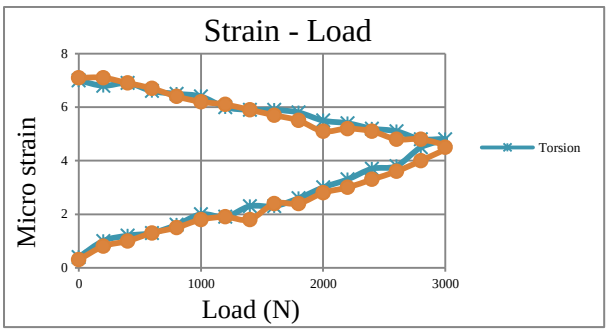

Figure AA60 Strain-Load curve at SG 3 (Tendon)

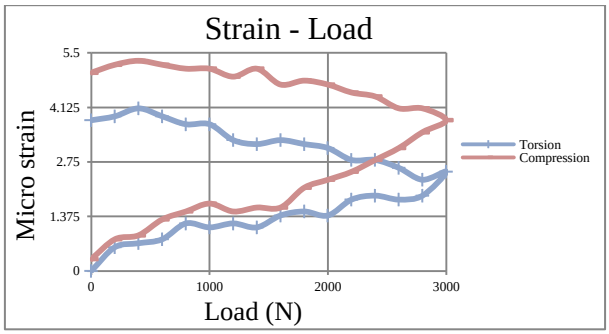

Figure AA61 Strain-Load curve at SG 4 (Tendon)

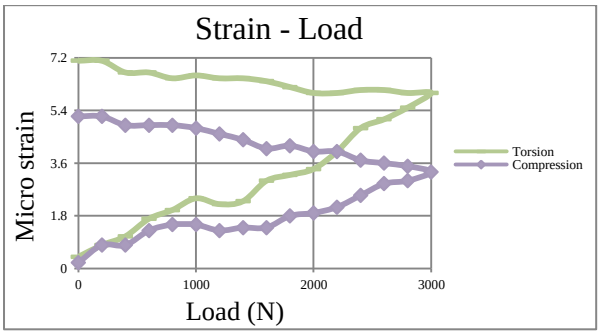

Figure AA62 Strain-Load curve at SG 5 (Tendon)

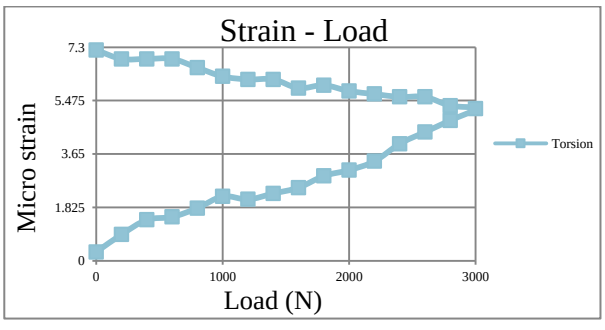

Figure AA63 Strain-Load curve at SG 6 (Tendon)

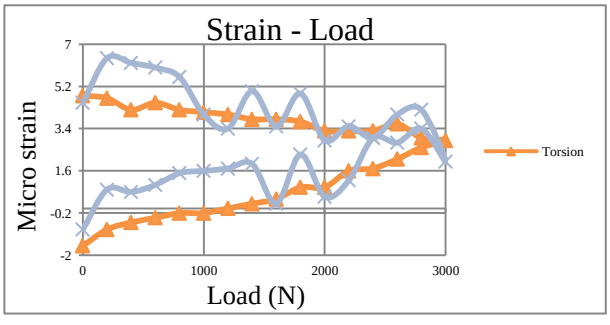

Figure AA64 Strain-Load curve at SG 7 (Tendon)

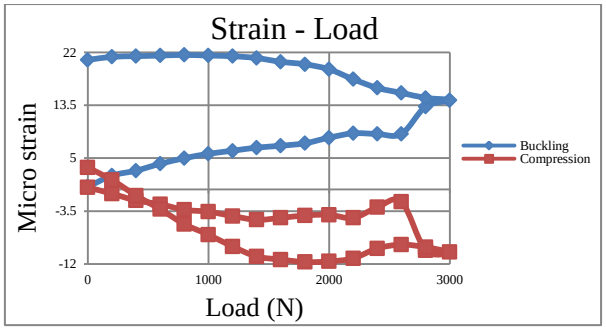

Figure AA65 Strain-Load curve at SG 1 (Outer Tube)

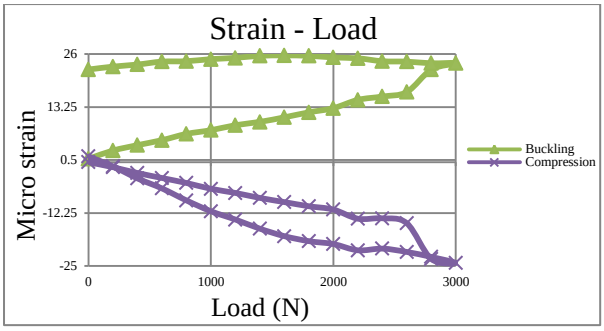

Figure AA66 Strain-Load curve at SG 2 (Outer Tube)

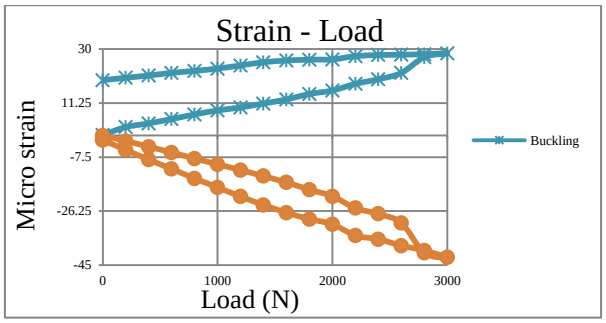

Figure AA67 Strain-Load curve at SG 3 (Outer Tube)

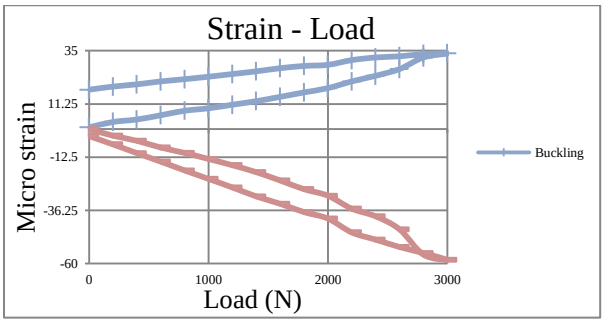

Figure AA68 Strain-Load curve at SG 4 (Outer Tube)

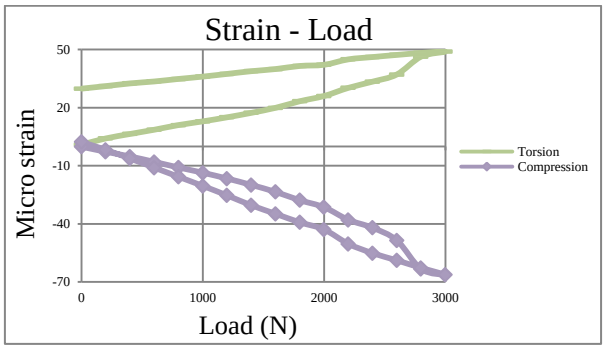

Figure AA69 Strain-Load curve at SG 5 (Outer Tube)

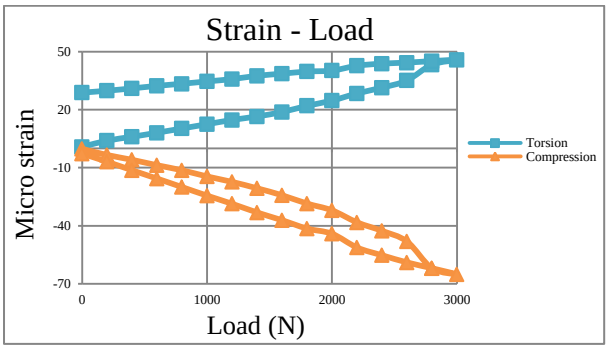

Figure AA70 Strain-Load curve at SG 6 (Outer Tube)

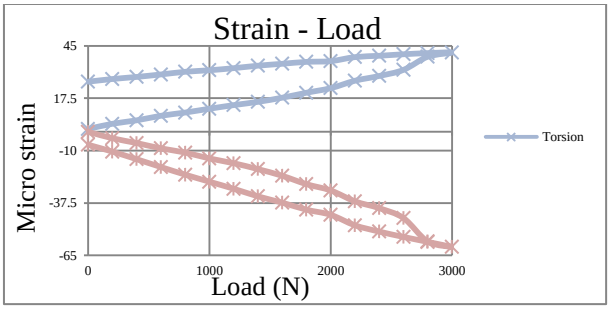

Figure AA71 Strain-Load curve at SG 7 (Outer Tube)

Outer Tube and Tendon, Max Load= 3000N, Increment= 200N, Pressure= 1bar

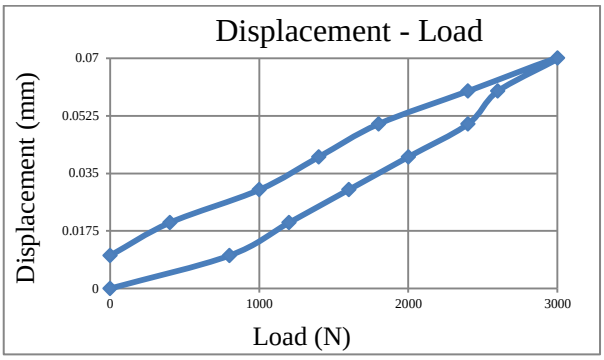

Figure AA72 Displacement-Load curve (Tendon and Outer Tube)

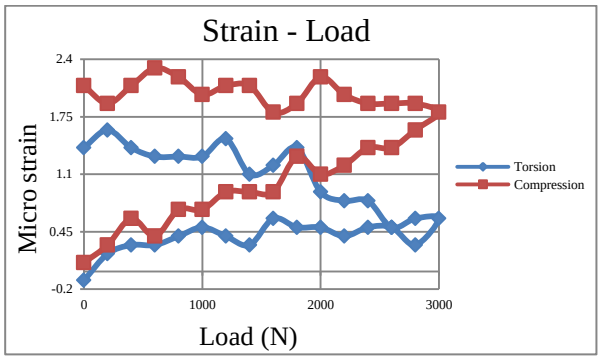

Figure AA73 Strain-Load curve at SG 1 (Tendon)

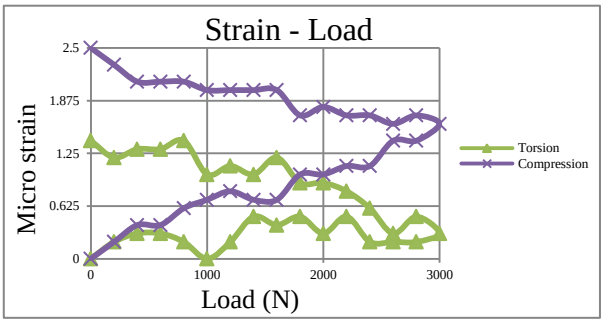

Figure AA74 Strain-Load curve at SG 2 (Tendon)

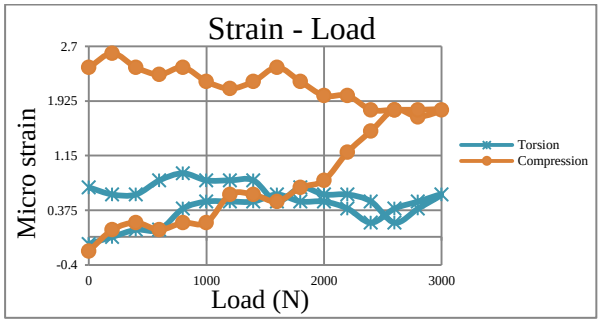

Figure AA75 Strain-Load curve at SG 3 (Tendon)

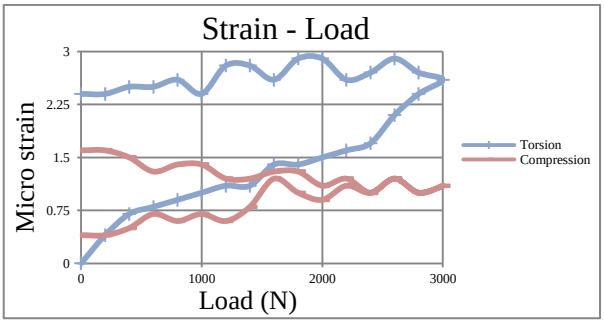

Figure AA76 Strain-Load curve at SG 4 (Tendon)

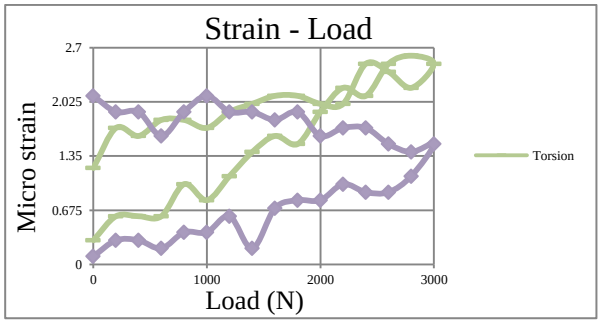

Figure AA77 Strain-Load curve at SG 5 (Tendon)

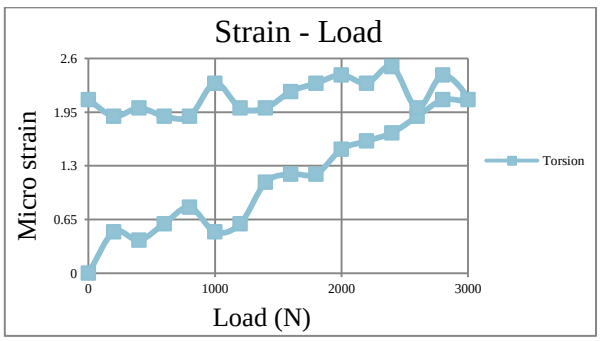

Figure AA78 Strain-Load curve at SG 6 (Tendon)

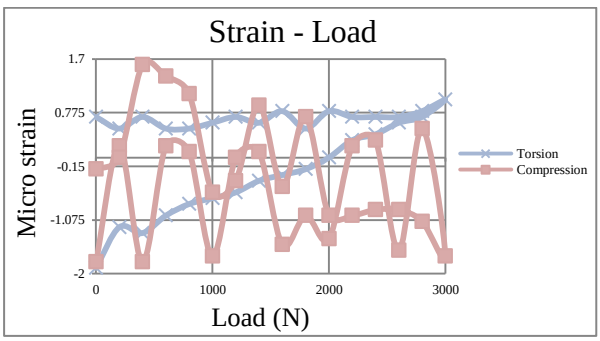

Figure AA79 Strain-Load curve at SG 7 (Tendon)

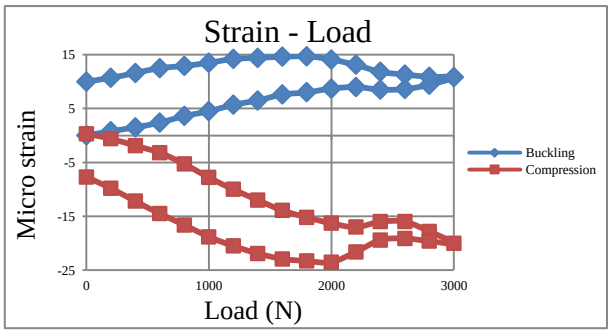

Figure AA80 Strain-Load curve at SG 1 (Outer Tube)

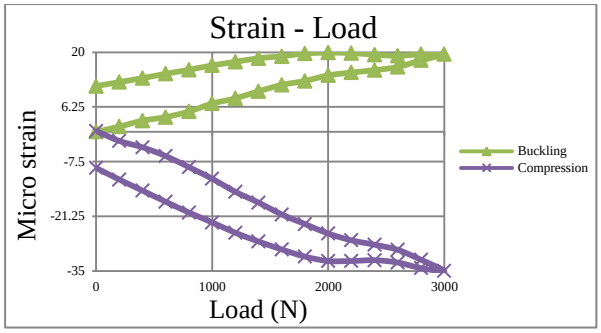

Figure AA81 Strain-Load curve at SG 2 (Outer Tube)

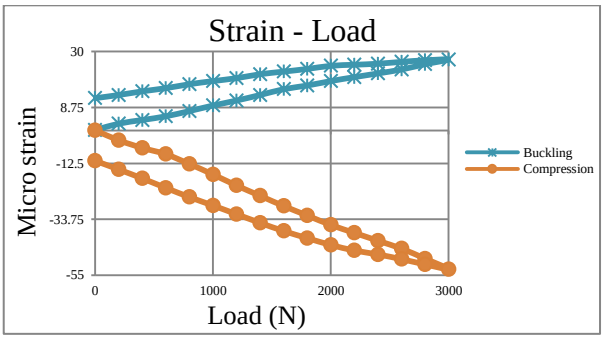

Figure AA82 Strain-Load curve at SG 3 (Outer Tube)

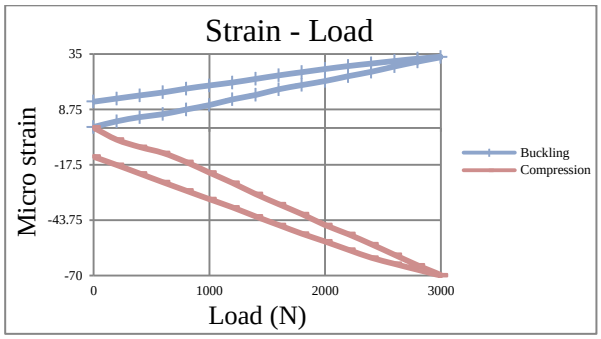

Figure AA83 Strain-Load curve at SG 4 (Outer Tube)

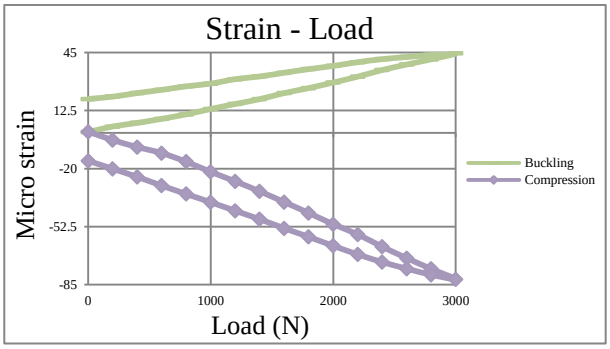

Figure AA84 Strain-Load curve at SG 5 (Outer Tube)

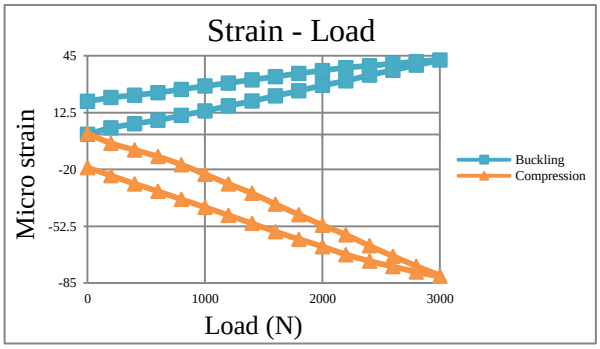

Figure AA85 Strain-Load curve at SG 6 (Outer Tube)

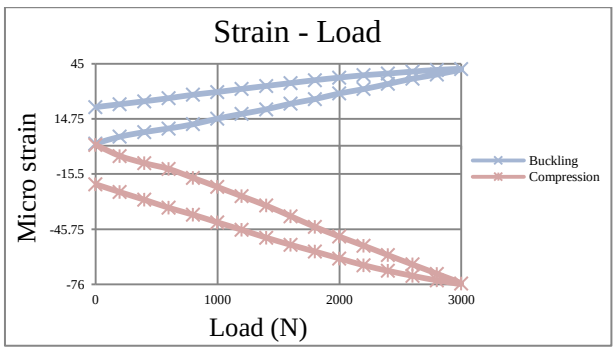

Figure AA86 Strain-Load curve at SG 7 (Outer Tube)

Outer Tube and Tendon, Max Load= 3000N, Increment= 200N, Pressure= 5bar

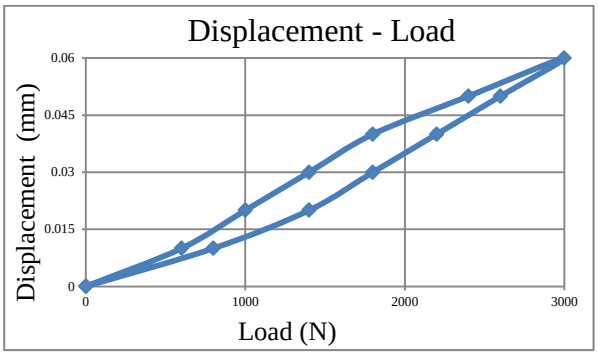

Figure AA87 Displacement-Load curve (Tendon and Outer Tube)

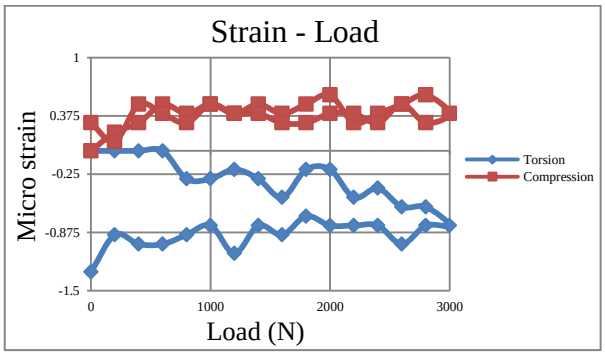

Figure AA88 Strain-Load curve at SG 1 (Tendon)

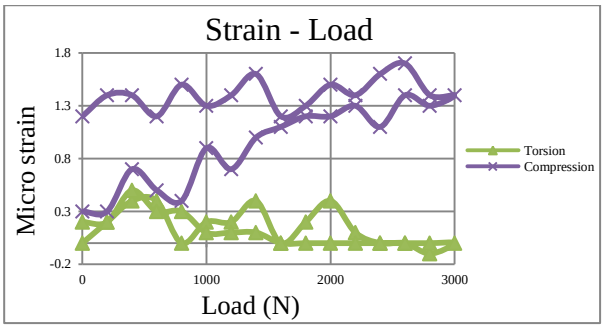

Figure AA89 Strain-Load curve at SG 2 (Tendon)

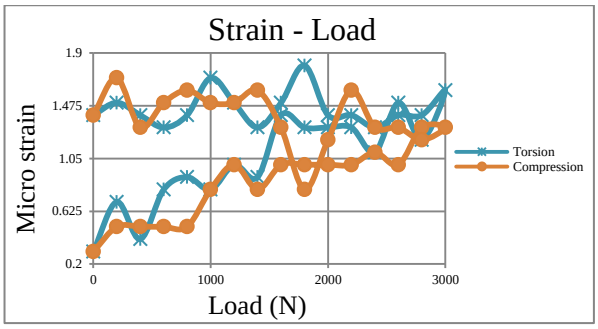

Figure AA90 Strain-Load curve at SG 3 (Tendon)

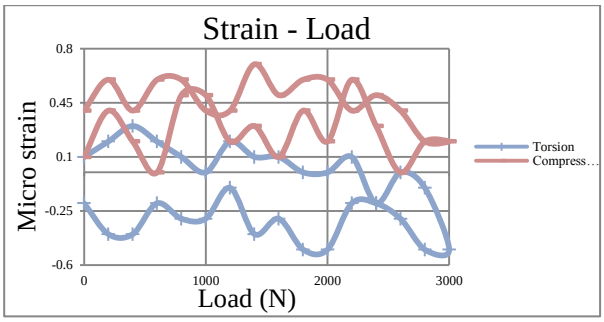

Figure AA91 Strain-Load curve at SG 4 (Tendon)

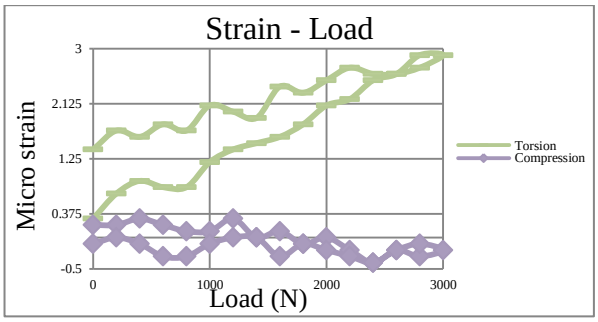

Figure AA92 Strain-Load curve at SG 5 (Tendon)

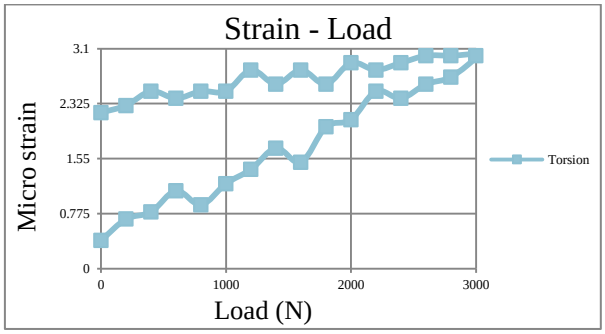

Figure AA93 Strain-Load curve at SG 6 (Tendon)

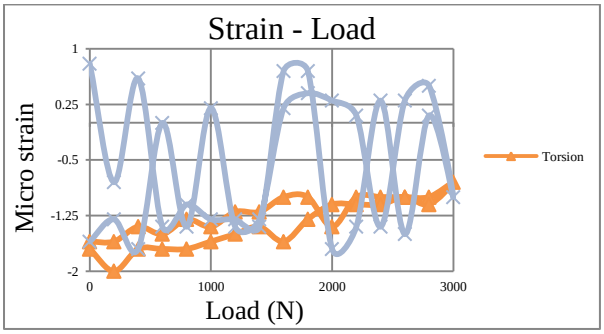

Figure AA94 Strain-Load curve at SG 7 (Tendon)

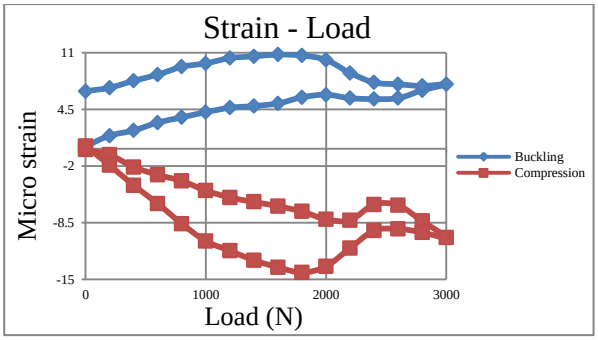

Figure AA95 Strain-Load curve at SG 1 (Outer Tube)

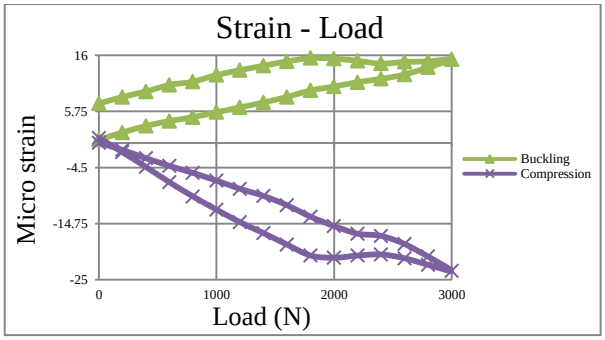

Figure AA96 Strain-Load curve at SG 2 (Outer Tube)

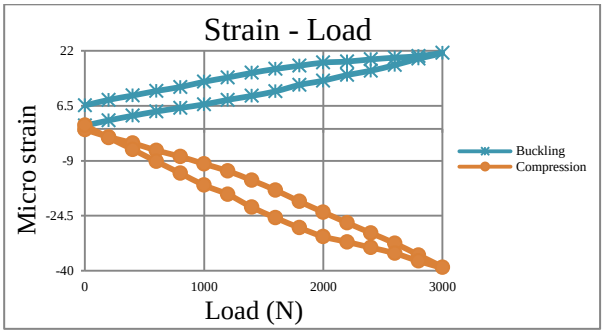

Figure AA97 Strain-Load curve at SG 3 (Outer Tube)

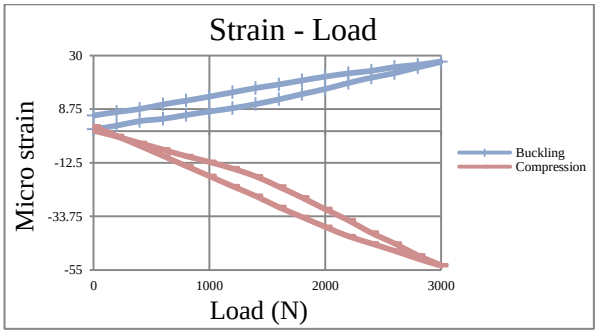

Figure AA98 Strain-Load curve at SG 4 (Outer Tube)

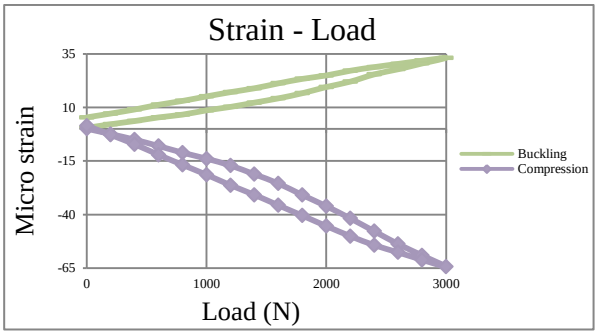

Figure AA99 Strain-Load curve at SG 5 (Outer Tube)

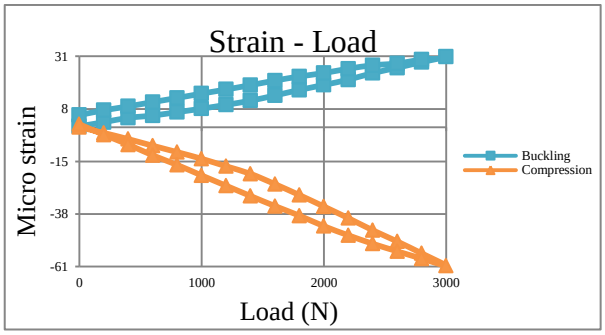

Figure AA100 Strain-Load curve at SG 6 (Outer Tube)

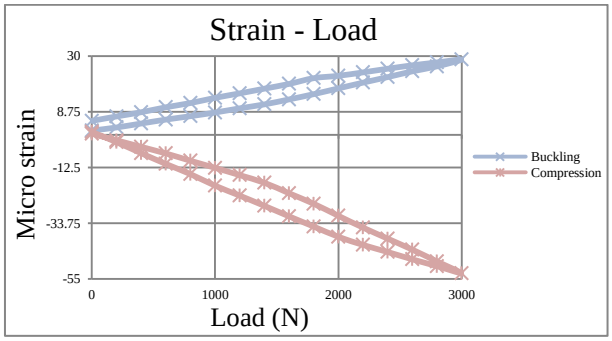

Figure AA101 Strain-Load curve at SG 7 (Outer Tube)

Outer Tube and Tendon, Max Load= 3000N, Increment= 200N, Pressure= 10bar

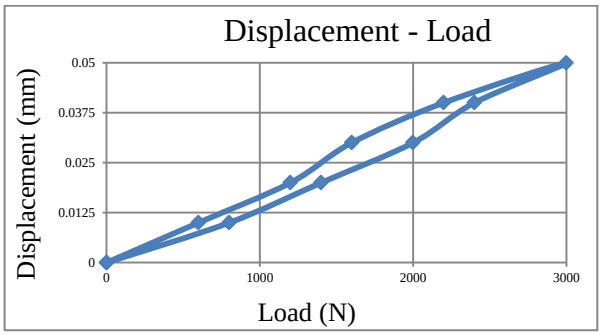

Figure AA102 Displacement-Load curve (Tendon and Outer Tube)

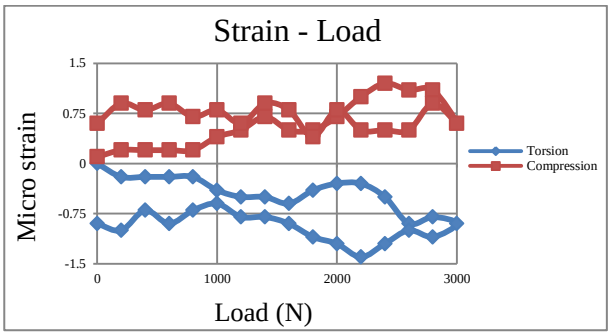

Figure AA103 Strain-Load curve at SG 1 (Tendon)

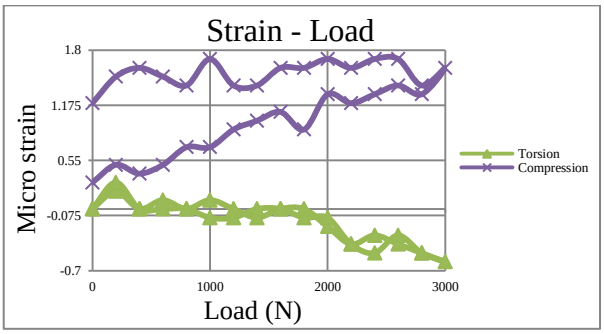

Figure AA104 Strain-Load curve at SG 2 (Tendon)

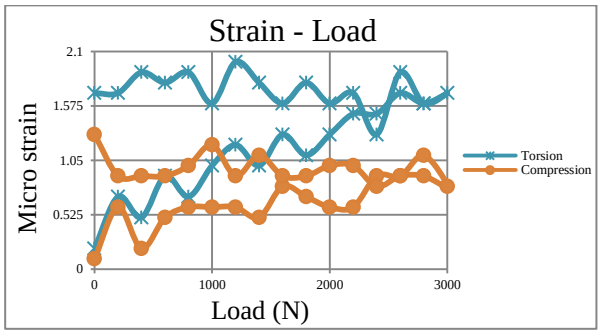

Figure AA105 Strain-Load curve at SG 3 (Tendon)

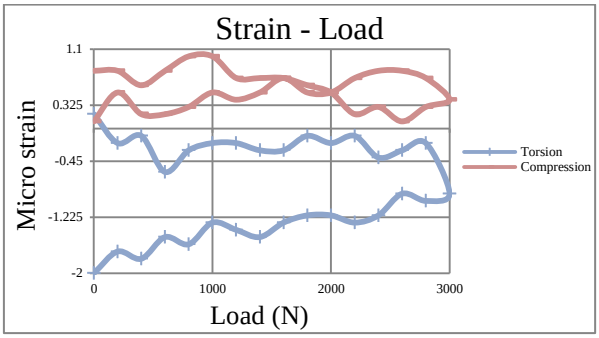

Figure AA106 Strain-Load curve at SG 4 (Tendon)

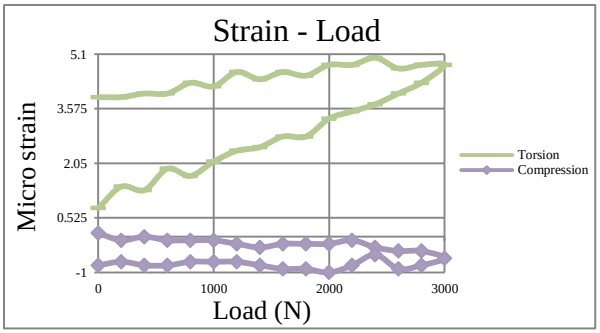

Figure AA107 Strain-Load curve at SG 5 (Tendon)

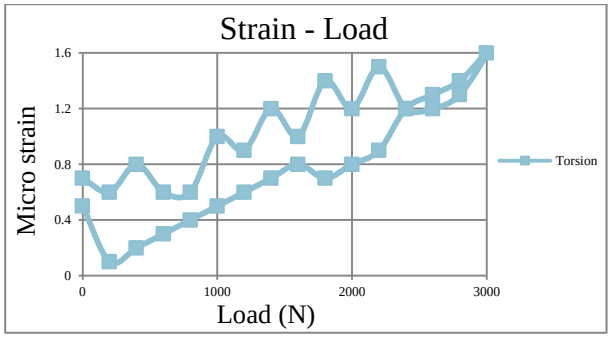

Figure AA108 Strain-Load curve at SG 6 (Tendon)

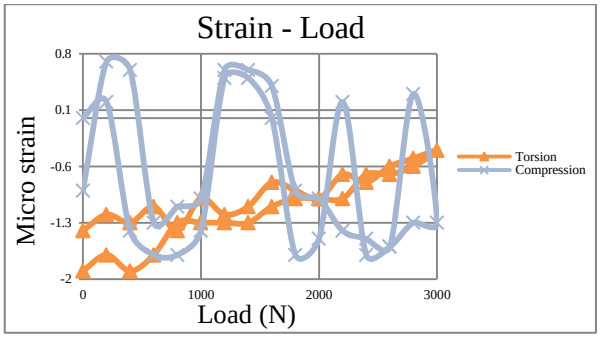

Figure AA109 Strain-Load curve at SG 7 (Tendon)

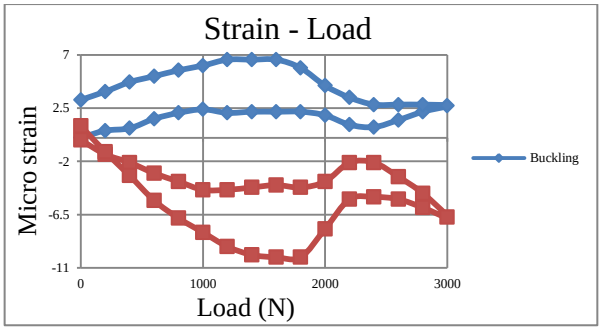

Figure AA110 Strain-Load curve at SG 1 (Outer Tube)

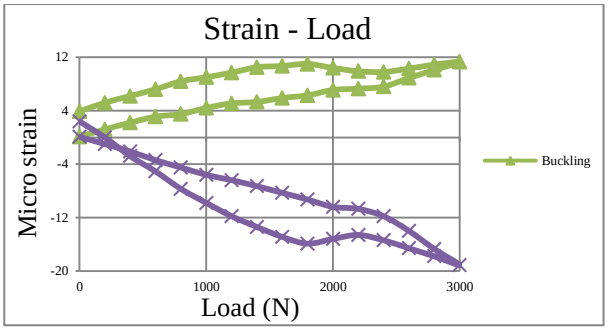

Figure AA111 Strain-Load curve at SG 2 (Outer Tube)

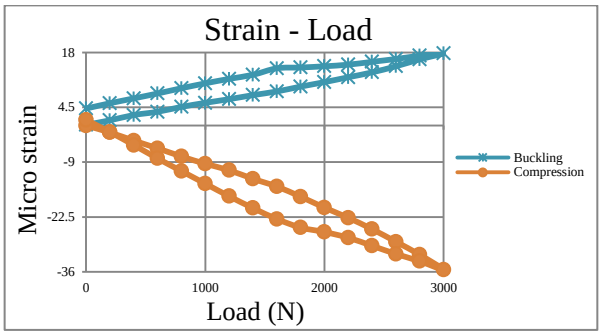

Figure AA112 Strain-Load curve at SG 3 (Outer Tube)

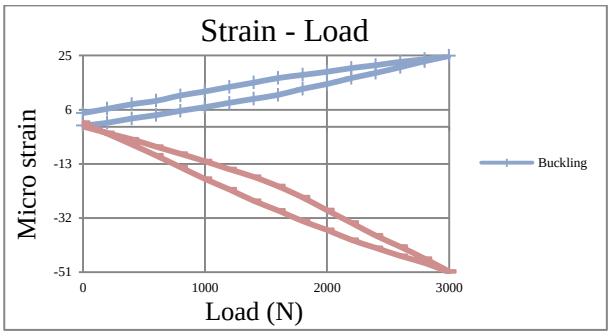

Figure AA113 Strain-Load curve at SG 4 (Outer Tube)

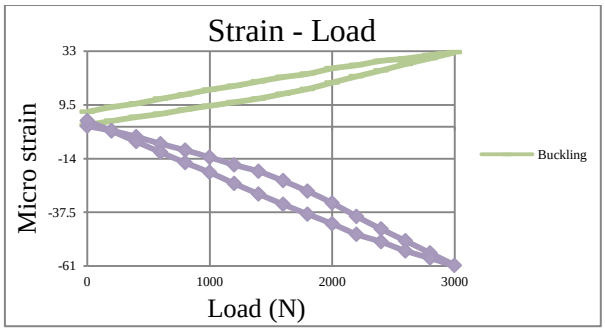

Figure AA114 Strain-Load curve at SG 5 (Outer Tube)

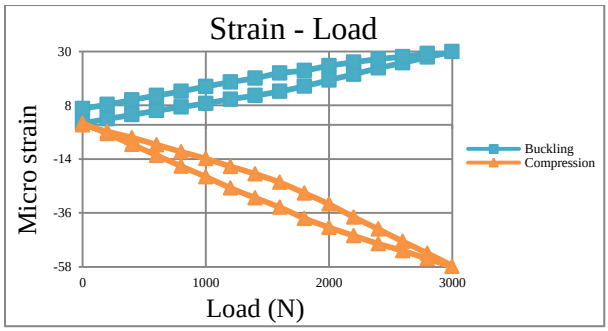

Figure AA115 Strain-Load curve at SG 6 (Outer Tube)

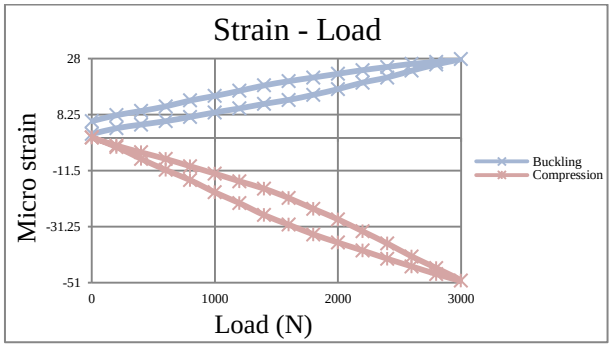

Figure AA116 Strain-Load curve at SG 7 (Outer Tube)

Outer Tube and Tendon, Max Load = 3000 N, Increment = 200 N, Pressure = 15 bar

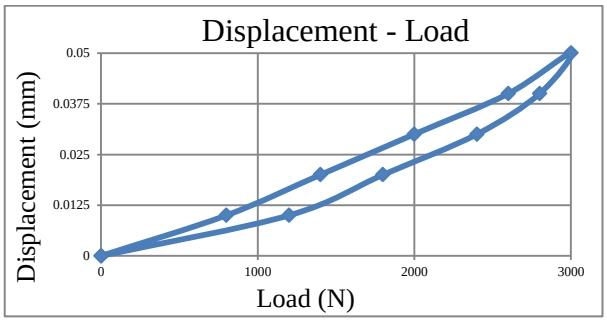

Figure AA117 Displacement-Load curve (Tendon and Outer Tube)

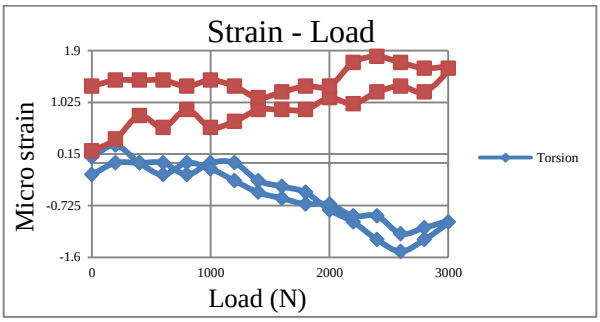

Figure AA118 Strain-Load curve at SG 1 (Tendon)

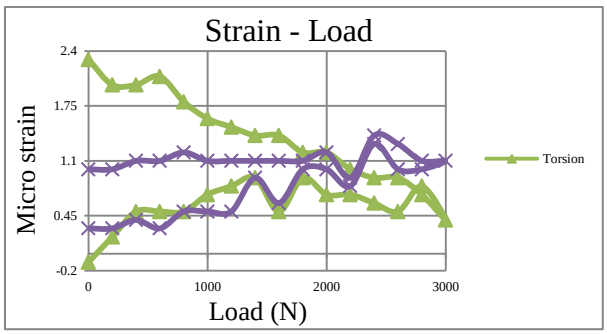

Figure AA119 Strain-Load curve at SG 2 (Tendon)

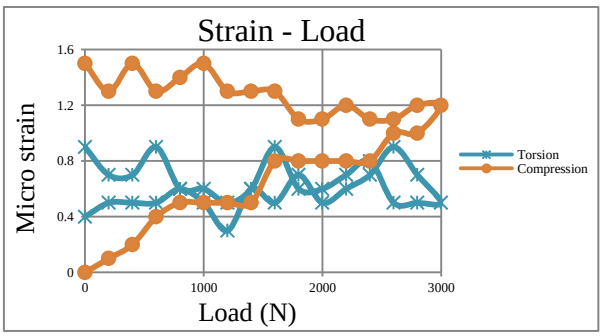

Figure AA120 Strain-Load curve at SG 3 (Tendon)

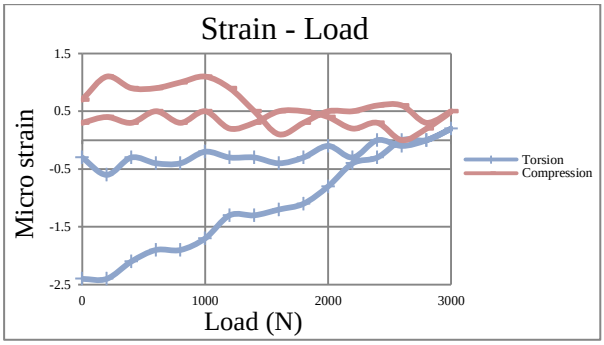

Figure AA121 Strain-Load curve at SG 4 (Tendon)

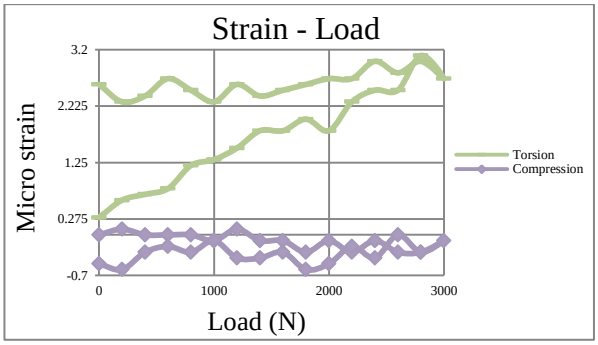

Figure AA122 Strain-Load curve at SG 5 (Tendon)

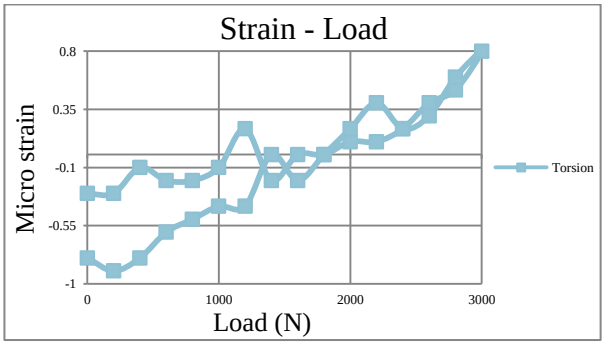

Figure AA123 Strain-Load curve at SG 6 (Tendon)

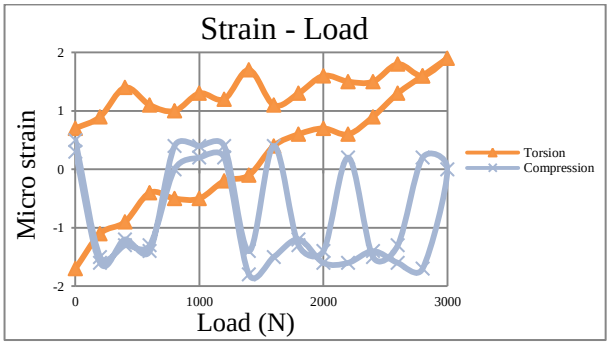

Figure AA124 Strain-Load curve at SG 7 (Tendon)

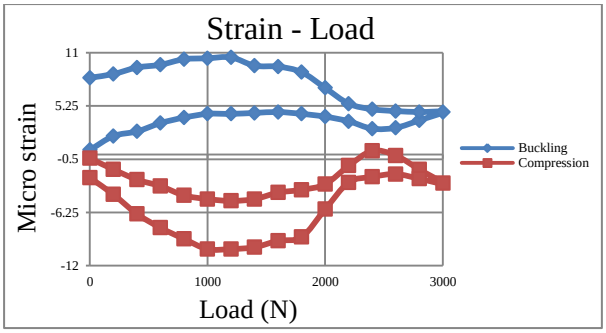

Figure AA125 Strain-Load curve at SG 1 (Outer Tube)

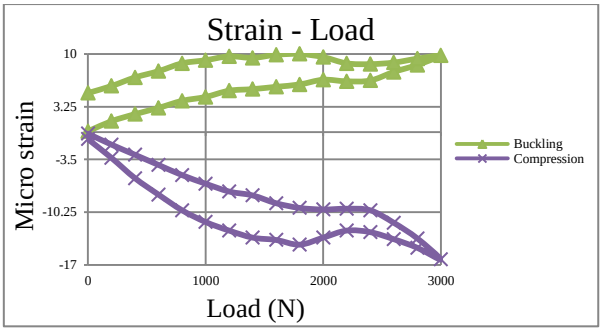

Figure AA126 Strain-Load curve at SG 2 (Outer Tube)

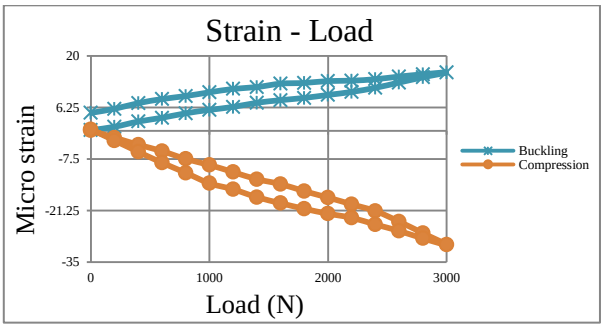

Figure AA127 Strain-Load curve at SG 3 (Outer Tube)

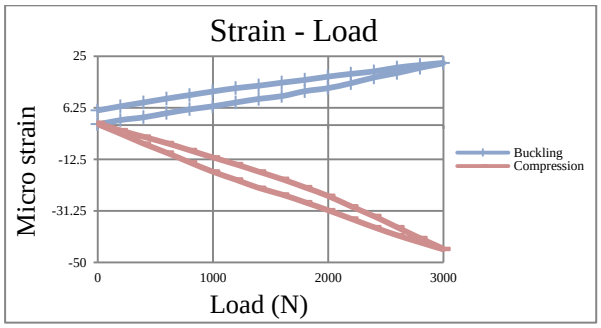

Figure AA128 Strain-Load curve at SG 4 (Outer Tube)

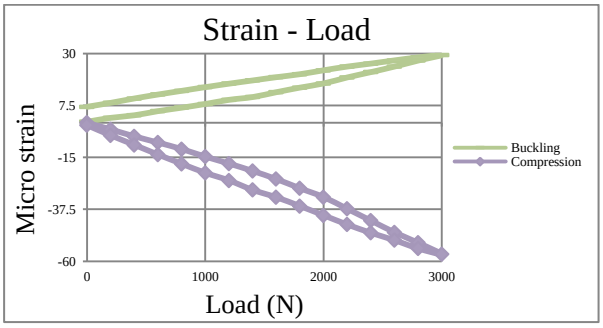

Figure AA129 Strain-Load curve at SG 5 (Outer Tube)

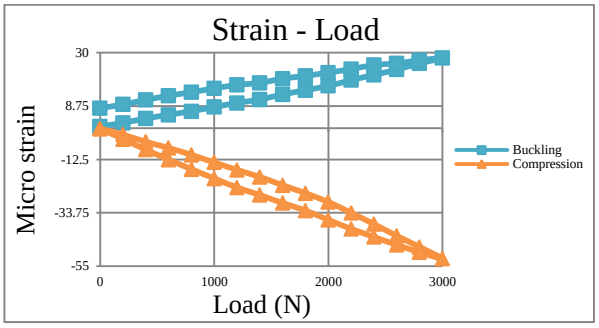

Figure AA130 Strain-Load curve at SG 6 (Outer Tube)

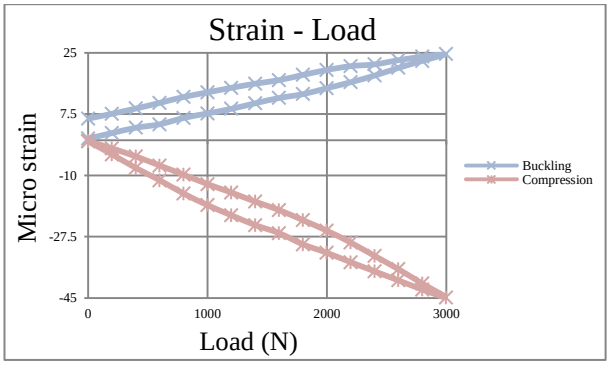

Figure AA131 Strain-Load curve at SG 7 (Outer Tube)

Outer Tube and Tendon, Max Load= 3000N, Increment= 200N, Pressure= 20bar

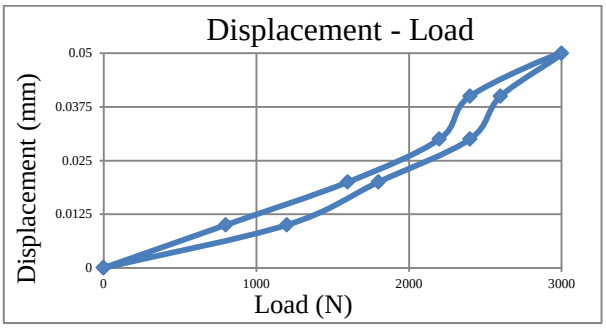

Figure AA132 Displacement-Load curve (Tendon and Outer Tube)

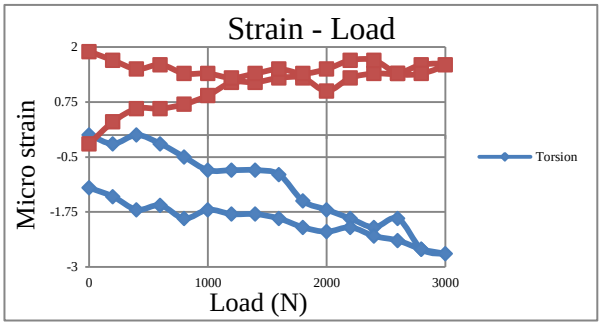

Figure AA133 Strain-Load curve at SG 1 (Tendon)

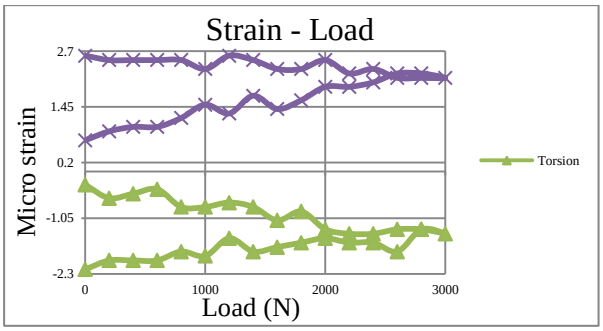

Figure AA134 Strain-Load curve at SG 2 (Tendon)

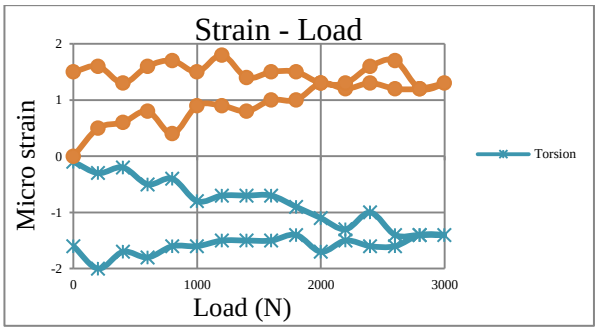

Figure AA135 Strain-Load curve at SG 3 (Tendon)

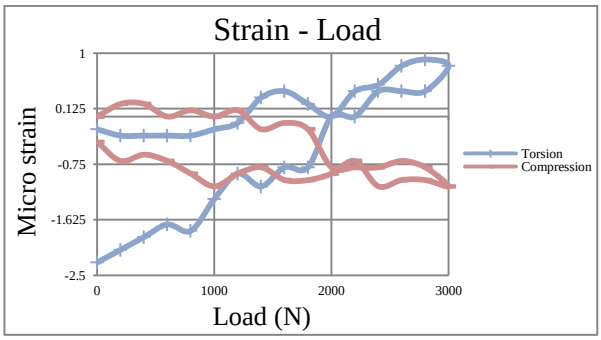

Figure AA136 Strain-Load curve at SG 4 (Tendon)

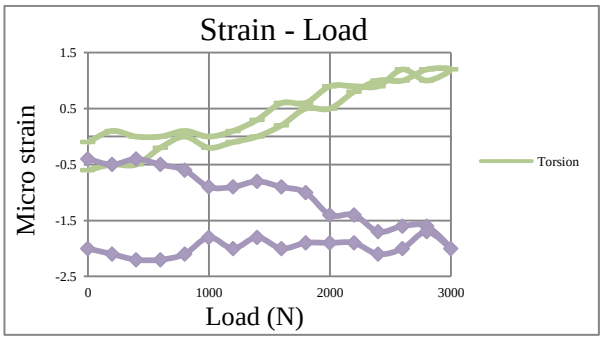

Figure AA137 strain-Load curve at SG 5 (Tendon)

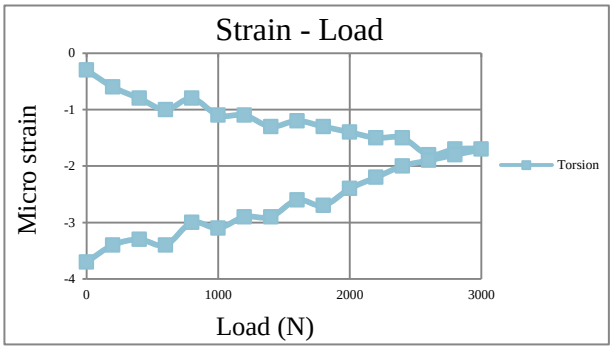

Figure AA138 Strain-Load curve at SG 6 (Tendon)

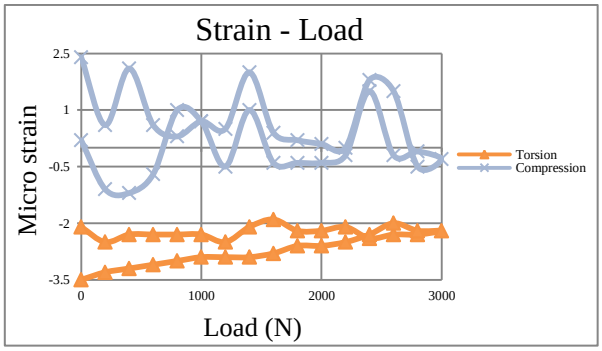

Figure AA139 Strain-Load curve at SG 7 (Tendon)

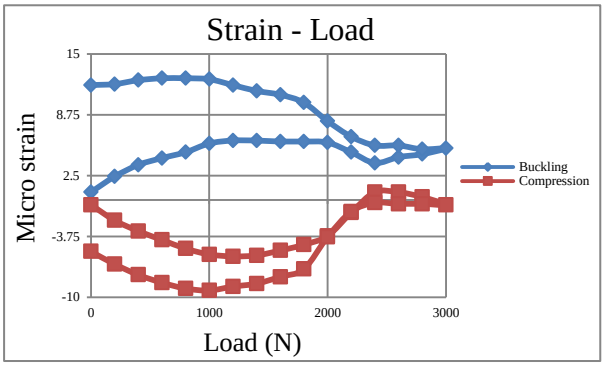

Figure AA140 Strain-Load curve at SG 1 (Outer Tube)

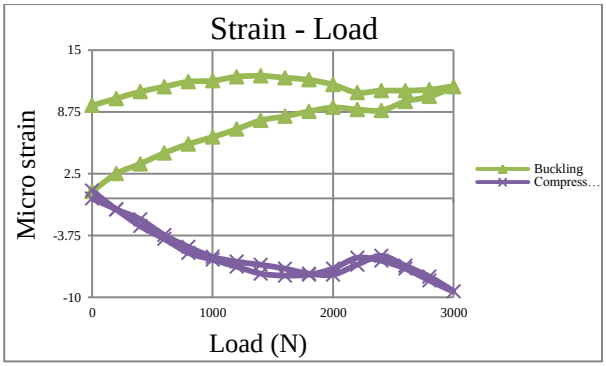

Figure AA141 Strain-Load curve at SG 2 (Outer Tube)

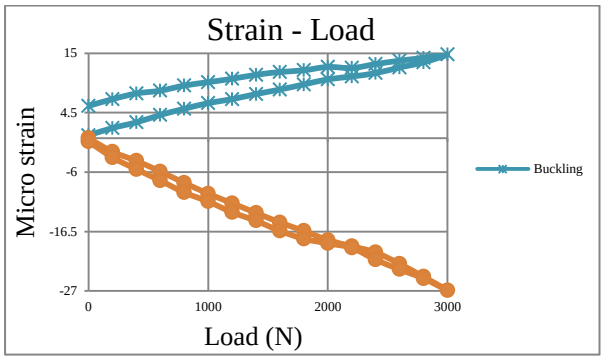

Figure AA142 Strain-Load curve at SG 3 (Outer Tube)

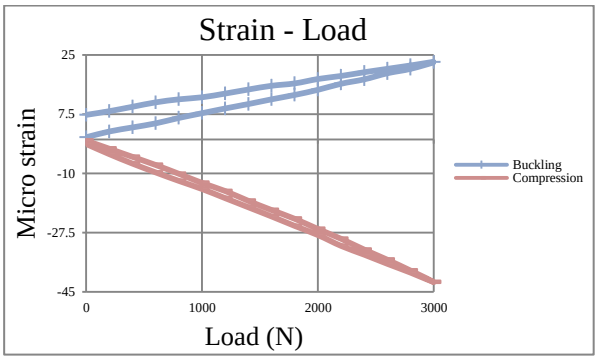

Figure AA143 Strain-Load curve at SG 4 (Outer Tube)

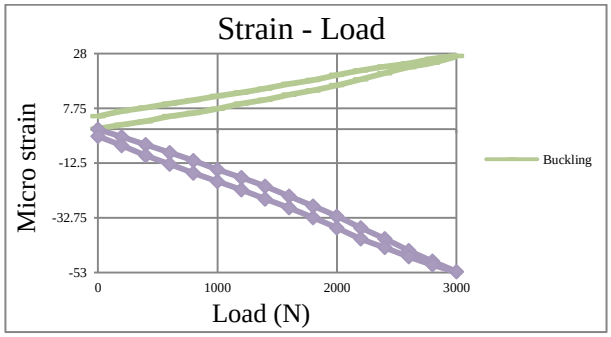

Figure AA144 Strain-Load curve at SG 5 (Outer Tube)

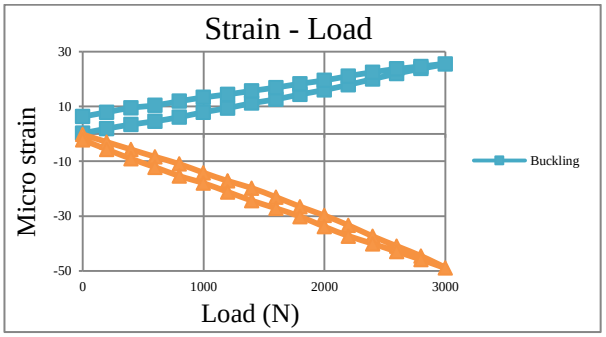

Figure AA145 Strain-Load curve at SG 6 (Outer Tube)

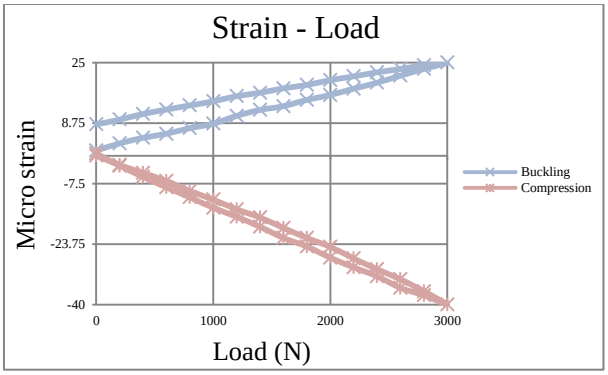

Figure AA146 Strain-Load curve at SG 7 (Outer Tube)

Outer Tube and Tendon, No Load, Increasing Pressure effects, Max Pressure= 20bar

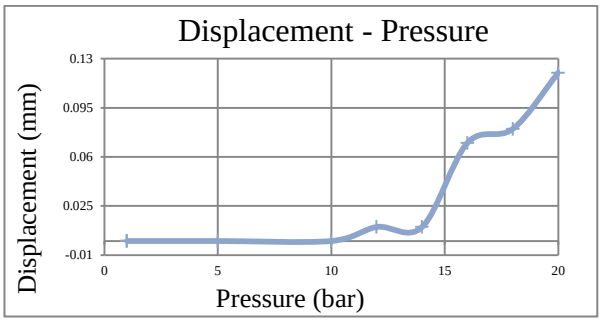

Figure AA147 Displacement-Pressure curve (Tendon + Outer Tube)

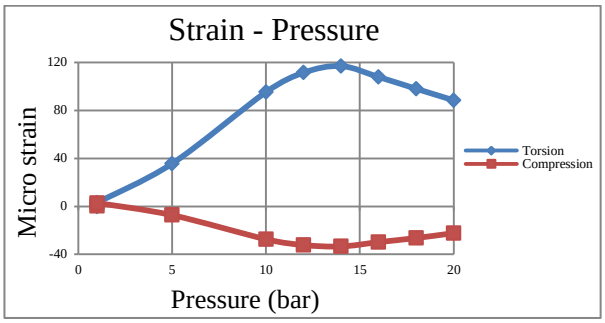

Figure AA148 Strain-Pressure curve at SG 1 (Tendon)

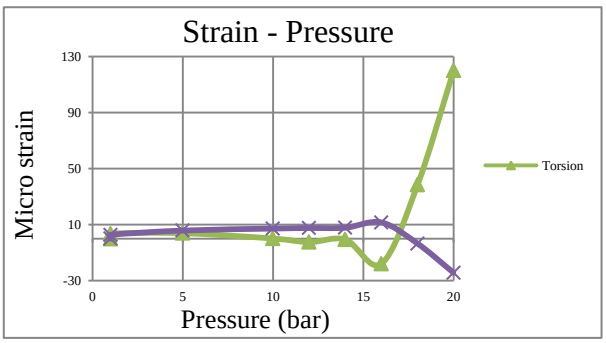

Figure AA149 Strain-Pressure curve at SG 2 (Tendon)

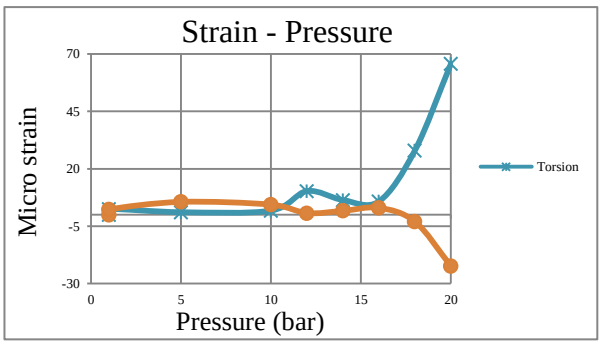

Figure AA150 Strain-Pressure curve at SG 3 (Tendon)

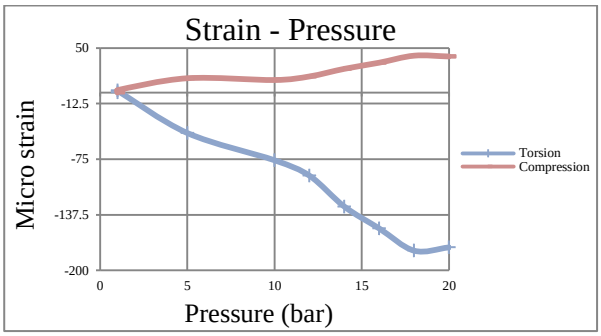

Figure AA151 Strain-Pressure curve at SG 4 (Tendon)

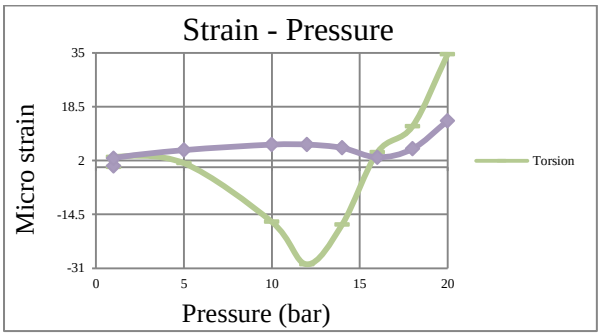

Figure AA152 Strain-Pressure curve at SG 5 (Tendon)

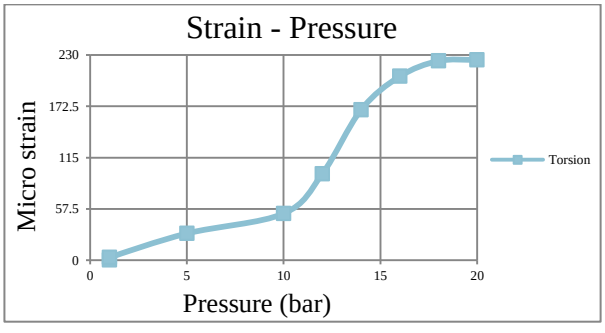

Figure AA153 Strain-Pressure curve at SG 6 (Tendon)

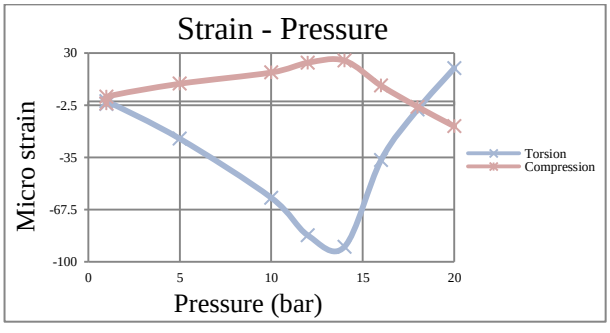

Figure AA154 Strain-Pressure curve at SG 7 (Tendon)

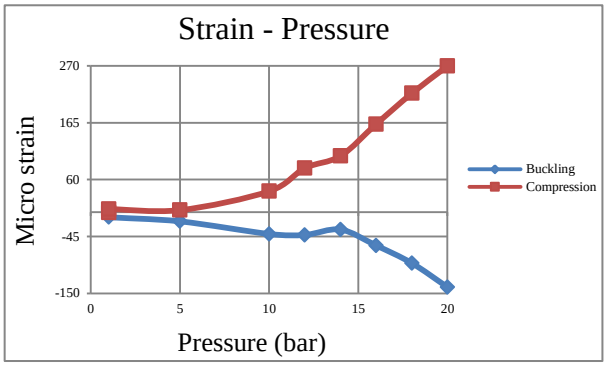

Figure AA155 Strain-Pressure curve at SG 1 (Outer tube)

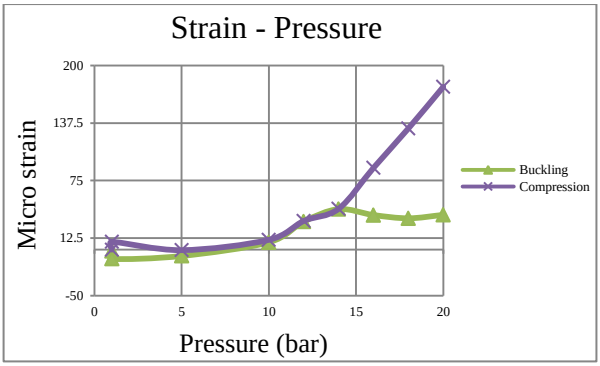

Figure AA156 Strain-Pressure curve at SG 2 (Outer Tube)

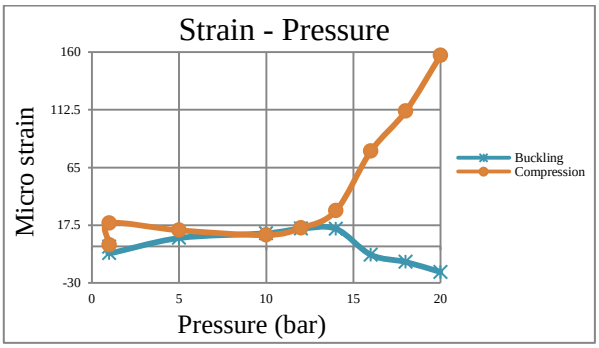

Figure AA157 Strain-Pressure curve at SG 3 (Outer Tube)

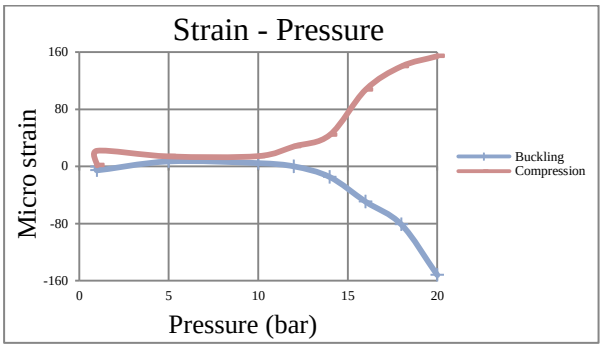

Figure AA158 Strain-Pressure curve at SG 4 (Outer Tube)

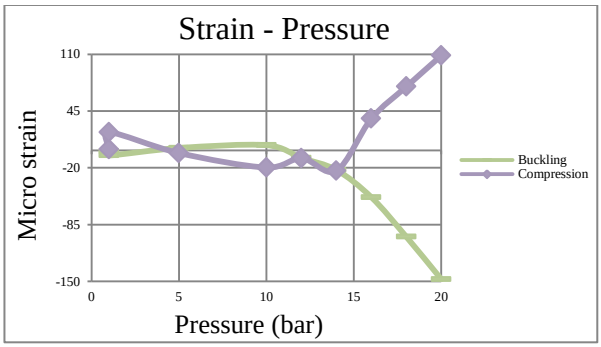

Figure AA159 Strain-Pressure curve at SG 5 (Outer Tube)

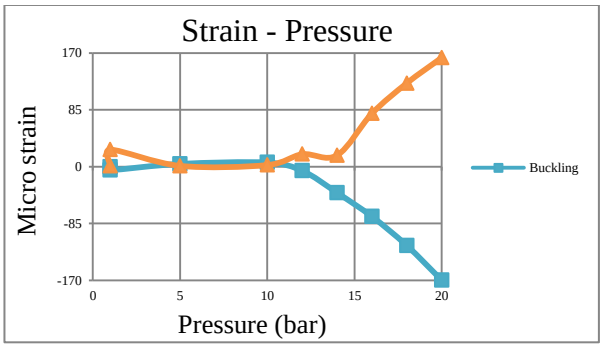

Figure AA160 Strain-Pressure curve at SG 6 (Outer Tube)

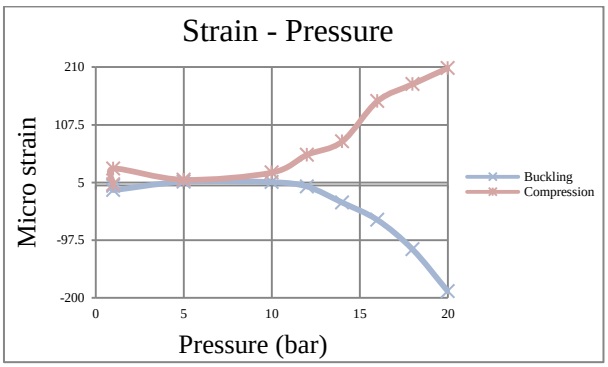

Figure AA161 Strain-Pressure curve at SG 7 (Outer Tube)

Appendix B

Blueprints and 3D view of Components

In this section, blueprints and three-dimensional views of the prototype layers and other components designed to keep the layers in right place, to seal the prototype when necessary, or to apply the external load are shown. These components are:

(1) Outer Tube: designed similar to outer sheath layer in real flexible risers, covered all other layers of the prototype, and was made of clear poly-carbonate (see figure AB1).

(2) Single Helical Armour (or Tendon): was covered by outer sheath and surrounded the inner cylinder and the material used was CR4 steel (figures AB2 to AB4).

(3) Inner Tube: was made of clear poly-carbonate similar to outer tube, yet it was designed more accurately in order to seal the pressurized oil inside it; this layer was placed inside tendon and covered carcass (figure AB5).

(4) Helical Carcass: was made of CR4 yet had more pitch comparing to tendon layer, was placed inside the inner tube (figure AB6).

(5) End-Caps: were designed to keep the layers of test specimen in desired position, to help other components seal the fluid inside inner-tube, and to help applying load; they were installed at each end of the specimen (figures AB7 to AB10).

(6) Threaded Rod: was designed to help the end-caps keep the test layers in place. It was adjusted by two nuts at its both ends which are sealed by washers and grease (figure AB11).

(7) Load Part: was designed to apply the external load (figures AB12 to AB14 and AB16).

(8) Bending bed: was designed and made for the bending test; both bending end-caps were installed on the bed which was installed on loading machine at bottom (magenta in figure AB15).

A schematic view of total assembly for axial loading is demonstrated in figure AB16.

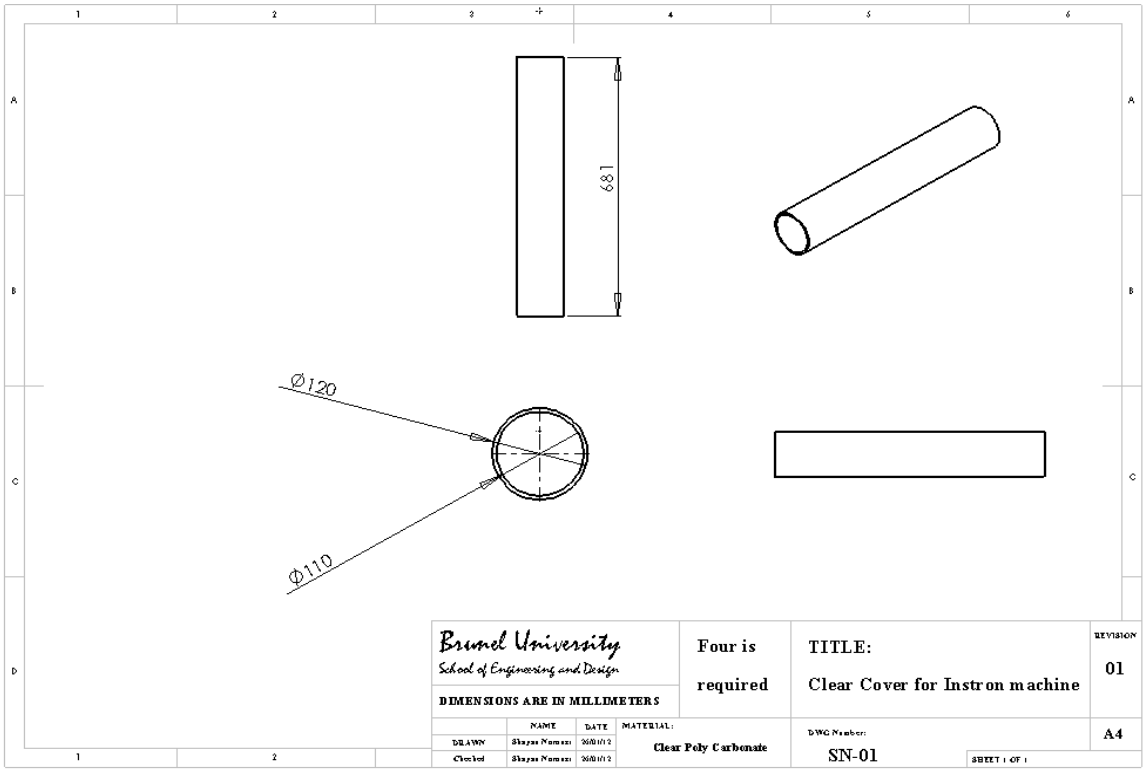

Figure AB1 Outer tube blueprint

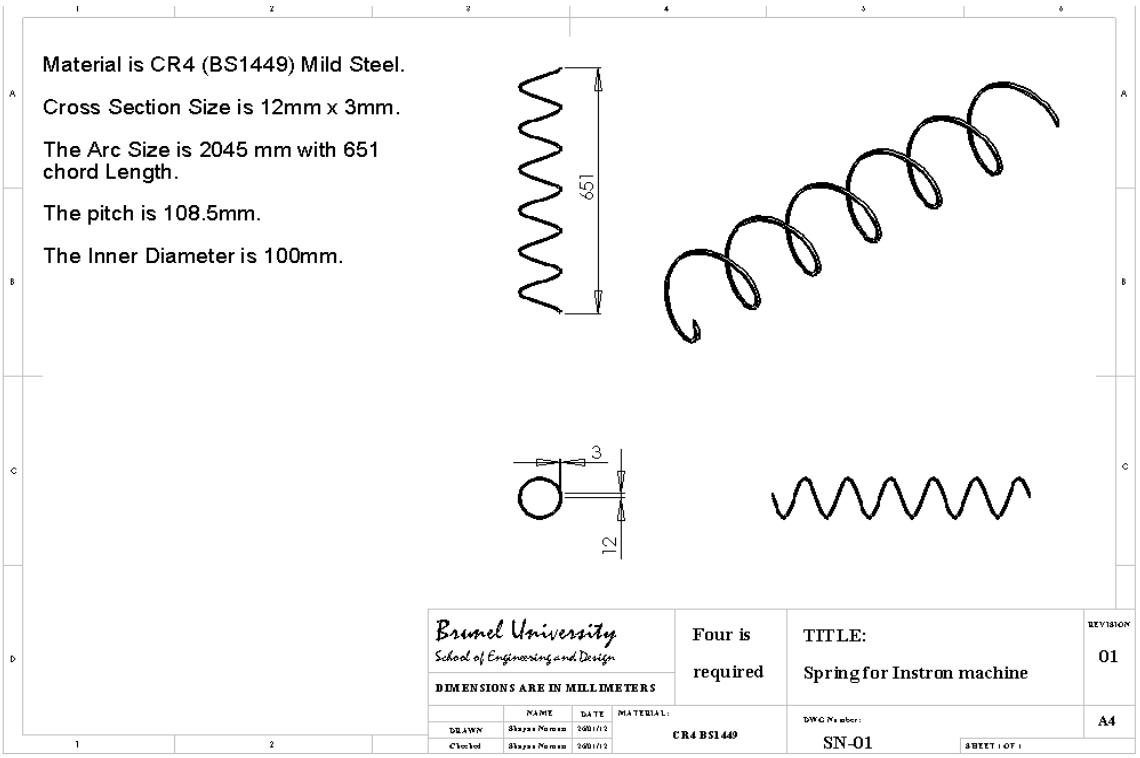

Figure AB2 Tendon blueprint

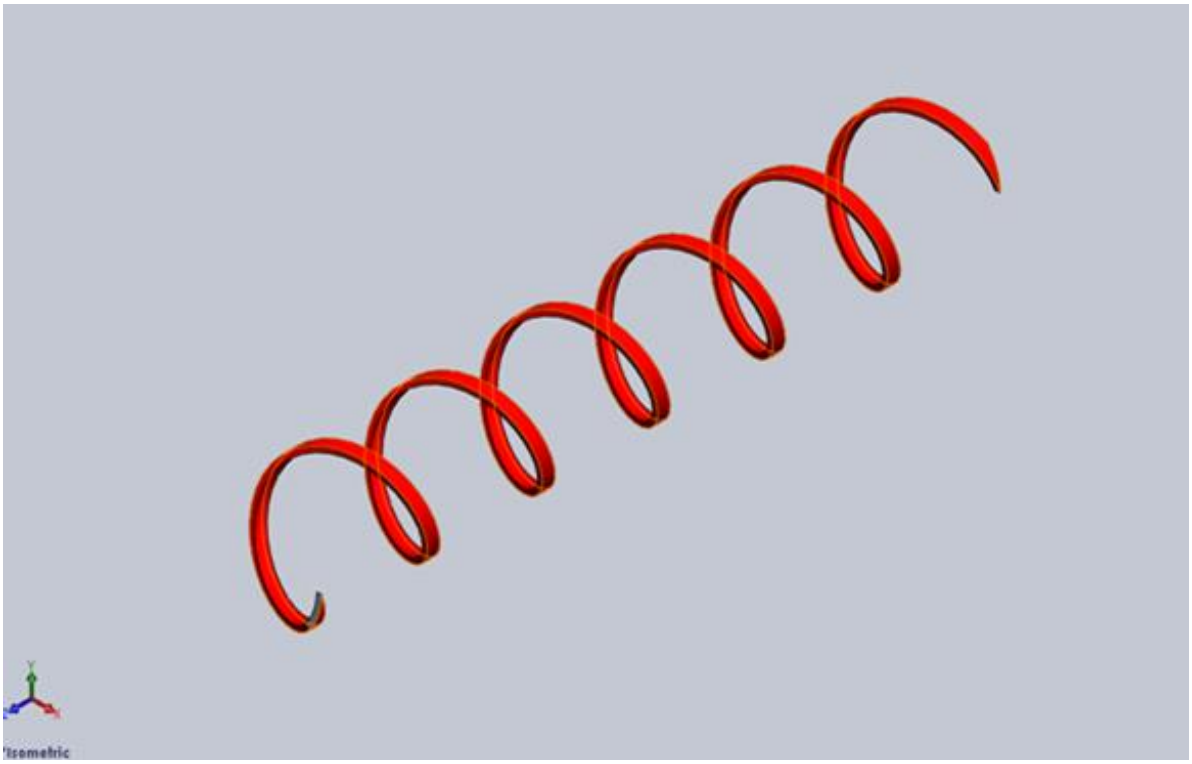

Figure AB3 Tendon 3D view

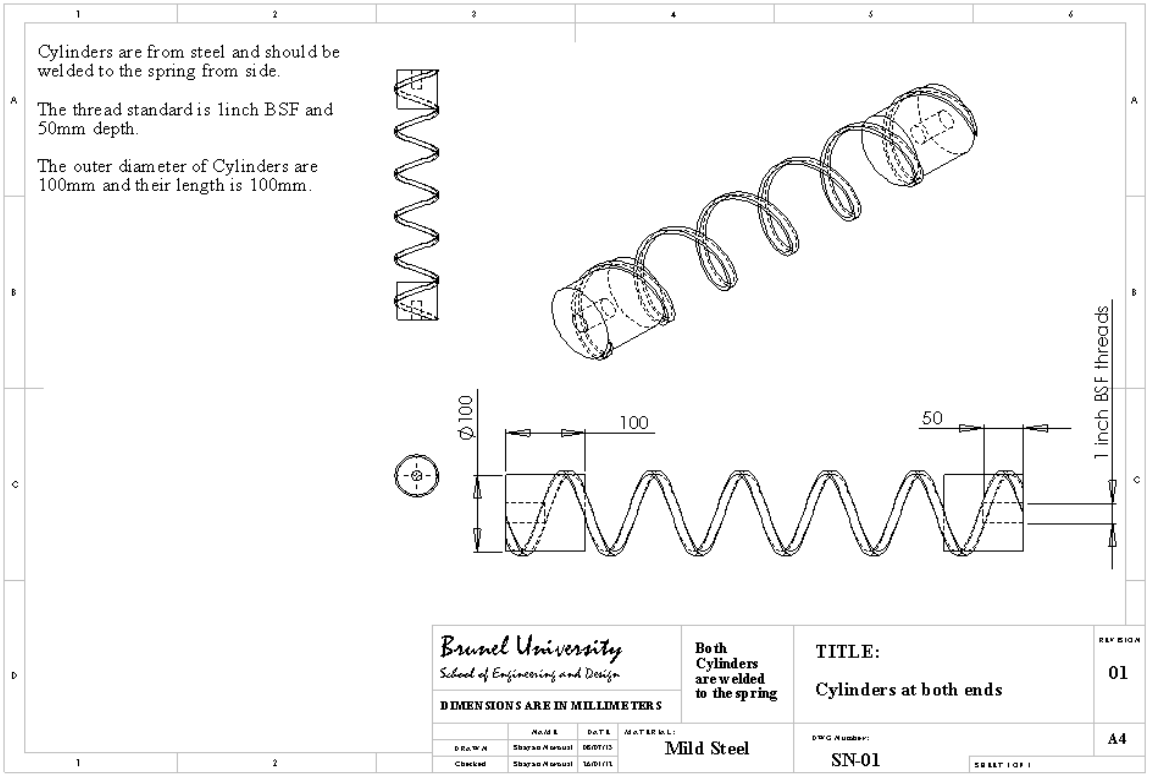

Figure AB4 Single tendon testing blueprint

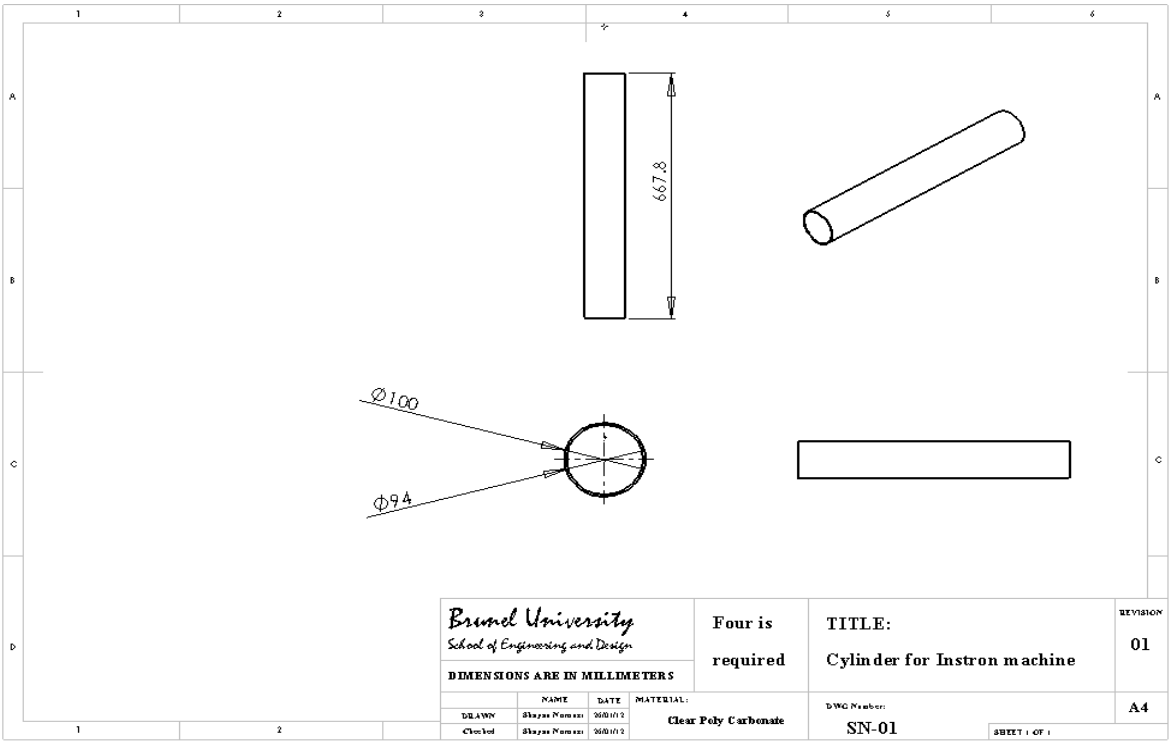

Figure AB5 Inner-tube blueprint

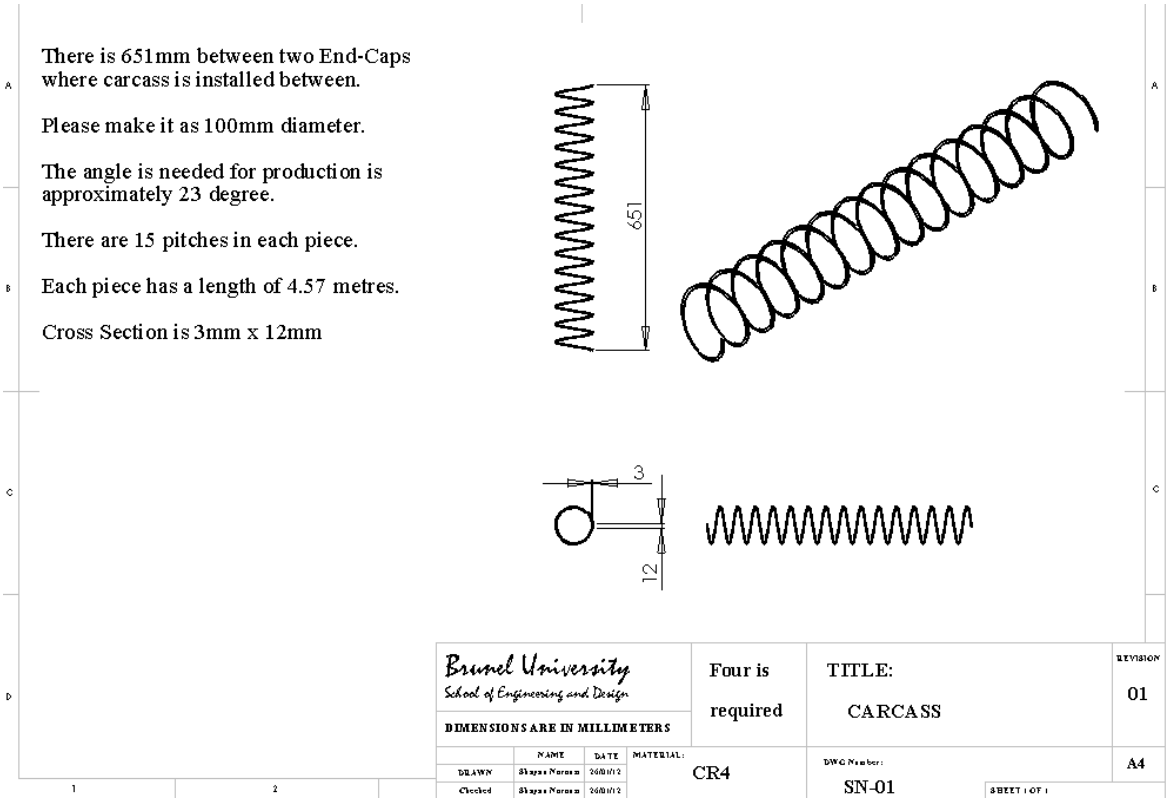

Figure AB6 Carcass blueprint

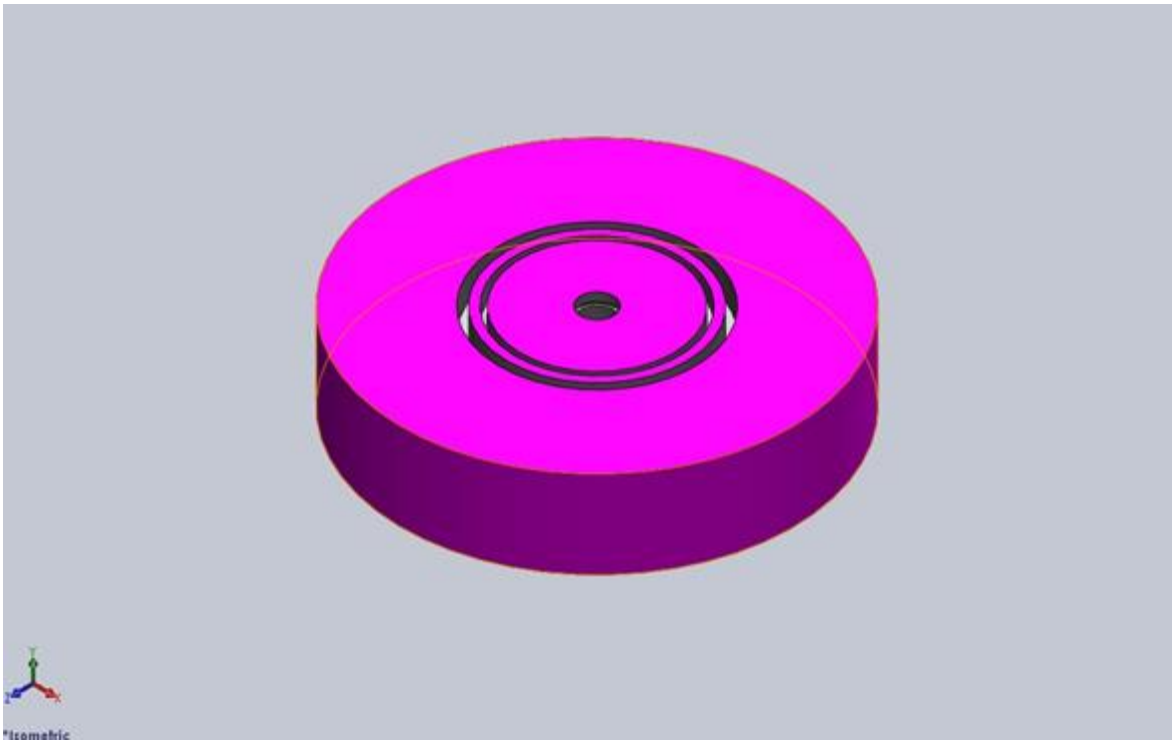

Figure AB7 End-Cap for axial test 3D view

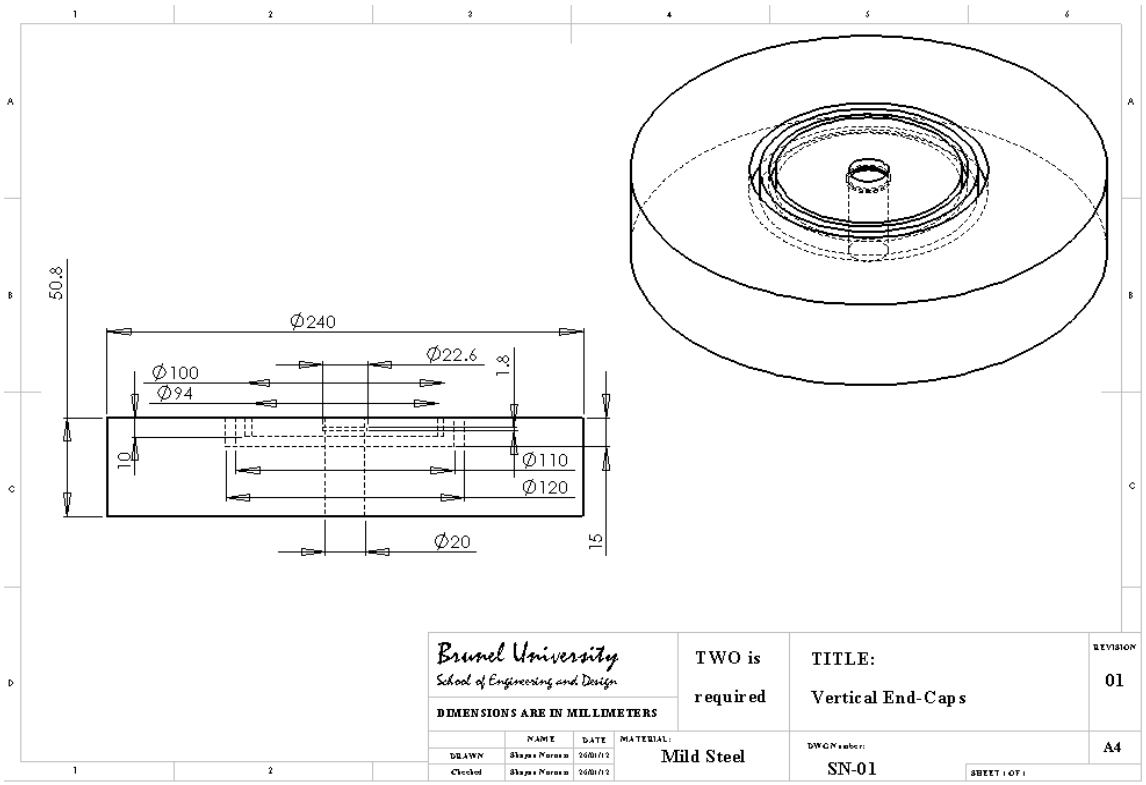

Figure AB8 End-Cap for axial test blueprint

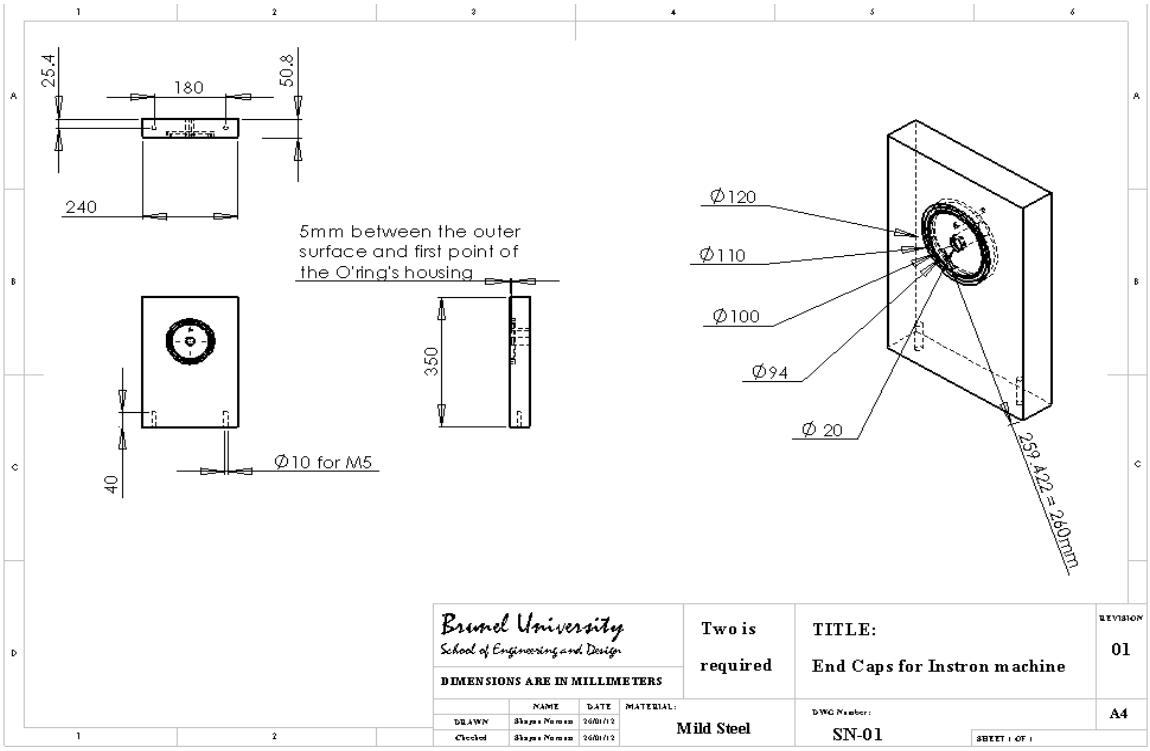

Figure AB9 End-Cap of bending test blueprint 1

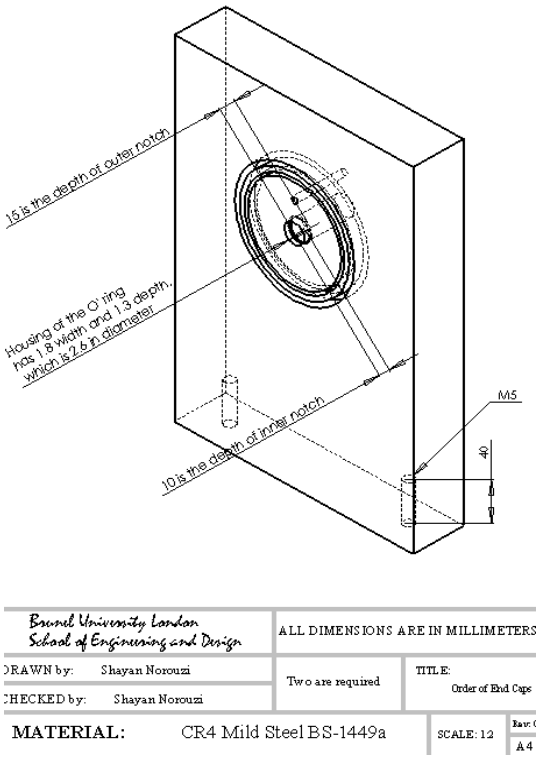

Figure AB10 End-Cap of bending test blueprint 2

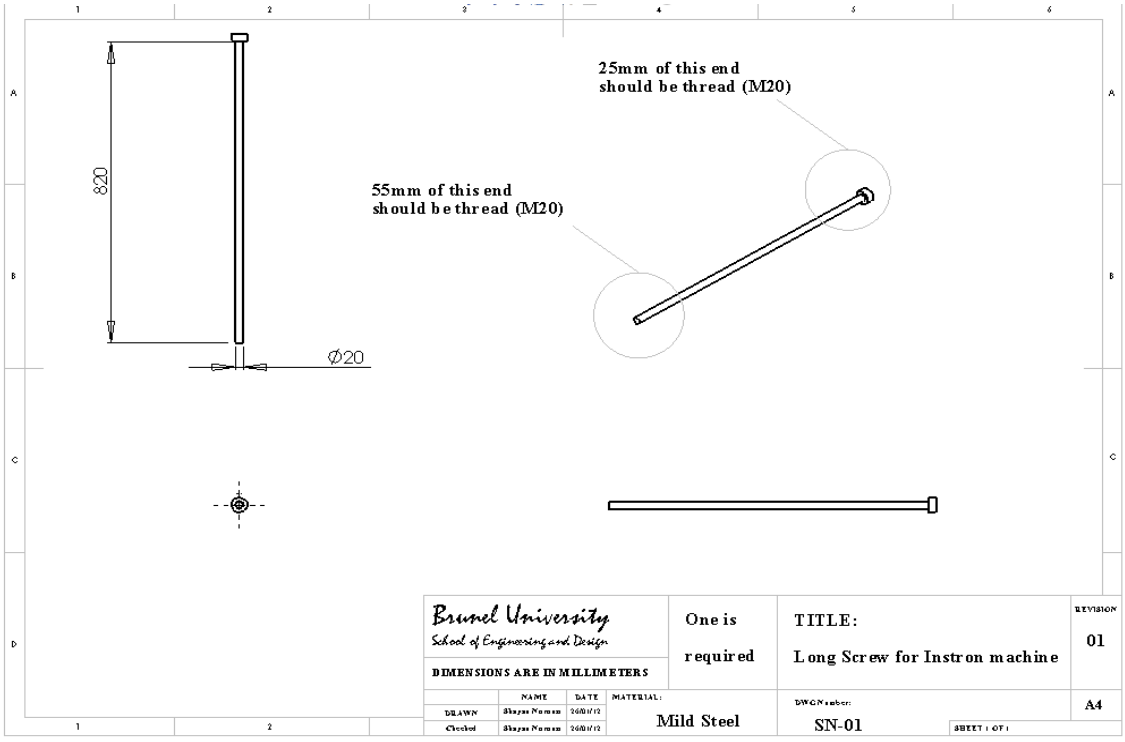

Figure AB11 Thread rod dimensions blueprint

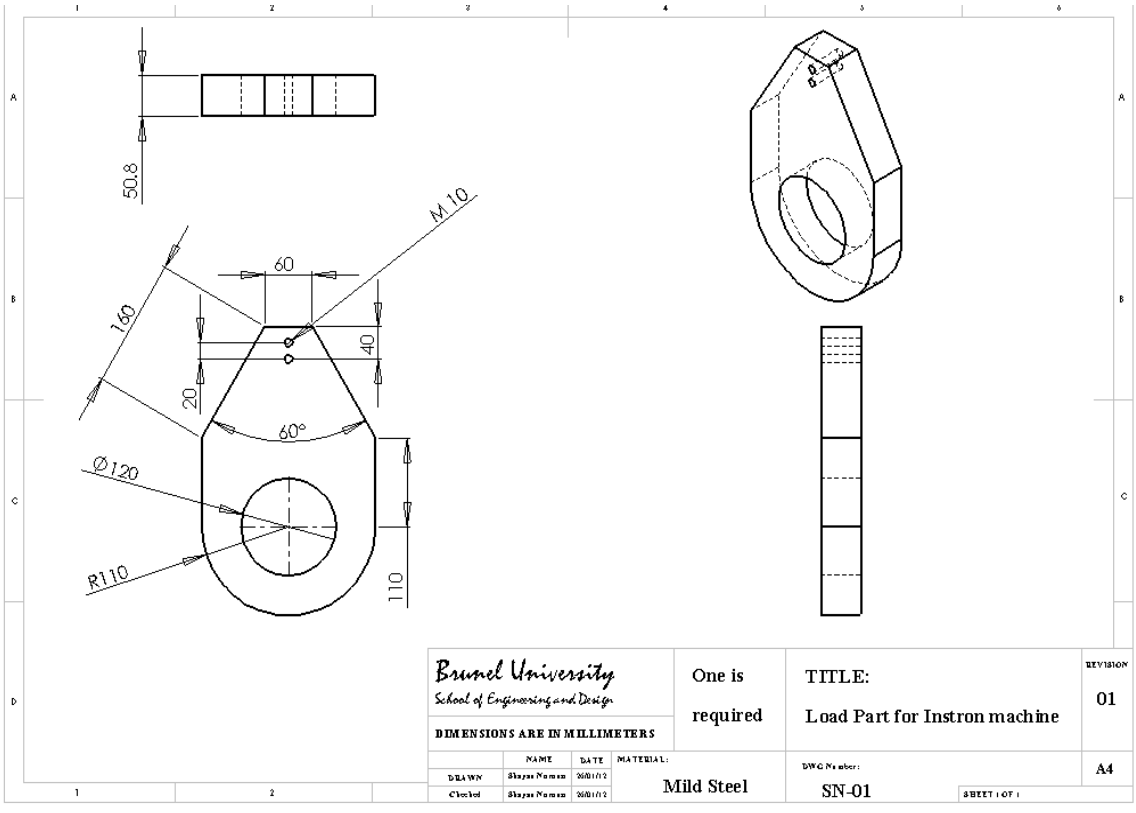

Figure AB12 Load Part for cyclic loading dimensions blueprint

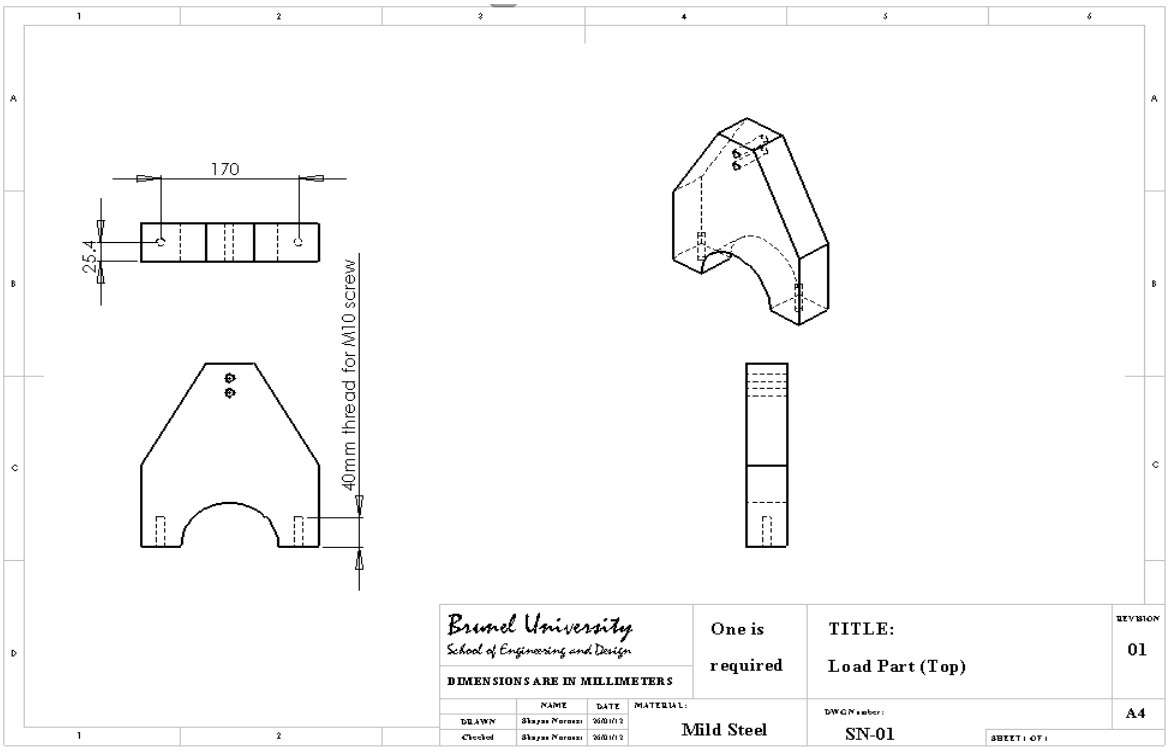

Figure AB13 Load Part for static loading blueprint

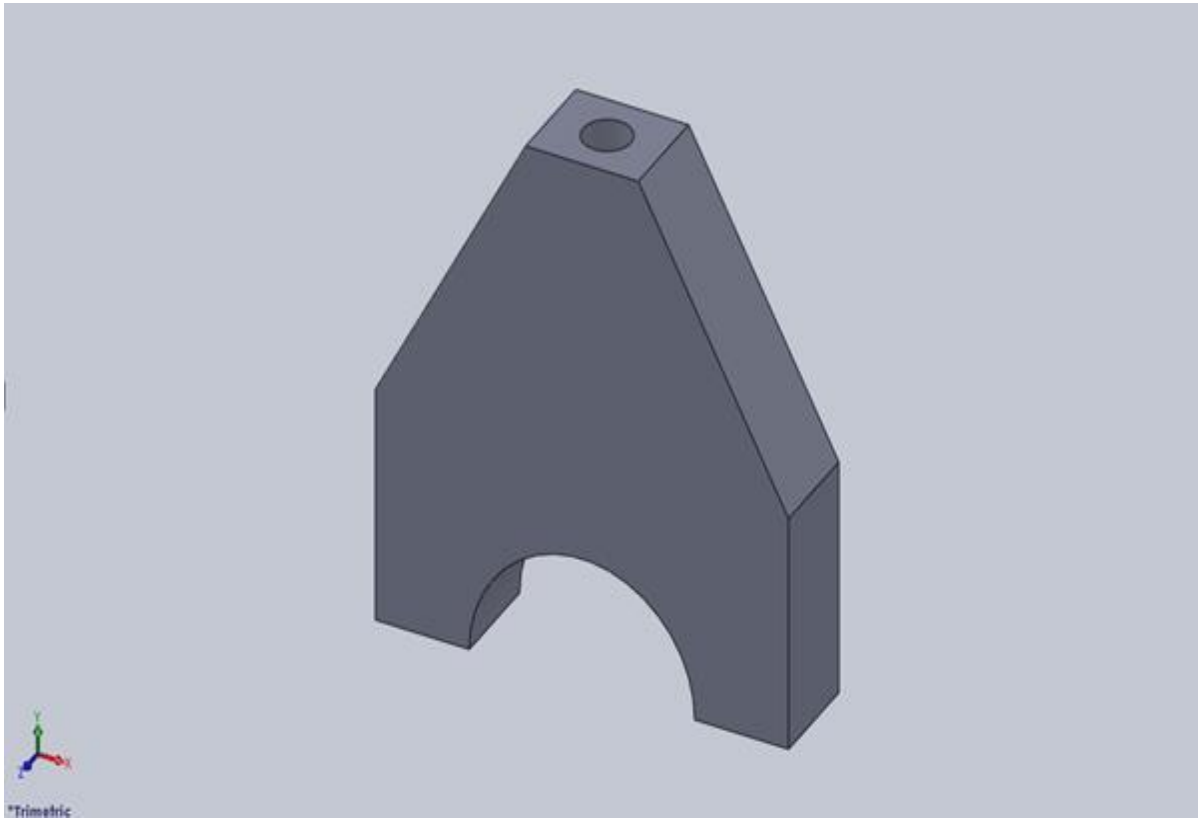

Figure AB14 Load Part for static loading 3D view

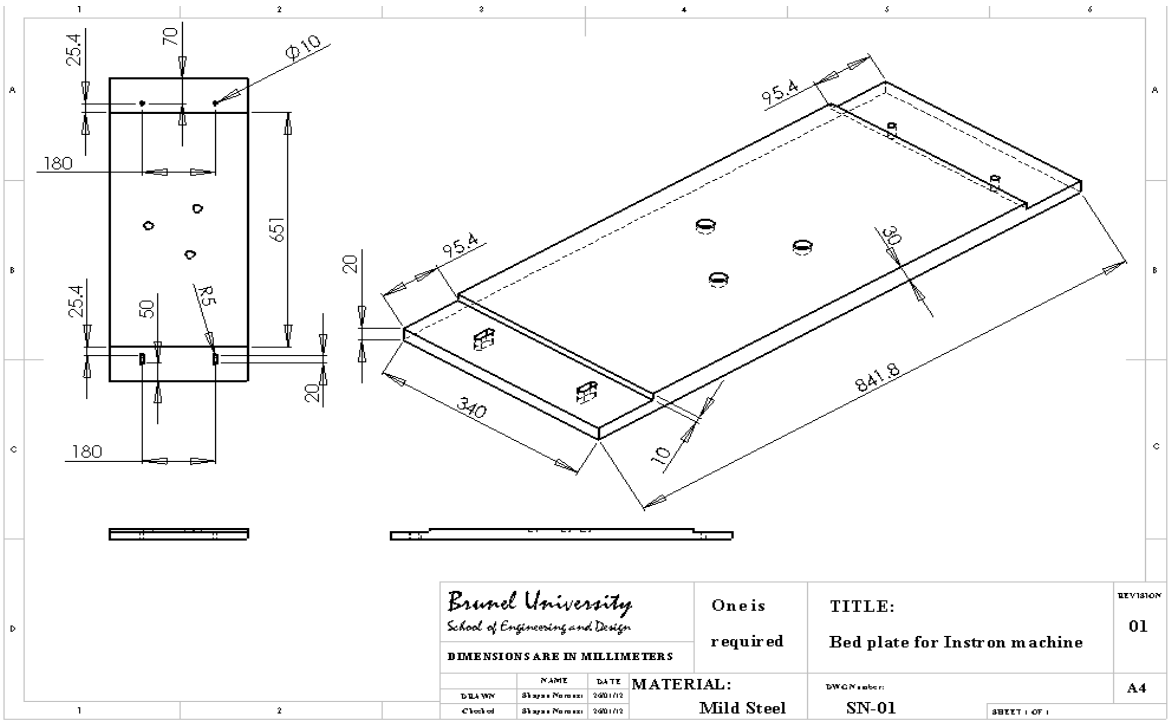

Figure AB15 Bending bed blueprint

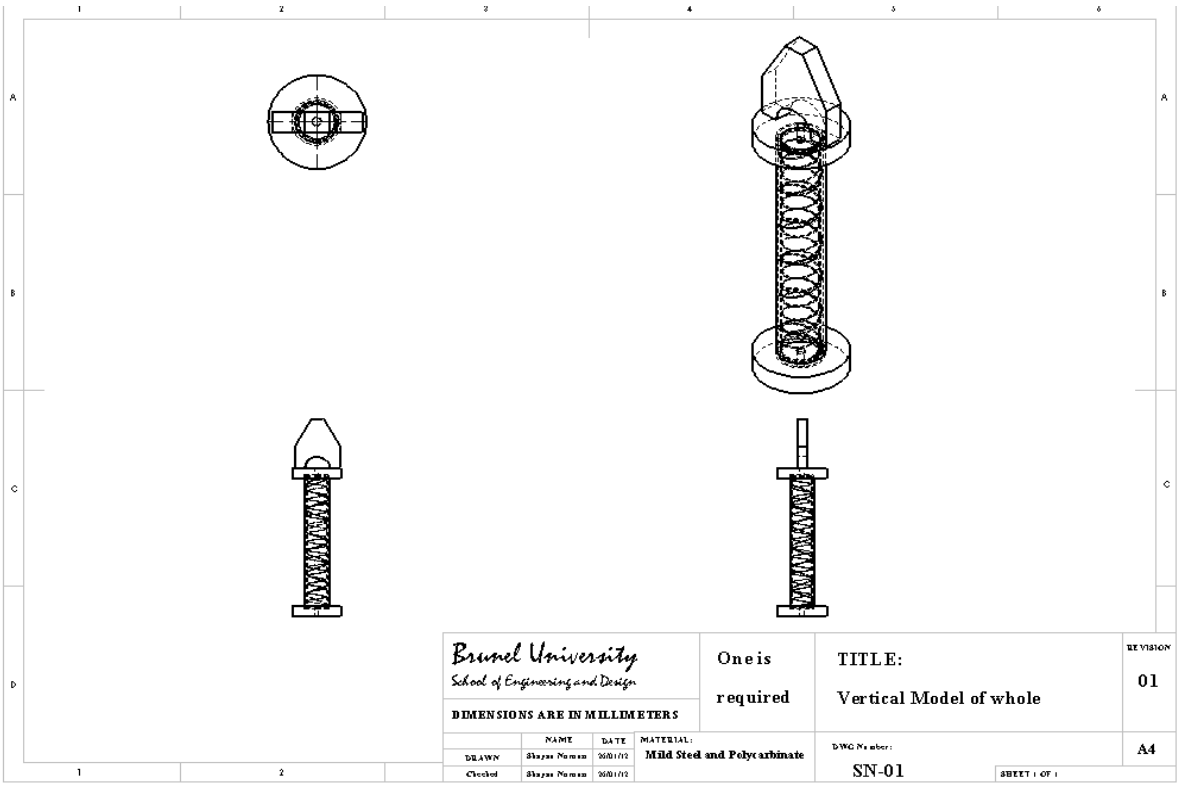

Figure AB16 Schematic view of axial loading assembly blueprint

Appendix C

Lagrange Multiplier

Method Equations

Internal energy term is:

$$\delta W = \int \sigma_{ij} \delta e_{ij} \, dV \tag{AC.1}$$

After using this method, internal energy term augmented form would be:

$$\delta W' = \delta W + \int \delta \bar{\lambda}^T \bar{\Phi}(\bar{u}) \, dV + \int \bar{\lambda}^T \delta \bar{\Phi}(\bar{u}) \, dV \tag{AC.2}$$

where W' is augmented potential and:

$$\bar{\Phi}(\bar{u}) = \bar{0} \tag{AC.3}$$

is the constraints set to be applied. The variation of the augmented potential is equal to zero.

$\bar{\Phi}(\bar{u}) = \bar{0}$ (thus: $\delta\bar{\Phi} = \bar{0}$) and simultaneously:

$$\delta W = 0 \tag{AC.4}$$

Augmented potential equation (eq. 4.2) is made of η_{tot} eqautions; thus:

$$\eta_{tot} = \eta_{dof} + \eta_c \tag{AC.5}$$

where:

η_{dof} = number of DOF of the model, η_c = number of Lagrange multiplier

The solution vector consists of the displacement DOFs $\bar{u}$ and the Lagrange multiplier.

The stiffness matrix is:

$$\begin{bmatrix} \bar{K} + \bar{\lambda}\bar{H} & \bar{B}^T \\ \bar{B} & \bar{0} \end{bmatrix} \begin{Bmatrix} \Delta\bar{u} \\ \Delta\bar{\lambda} \end{Bmatrix} = \begin{Bmatrix} -\bar{r} - \bar{\lambda}^T \bar{B} \\ \bar{\Phi}(\bar{u}) \end{Bmatrix} \tag{AC.6}$$

where $\Delta\bar{u}$ and $\Delta\bar{\lambda}$ are displacement increments and Lagrange multiplier respecively and:

$$\bar{r} = \bar{f}_{int} - \bar{f}_{ext} = \int \sigma_{ij}\delta e_{ij} - \int f_i^B \delta u_i \, dv - \int f_i^s \delta u_i \, ds \quad \text{(AC.7)}$$

$$K = \delta\bar{r} \quad \text{(AC.8)}$$

$$\bar{B} = \frac{\partial\bar{\Phi}(\bar{u})}{\partial\bar{u}} \quad \text{(AC.9)}$$

$$\bar{H} = \frac{\partial\bar{B}}{\partial\bar{u}} \quad \text{(AC.10)}$$